LBL-16826
Preprint c.2

Lawrence Berkeley Laboratory
UNIVERSITY OF CALIFORNIA

RECEIVED
LAWRENCE
BERKELEY LABORATORY
MAR 14 1984
LIBRARY AND
DOCUMENTS SECTION

Submitted to Nuclear Physics A

DYNAMICAL EVOLUTION OF ANGULAR MOMENTUM IN DAMPED NUCLEAR REACTIONS. II. OBSERVATION OF ANGULAR MOMENTUM THROUGH SEQUENTIAL DECAY

T. Døssing and J. Randrup

December 1983

LBL-16826
c.2

Prepared for the U.S. Department of Energy under Contract DE-AC03-76SF00098

DISCLAIMER

This document was prepared as an account of work sponsored by the United States Government. While this document is believed to contain correct information, neither the United States Government nor any agency thereof, nor the Regents of the University of California, nor any of their employees, makes any warranty, express or implied, or assumes any legal responsibility for the accuracy, completeness, or usefulness of any information, apparatus, product, or process disclosed, or represents that its use would not infringe privately owned rights. Reference herein to any specific commercial product, process, or service by its trade name, trademark, manufacturer, or otherwise, does not necessarily constitute or imply its endorsement, recommendation, or favoring by the United States Government or any agency thereof, or the Regents of the University of California. The views and opinions of authors expressed herein do not necessarily state or reflect those of the United States Government or any agency thereof or the Regents of the University of California.

LBL-16826

Dynamical Evolution of Angular Momentum in Damped Nuclear Reactions

II. Observation of Angular Momentum through Sequential Decay

Thomas Døssing and Jørgen Randrup

Nuclear Science Division
Lawrence Berkeley Laboratory
University of California
Berkeley, California 94720

December 1983

This work was supported by the Director, Office of Energy Research Division, of Nuclear Physics of the Office of High Energy and Nuclear Physics of the U.S. Department of Energy under Contract DE-AC03-76SF00098.

Abstract

The sequential decay of nuclei resulting from damped nuclear reactions is considered with an emphasis on observables related to the angular momentum accumulated during the reaction. Two types of observable are cosidered: multiplicity distributions and angular correlations. For both types, the effect of particle evaporation prior to the observed decay is derived, and particularly detailed calculations are made for bump-region γ-rays and fission.

The derived expressions are employed for confronting the nucleon exchange transport model with data. Overall good agreement is obtained with a few exceptions. A significant discrepancy is found for small total kinetic energy losses, where the calculated spin magnitude increases too rapidly (by approximately a factor of two). This discrepancy may be reduced somewhat by certain modifications in the treatment of the neck dynamics. Other discrepancies are mostly ascribed to uncertainties in the knowledge of the properties of the sequential decay. A modified description is tentatively proposed for fission of highly excited reaction products. It is based upon the assumption that the relaxation of the K quantum number is relatively slow, so that the angular correlation is determined by the precessional motion of the fissioning reaction product.

A separate discussion is made for double fission angular correlations. The existence of covariances between the spins of the two reaction products implies that the detection of fission from one nucleus may break the reflection symmetry of the angular correlation of fission from the other nucleus. The nucleon exchange transport theory predicts a substantial symmetry breaking (up to a factor of two) while a statistical model, which yields much smaller spin covariances, predicts a 20 percent effect only.

1. Introduction

In the preceding paper, henceforth referred to as I, we discussed the accumulation of angular momentum as caused by stochastic nucleon transfer in a damped nuclear reaction. After the reaction stage, the excited product nuclei dispose of their angular momentum by various decay processes. Only the observation of ejectiles from this secondary reaction stage enables us to ascertain the amount of angular momentum carried by the product nuclei at the end of the primary reaction stage.

Ever since the first experiment[1)], increasingly detailed information has been obtained about damped nuclear reactions by observation of sequential decay products. Measurements[1-4)] of the multiplicity of γ-rays indicated that damped reactions endow the product nuclei with substantial angular momenta. Studies[5)] of the circular polarization of γ-rays gave evidence of negative-angle scattering. Investigations[6-7)] of the angular correlation of sequential fission fragments demonstrated that there is not a unique relation between impact parameter and energy loss.

The damped reaction product nuclei have a distribution of excitation energy and angular momentum which is different from that in compound nuclei produced in fusion reactions. Therefore caution must be exercised in the theoretical treatment of their sequential decay. For studies of light-particle sequential decay (including γ-emission) one may make use of data gathered from (HI,xn) reactions, but often this information must be extrapolated to higher excitation energies and, sometimes, also to higher angular momenta.

Fission of very heavy damped reaction products present a special problem. The fission angular distributions observed in fusion reactions[8] do not agree with the angular correlation data for sequential fission following damped reactions,[9] and both are in disagreement with the standard theory which relates the fission angular distribution to the effective moment of inertia of the fission saddle shape, as predicted by the rotating liquid drop model.[8-10]

Scalar quantities characterizing the sequential decay process, such as the γ-ray multiplicity and the fission probability, can readily be analyzed in sequential decay studies, provided that the model parameters are known from compound nucleus studies.

On the other hand, it is not so straigthforward to describe the correlations between the directions of motion of the nucleus and sequential ejectiles. The first analysis of angular correlations[6-7,11] employed special parametrizations of the distribution of angular momentum directions. Some of these[7,11] use a gaussian form of the spin distribution, in good accordance with the theoretical distributions. Under certain conditions,[11] analytical expressions can be derived, and a comparison between theory and data, though not very accurate, can be carried out. Another method of analysis[12] takes a more fundamental starting point by deriving a general expression for the angular correlation. Applied to fission data this formulation has had some success in describing the alignment of the spin.[12-13]

The purpose of the present paper is to follow up on the calculations in I of the accumulation of angular momenta by addressing the sequential decay processes after the reaction and, in turn, compare the theoretical results with available data.

For those quantities which involve only the spin in one of the two reaction products, we aim at a rather precise calculation of the sequential decay properties, integrating over the entire spin distribution and employing detailed information about the decay processes.

For quantities involving both nuclei simultaneously, such as the width of the γ-multiplicity distribution and the double fission angular correlation, we resort to analytical approximations.

First, in Section 2, we give an introductory discussion of the symmetries of the spin distributions and of the experimental quantities. Then, in Section 3, approximate analytical expressions are derived for average values and variances of the spin magnitude distributions, as relevant for γ-multiplicity studies. Section 4 presents the main expressions for the angular correlation and gives angular correlation parameters for continuous γ-rays and fission products. In Section 5 we compare the calculated results to data. In Section 6 we derive analytical expressions for double fission angular distributions and discuss, with reference to a specific reaction of experimental interest, how the correlation between the spins in the two reaction products can be probed in such an experiment. Section 7 concludes our study and attempts to evaluate how well the data can be described by the nucleon exchange transport model.

Appendix A evaluates the change of the spin distribution, both with regard to magnitude and direction, caused by unobserved neutron decay prior to the sequential decay actually observed. Appendix B describes our calculation of the fission angular correlation parameters and compares the results with more involved and consistent calculations, and with experiment.

2. General remarks

We first make some general remarks about the spin distributions and the related observables.

2.1 Reflection in the reaction plane

The detection of one of the damped nuclear reaction products defines the reaction plane. If only scalar quantities, such as the charge and the kinetic energy, are measured together with the direction of motion, the density matrix for the system is invariant under an overall reflection in the reaction plane. Assuming that the forces acting during the reaction conserve parity, the expectation value must vanish for any quantity which changes sign under such a reflection. Specifically, for the angular momentum the two components in the reaction plane change sign under the reflection while the component along the reaction normal is invariant.

2.2 Coordinate system

As we have discussed in I, when studying the reaction dynamics it is convenient to use the relative dinuclear position as the z-axis and the instantaneous direction of relative tangential motion as the x-axis so that the instantaneous reaction normal is the y-axis. Therefore, when discussing observables in an externally defined reference system, it is natural to adopt the reaction normal as the Y-axis, (and also as the polar direction). The XZ-plane is then the reaction plane, but the orientation of the in-plane axes will depend on convenience.

Let the angular momenta of the two reaction products be $\vec{S}^A$ and $\vec{S}^B$. It then follows from the above symmetry considerations that the following mean values and covariances vanish,

$$\langle S_X^F \rangle = \langle S_Z^F \rangle = 0$$
$$\sigma_{XY}^{FG} = \sigma_{YZ}^{FG} = 0 \tag{2.1}$$

so that only the following moments are non-trivial

$$\langle S_Y^F \rangle$$
$$\sigma_{XX}^{FG}, \sigma_{YY}^{FG}, \sigma_{ZZ}^{FG}, \sigma_{XZ}^{FG}, \sigma_{ZX}^{FG} \tag{2.2}$$

where the labels F,G refer to either of the nuclei A,B. (For explanation of the notation we refer to I.) Spin distributions satisfying the above requirements are said to be of standard form.

The symmetry requirement is also valid at any time during the reaction when the quantities are referred to the body-fixed (L-aligned) system xyz mentioned above. Therefore the dynamical spin distributions are always of standard form and generally all the non-trivial moments are non-vanishing. [Although any individual nucleon transfer may produce a non-zero in-plane spin component, there is an equal probability for a transfer producing the opposite in-plane spin component so that the distribution remains on standard form.]

2.3 Higher moments

In our current treatment, only the mean values and the covariances of the spins are determined, rather than the entire distribution. When higher moments are required to make contact with the experimental quantities, we assume the theoretical spin distribution to be of multivariate gaussian form . The higher moments can then be expressed in terms of the first and second moments. For example, for the product of four spin variables with vanishing mean values,

$$\langle S_i \rangle = \langle S_j \rangle = \langle S_k \rangle = \langle S_\ell \rangle = 0 \quad , \tag{2.3}$$

the expectation value is

$$\langle S_i S_j S_k S_\ell \rangle = \sigma_{ij}\, \sigma_{k\ell} + \sigma_{ik}\, \sigma_{j\ell} + \sigma_{i\ell}\, \sigma_{jk} \tag{2.4}$$

2.4 Experimental quantities

At present, our information about angular momentum in damped nuclear reactions arises from three types of observable: the multiplicity of γ-rays, the circular polarization of γ-rays, and the angular correlation between the direction of motion of a reaction product and a sequential ejectile. In the present study we shall not address the polarization data since they are yet fairly crude with respect to the dependence on energy loss.

The γ-multiplicity data gives information about the distribution of the total magnitude of fragment spin, specifically,

$$\langle |\vec{S}^A| + |\vec{S}^B| \rangle$$
$$\sigma^2_{|\vec{S}^A|+|\vec{S}^B|} \tag{2.5}$$

The angular correlation data gives information about the distribution of the spin directions. The moments of the directional distribution are the statistical spherical tensors. The information about the statistical tensors is modulated by the angular distribution coefficients and the decay probabilities, which depend on the spin size. The most important tensors are those of rank two, namely the <u>alignment</u> along the reaction normal

$$P_{YY} = \left\langle \frac{3 S_Y^2 - \vec{S}^2}{2 \vec{S}^2} \right\rangle \tag{2.6}$$

and the <u>asymmetry</u> between the in-plane components

$$P_{XZ} = \left\langle \frac{S_X^2 - S_Z^2}{\vec{S}^2} \right\rangle \tag{2.7}$$

2.5 Unobserved intermediate decay

Most of the observed decay products are not emitted directly from the primary reaction product. Indeed, γ-rays, and also fission to some extent, are preceded by the emission of (usually unobserved) light particles, mostly neutrons. Therefore it is necessary to determine how the moments of the spin distribution and the statistical tensors are affected by a neutron cascade. The appropriate expressions are derived in Appendix A.

3. The spin magnitude distribution

In this section we derive expressions for mean values and variances of the spin magnitude distributions. We assume that the spin distribution for the two reaction products is of normal form and, furthermore, that the fluctuations are not dominant, i.e.

$$\langle S_Y^F \rangle \langle S_Y^G \rangle > \mathrm{tr}\, \sigma^{FG} \tag{3.1}$$

We shall then derive results to second order in $\sigma_{ij}^{FG}/\langle S_Y^F\rangle\langle S_Y^G\rangle$.

First, we consider the spin $\vec{S}$ in one of the nuclei and expand its magnitude $S = |\vec{S}|$ to fourth order in the deviation $\Delta\vec{S} \equiv \vec{S} - \langle\vec{S}\rangle$:

$$\begin{aligned}
S &= \left[(\langle\vec{S}\rangle + \Delta\vec{S})^2 \right]^{1/2} \\
&= |\langle\vec{S}\rangle| \left[1 + 2\,\frac{\vec{S}\cdot\Delta\vec{S}}{|\langle\vec{S}\rangle|^2} + \frac{\Delta\vec{S}\cdot\Delta\vec{S}}{|\langle\vec{S}\rangle|^2} \right]^{1/2} \\
&\approx |\langle\vec{S}\rangle| \Bigg\{ 1 + \frac{\langle\vec{S}\rangle}{|\langle\vec{S}\rangle|}\cdot\Delta\vec{S} + \frac{|\Delta\vec{S}|^2}{2|\langle\vec{S}\rangle|^2} \\
&\quad - \frac{1}{8}\frac{1}{|\langle\vec{S}\rangle|^4}\left[4(\vec{S}\cdot\Delta\vec{S})^2 + 4(\vec{S}\cdot\Delta\vec{S})|\Delta\vec{S}|^2 + |\Delta\vec{S}|^4 \right] \\
&\quad + \frac{1}{16}\frac{1}{|\langle\vec{S}\rangle|^6}\left[8(\vec{S}\cdot\Delta\vec{S})^3 + 12(\vec{S}\cdot\Delta\vec{S})^2|\Delta\vec{S}|^2 + 6(\langle\vec{S}\rangle\cdot\Delta\vec{S})|\Delta\vec{S}|^4 \right] \\
&\quad - \frac{5}{128}\frac{1}{|\langle\vec{S}\rangle|^8}\left[16(\vec{S}\cdot\Delta\vec{S})^4 + \dots \right] + \dots \Bigg\}
\end{aligned} \tag{3.2}$$

By applying relations similar to (2.4), valid for gaussian distributions, we obtain, to second order in $\sigma_{ij}^{FF}/\langle S_Y^F\rangle^2$:

$$\langle S^F\rangle = \langle S_Y^F\rangle + \frac{\sigma_{\perp\perp}^{FF}}{2\langle S_Y^F\rangle} + \frac{1}{8}\frac{1}{\langle S_Y^F\rangle^3}\left[4\sigma_{YY}^{FF}\sigma_{\perp\perp}^{FF} - \sigma_{\perp\perp}^{FF\,2} - 2\left(\sigma_{XX}^{FF\,2} + 2\sigma_{XZ}^{FF\,2} + \sigma_{ZZ}^{FF\,2}\right)\right] \tag{3.3}$$

where $\sigma_{\perp\perp}^{FF} \equiv \sigma_{XX}^{FF} + \sigma_{ZZ}^{FF}$. For the second moment we obtain

$$\langle S^{F\,2}\rangle = \langle S_Y^F\rangle^2 + \sigma_{YY}^{FF} + \sigma_{\perp\perp}^{FF} \tag{3.4}$$

so that the variance of S^F is

$$\sigma_{S^F}^2 = \sigma_{YY}^{FF} + \frac{1}{2}\frac{1}{\langle S_Y^F\rangle^2}\left[\sigma_{XX}^{FF\,2} + 2\sigma_{XZ}^{FF\,2} + \sigma_{ZZ}^{FF\,2} - 2\sigma_{YY}^{FF}\sigma_{\perp\perp}^{FF}\right] \tag{3.5}$$

Considering now both reaction products, we find that the mean value of the sum of the two spin magnitudes is just the sum of the individual mean values,

$$\langle S^A + S^B\rangle = \langle S^A\rangle + \langle S^B\rangle \tag{3.6}$$

while the variance on this quantity depends on the correlation between $\vec{S}^A$ and $\vec{S}^B$:

$$\sigma_{S^A+S^B}^2 = \sigma_{S^A}^2 + \sigma_{S^B}^2 + 2\left(\langle S^A S^B\rangle - \langle S^A\rangle\langle S^B\rangle\right) \tag{3.7}$$

To second order, the result for the variance is then

$$\sigma^2_{S^A+S^B} = \sigma^2_{S^A} + \sigma^2_{S^B} + 2\sigma^{AB}_{YY}$$

$$+ \frac{1}{\langle S^A_Y\rangle}\frac{1}{\langle S^B_Y\rangle}\left(\sigma^{AB\,2}_{XX} + \sigma^{AB\,2}_{XZ} + \sigma^{AB\,2}_{ZX} + \sigma^{AB\,2}_{ZZ}\right) \tag{3.8}$$

$$- \left(\frac{1}{\langle S^A_Y\rangle^2}\sigma^{AA}_{\perp\perp} + \frac{1}{\langle S^B_Y\rangle^2}\sigma^{BB}_{\perp\perp}\right)\sigma^{AB}_{YY}$$

3.1 Effects of neutron evaporation

The evaporation of neutrons from the primary reaction products modifies the spin distribution. In this section we derive approximate analytical expressions for the changes in mean spin magnitudes and the associated covariances. We thus consider the evaporation chains

$S^A_0 \to S^A_1 \to \ldots \to S^A_i \to \ldots$ and $S^B_0 \to S^B_1 \to \ldots \to S^B_j \to \ldots$

in the projectile-like and target-like nuclei, respectively. As shown in Appendix A (A.17), at a given stage, when the evaporating nuclei have definite spin magnitudes S^A_{i-1} and S^B_{j-1}, the change in spin magnitude and the incurred variance are approximately given by

$$\langle\Delta_i\rangle \equiv \langle S^A_i - S^A_{i-1}\rangle \approx \left(1 - \frac{2}{3}\frac{\mathcal{J}_a}{\mathcal{J}_A}\right) S^A_{i-1}$$

$$\langle\Delta_j\rangle \equiv \langle S^B_j - S^B_{j-1}\rangle \approx \left(1 - \frac{2}{3}\frac{\mathcal{J}_b}{\mathcal{J}_B}\right) S^B_{j-1}$$

$$\sigma_i^2 \equiv \langle (S^A_i - S^A_{i-1})^2\rangle - \Delta_i^2 \approx \frac{2}{3}\mathcal{J}_a T_i \tag{3.9}$$

$$\sigma_j^2 \equiv \langle (S^B_j - S^B_{j-1})^2\rangle - \Delta_j^2 \approx \frac{2}{3}\mathcal{J}_b T_j$$

where $\mathcal{J}_a = mR_A^2$ and $\mathcal{J}_b = mR_B^2$ are the respective moments of inertia of the evaporated neutron at the barrier.

In general, the evaporating nuclei have an entire distribution of spin magnitudes, rather than a definite value. After i evaporations from A and j evaporations from B the spin magnitude distribution is characterized by the mean magnitudes $\langle S_i^A \rangle$ and $\langle S_j^B \rangle$, the corresponding variances $\sigma^2_{S_i^A}$ and $\sigma^2_{S_j^B}$, and the covariance $\sigma_{S_i^A S_j^B}$. By use of (3.9) it is easy to calculate the change in these quantities effected by a single step in the evaporation chain, for example $(S_{i-1}^A, S_j^B) \to (S_i^A, S_j^B)$:

$$\langle S_i^A + S_j^B \rangle = \left(1 - \frac{2}{3}\frac{\mathcal{J}_a}{\mathcal{J}_A}\right)\langle S_{i-1}^A \rangle + \langle S_j^B \rangle$$

$$\sigma^2_{S_i^A} = \left(1 - \frac{2}{3}\frac{\mathcal{J}_a}{\mathcal{J}_A}\right)^2 \sigma^2_{S_{i-1}^A} + \frac{2}{3}\mathcal{J}_a T_i$$

$$\begin{aligned}
\sigma^2_{S_i^A + S_j^B} &= \sigma^2_{S_i^A} + \sigma^2_{S_j^B} + 2\langle S_i^A S_j^B \rangle - 2\langle S_i^A \rangle \langle S_j^B \rangle \\
&= \left(1 - \frac{2}{3}\frac{\mathcal{J}_a}{\mathcal{J}_A}\right)^2 \sigma^2_{S_{i-1}^A} + \frac{2}{3}\mathcal{J}_a T_i + \sigma^2_{S_j^B} \\
&\quad + 2\left(1 - \frac{2}{3}\frac{\mathcal{J}_a}{\mathcal{J}_A}\right)\langle S_{i-1}^A S_j^B \rangle - 2\left(1 - \frac{2}{3}\frac{\mathcal{J}_a}{\mathcal{J}_A}\right)\langle S_{i-1}^A \rangle \langle S_j^B \rangle \\
&= \left(1 - \frac{2}{3}\frac{\mathcal{J}_a}{\mathcal{J}_A}\right)\sigma^2_{S_{i-1}^A + S_j^B} + \frac{2}{3}\mathcal{J}_a T_i \\
&\quad - \frac{2}{3}\frac{\mathcal{J}_a}{\mathcal{J}_A}\left(1 - \frac{2}{3}\frac{\mathcal{J}_a}{\mathcal{J}_A}\right)\sigma^2_{S_{i-1}^A} + \frac{2}{3}\frac{\mathcal{J}_a}{\mathcal{J}_A}\sigma^2_{S_j^B}
\end{aligned} \tag{3.10}$$

By recursive use of this result, the effects of the entire neutron cascade of n_A neutrons from A and n_B neutrons from B can be calculated:

$$\langle S^A_{n_A} + S^B_{n_B} \rangle = \left(1 - \frac{2}{3}\frac{\mathcal{J}_a}{\mathcal{J}_A}\right)^{n_A} \langle S^A_0 \rangle + \left(1 - \frac{2}{3}\frac{\mathcal{J}_b}{\mathcal{J}_B}\right)^{n_B} \langle S^B_0 \rangle$$

$$\begin{aligned}
\sigma^2_{S^A_{n_A} + S^B_{n_B}} = {} & \left(1 - \frac{2}{3}\frac{\mathcal{J}_a}{\mathcal{J}_A}\right)^{n_A} \left(1 - \frac{2}{3}\frac{\mathcal{J}_b}{\mathcal{J}_B}\right)^{n_B} \sigma^2_{S^A_0 + S^B_0} \\
& + \sum_{i=1}^{n_A} \left(1 - \frac{2}{3}\frac{\mathcal{J}_a}{\mathcal{J}_A}\right)^{2(n_A - i)} \frac{2}{3}\mathcal{J}_a \tau_i \\
& + \sum_{j=1}^{n_B} \left(1 - \frac{2}{3}\frac{\mathcal{J}_b}{\mathcal{J}_B}\right)^{2(n_B - j)} \frac{2}{3}\mathcal{J}_b \tau_j \\
& + \left(1 - \frac{2}{3}\frac{\mathcal{J}_a}{\mathcal{J}_A}\right)^{n_A} \left[\left(1 - \frac{2}{3}\frac{\mathcal{J}_a}{\mathcal{J}_A}\right)^{n_A} - \left(1 - \frac{2}{3}\frac{\mathcal{J}_b}{\mathcal{J}_B}\right)^{n_B}\right] \sigma^2_{S^A_0} \\
& + \left(1 - \frac{2}{3}\frac{\mathcal{J}_b}{\mathcal{J}_B}\right)^{n_B} \left[\left(1 - \frac{2}{3}\frac{\mathcal{J}_b}{\mathcal{J}_B}\right)^{n_B} - \left(1 - \frac{2}{3}\frac{\mathcal{J}_a}{\mathcal{J}_A}\right)^{n_A}\right] \sigma^2_{S^B_0}
\end{aligned} \tag{3.11}$$

When the temperatures in the primary nuclei are nearly equal, as is expected for not too small energy losses,[14] we have approximately

$$\frac{n_A}{n_B} \approx \frac{A}{B} \tag{3.12}$$

When this is the case, the last two terms in the above expression (3.11) for the variance of $S^A_{n_B}$ and $S^B_{n_B}$ are quite small, since $\mathcal{J}_a/\mathcal{J}_A \sim 1/A$ and $\mathcal{J}_b/\mathcal{J}_B \sim 1/B$:

$$\begin{aligned}
& \left(1 - \frac{2}{3}\frac{\mathcal{J}_a}{\mathcal{J}_A}\right)^{n_A} - \left(1 - \frac{2}{3}\frac{\mathcal{J}_b}{\mathcal{J}_B}\right)^{n_B} \\
& \approx \exp\left(-n_A \frac{2}{3}\frac{\mathcal{J}_a}{\mathcal{J}_A}\right) - \exp\left(-n_B \frac{2}{3}\frac{\mathcal{J}_b}{\mathcal{J}_B}\right) \approx 0
\end{aligned} \tag{3.13}$$

The sums in (3.11) can be approximated by integrals,

$$\sum_{i=1}^{n_A} \left(1-\frac{2}{3}\frac{\mathcal{J}_a}{\mathcal{J}_A}\right)^{2(n_A-i)} \frac{2}{3}\mathcal{J}_a T_i$$

$$\approx \frac{2}{3}\mathcal{J}_a T_1 \int_0^{n_A} \sqrt{\frac{n_A-i}{n_A}}\left(1-\frac{2}{3}\frac{\mathcal{J}_a}{\mathcal{J}_A}\right)^{2(n_A-i)} di \tag{3.14}$$

For the relation between excitation energy and number of evaporated neutrons we shall use (A.25). Since the integral can be approximated as

$$\int_0^{\alpha} \sqrt{x}\, e^{\beta x} = \int_0^{\alpha} \sum_{n=0}^{\infty} \frac{\beta^n x^{n+\frac{1}{2}}}{n!}\, dx \tag{3.15}$$

$$= \frac{2}{3}\alpha^{3/2} + \frac{\beta\alpha^{5/2}}{5/2} + \frac{1}{2}\frac{\beta^2\alpha^{7/2}}{7/2} + \ldots \approx \frac{2}{3}\alpha^{3/2}\exp\left(\frac{3}{5}\beta\alpha\right)$$

the sum can finally be written as

$$\sum_{i=1}^{n_A} \left(1-\frac{2}{3}\frac{\mathcal{J}_a}{\mathcal{J}_A}\right)^{2(n_A-i)} \frac{2}{3}\mathcal{J}_a T_i \tag{3.16}$$

$$\approx \frac{4}{9}\mathcal{J}_a T_1 n_A \exp\left(-\frac{4}{5} n_A \frac{\mathcal{J}_a}{\mathcal{J}_A}\right)$$

Altogether we then obtain the following approximate result,

$$\langle S^A_{n_A} + S^B_{n_B} \rangle \approx \langle S^A_0 \rangle \exp\left(-n_A \tfrac{2}{3} \tfrac{\mathcal{J}_a}{\mathcal{J}_A}\right) + \langle S^B_0 \rangle \exp\left(-n_B \tfrac{2}{3} \tfrac{\mathcal{J}_b}{\mathcal{J}_B}\right)$$

$$\sigma^2_{S^A_{n_A} + S^B_{n_B}} \approx \sigma^2_{S^A_0 + S^B_0} \exp\left(-n_A \tfrac{2}{3} \tfrac{\mathcal{J}_a}{\mathcal{J}_A}\right) \exp\left(-n_B \tfrac{2}{3} \tfrac{\mathcal{J}_b}{\mathcal{J}_B}\right) \tag{3.17}$$

$$+ n_A \tfrac{4}{9} \mathcal{J}_a \tau_1 \exp\left(-n_A \tfrac{4}{5} \tfrac{\mathcal{J}_a}{\mathcal{J}_A}\right) + n_B \tfrac{4}{9} \mathcal{J}_b \tau_1 \exp\left(-n_B \tfrac{4}{5} \tfrac{\mathcal{J}_b}{\mathcal{J}_B}\right)$$

The temperatures in the first daughter nuclei can be calculated from (A.26) once the excitation energy in the primary nuclei A and B is known. In the above expression we have used the same temperature τ_1 for both daughter nuclei which is most often a good approximation.

3.2 Transport description of neutron evaporation

In the preceding, we have derived expressions for the effect of the neutron evaporation process by solving approximately the iterative equations (3.9) for the spin distribution. A simple approximate treatment of the same problem can be given within the framework of transport theory.

To this end we consider n_F, the number of neutrons evaporated from the nucleus $F = A,B$, to be a continuous variable. We then wish to consider the distribution of the total nuclear spin magnitude $\Sigma(n_A,n_B) \equiv S_A(n_A) + S_B(n_B)$ as a function of the number of evaporated neutrons. The evolution of Σ is a transport process with n_A and n_B acting as generalized time variables. The evolution of the individual nuclear spin magnitudes S_F is governed by the transport coefficients V_F and D_{FF} which can be determined by considering the

effect of a single evaporation step on a nucleus prepared with a sharply defined value of S_F. Thus, it follows from (3.9) that

$$V_F = -\frac{2}{3}\frac{\mathcal{J}_f}{\mathcal{J}_F} S_F$$

$$D_{FF} = \frac{1}{3}\mathcal{J}_f \tau_F \tag{3.18}$$

for the drift and diffusion coefficient, respectively, while the mixed diffusion coefficient D_{AB} vanishes. Here $\mathcal{J}_f = mr_n^2 F^{2/3}$ is the moment of inertia of the neutron at its barrier distance $r_n F^{1/3}$ and $\mathcal{J}_F = \frac{2}{5} mr_0^2 F^{5/3}$ is the moment of inertia of the nucleus F; τ_F is the nuclear temperature. As usual (see for example ref. [30]), the corresponding Fokker-Planck equation can be reduced to equations for the mean value and variances of S_F,

$$\frac{\partial}{\partial n_F}\langle S_F\rangle = \langle V_F\rangle = -\frac{2}{3}\frac{\mathcal{J}_f}{\mathcal{J}_F}\langle S_F\rangle$$

$$\frac{\partial}{\partial n_F}\sigma_{FF} = \langle 2 D_{FF} + 2\frac{\partial V_F}{\partial S_F}\sigma_{FF}\rangle \tag{3.19}$$

$$= \frac{2}{3}\mathcal{J}_f\tau_F - \frac{4}{3}\frac{\mathcal{J}_f}{\mathcal{J}_F}\sigma_{FF}$$

Assuming for the time being that the temperature τ_F, as well as $\mathcal{J}_f$ and $\mathcal{J}_F$, remain constant throughout the evaporation chain, we obtain the following solution for S_F:

$$\langle S_F\rangle(n_F) = \langle S_F\rangle(0)\, e^{-\frac{2}{3}\frac{\mathcal{J}_f}{\mathcal{J}_F} n_F}$$

$$\sigma_{FF}(n_F) = \sigma_{FF}(0)\, e^{-\frac{4}{3}\frac{\mathcal{J}_f}{\mathcal{J}_F} n_F} + \frac{\tau_F}{2}\mathcal{J}_f\left(1 - e^{-\frac{4}{3}\frac{\mathcal{J}_f}{\mathcal{J}_F} n_F}\right) \tag{3.20}$$

Furthermore, we find for the evolution of the covariance between the two spins

$$\frac{\partial}{\partial n_A}\sigma_{AB} = -\frac{2}{3}\frac{J_a}{J_A}\sigma_{AB}$$
$$\frac{\partial}{\partial n_B}\sigma_{AB} = -\frac{2}{3}\frac{J_b}{J_B}\sigma_{AB} \tag{3.21}$$

so that

$$\sigma_{AB}(n_A, n_B) = \sigma_{AB}(0,0)\, e^{-\frac{2}{3}\frac{J_a}{J_A}n_A}\, e^{-\frac{2}{3}\frac{J_b}{J_B}n_B} \tag{3.22}$$

For the total spin magnitude $\Sigma = S_A + S_B$ we therefore have

$$\langle\Sigma\rangle(n_A, n_B) = \langle S_A\rangle(n_A) + \langle S_B\rangle(n_B)$$
$$= \langle S_A\rangle(0)\, e^{-\frac{2}{3}\frac{J_a}{J_A}n_A} + \langle S_B\rangle(0)\, e^{-\frac{2}{3}\frac{J_b}{J_B}n_B} \tag{3.24}$$

which is identical to the expression in (3.17), and

$$\sigma_{\Sigma\Sigma}(n_A, n_B) = \sigma_{AA}(n_A) + \sigma_{BB}(n_B) + 2\sigma_{AB}(n_A, n_B)$$

$$= \sigma_{AA}(0)\, e^{-\frac{4}{3}\frac{\mathcal{J}_a}{\mathcal{J}_A} n_A} + \sigma_{BB}(0)\, e^{-\frac{4}{3}\frac{\mathcal{J}_b}{\mathcal{J}_B} n_B} + 2\sigma_{AB}(0,0)\, e^{-\frac{2}{3}\frac{\mathcal{J}_a}{\mathcal{J}_A} n_A} e^{-\frac{2}{3}\frac{\mathcal{J}_b}{\mathcal{J}_B} n_B}$$

$$+ \frac{\tau_A}{2}\mathcal{J}_a\left(1 - e^{-\frac{4}{3}\frac{\mathcal{J}_a}{\mathcal{J}_A} n_A}\right) + \frac{\tau_B}{2}\mathcal{J}_b\left(1 - e^{-\frac{4}{3}\frac{\mathcal{J}_b}{\mathcal{J}_B} n_B}\right) \tag{3.25}$$

$$= \sigma_{\Sigma\Sigma}(0,0)\, e^{-\frac{2}{3}\frac{\mathcal{J}_a}{\mathcal{J}_A} n_A}\, e^{-\frac{2}{3}\frac{\mathcal{J}_b}{\mathcal{J}_B} n_B}$$

$$+ \sigma_{AA}(0)\left(e^{-\frac{2}{3}\frac{\mathcal{J}_a}{\mathcal{J}_A} n_A} - e^{-\frac{2}{3}\frac{\mathcal{J}_b}{\mathcal{J}_B} n_B}\right) e^{-\frac{2}{3}\frac{\mathcal{J}_a}{\mathcal{J}_A} n_A} + \sigma_{BB}(0)\left(e^{-\frac{2}{3}\frac{\mathcal{J}_b}{\mathcal{J}_B} n_B} - e^{-\frac{2}{3}\frac{\mathcal{J}_a}{\mathcal{J}_A} n_A}\right) e^{-\frac{2}{3}\frac{\mathcal{J}_b}{\mathcal{J}_B} n_B}$$

$$+ \frac{\tau_A}{2}\mathcal{J}_a\left(1 - e^{-\frac{4}{3}\frac{\mathcal{J}_a}{\mathcal{J}_A} n_A}\right) + \frac{\tau_B}{2}\mathcal{J}_b\left(1 - e^{-\frac{4}{3}\frac{\mathcal{J}_b}{\mathcal{J}_B} n_B}\right)$$

If, as before, we assume that the excitation energy is initially equally partitioned between A and B we have that $n_F \sim F$ so that $\mathcal{J}_a n_a/\mathcal{J}_A \simeq \mathcal{J}_b n_b/\mathcal{J}_B$. The factors multiplying $\sigma_{AA}(0)$ and $\sigma_{BB}(0)$ in the last expression above then cancel and, furthermore, the remaining exponents are pairwise identical.

The nuclear temperatures τ_A and τ_B are initially equal and decrease to zero through the cascade. This variation of the temperature has been ignored so far but can be approximately accounted for by replacing the temperature in the final expression by the average temperature through the cascade, $\tau_A, \tau_B \to \frac{2}{3}\tau_1$. We then obtain

$$\sigma_{\Sigma\Sigma} \approx \sigma_{\Sigma\Sigma}(0)\, e^{-\frac{2}{3}\frac{\mathcal{J}_a}{\mathcal{J}_A} n_A}\, e^{-\frac{2}{3}\frac{\mathcal{J}_b}{\mathcal{J}_B} n_B}$$

$$+ \frac{\tau_1}{3}\mathcal{J}_A\left(1 - e^{-\frac{4}{3}\frac{\mathcal{J}_a}{\mathcal{J}_A} n_A}\right) + \frac{\tau_1}{3}\mathcal{J}_B\left(1 - e^{-\frac{4}{3}\frac{\mathcal{J}_b}{\mathcal{J}_B} n_B}\right)$$

$$\approx \sigma_{\Sigma\Sigma}(0)\, e^{-\frac{2}{3}\frac{\mathcal{J}_a}{\mathcal{J}_A} n_A}\, e^{-\frac{2}{3}\frac{\mathcal{J}_b}{\mathcal{J}_B} n_B} \tag{3.26}$$

$$+ \frac{4}{9}\tau_1 \mathcal{J}_a n_a\left(1 - \frac{2}{3}\frac{\mathcal{J}_a}{\mathcal{J}_A} n_A + \ldots\right) + \frac{4}{9}\tau_1 \mathcal{J}_b n_B\left(1 - \frac{2}{3}\frac{\mathcal{J}_b}{\mathcal{J}_B} n_B + \ldots\right)$$

In the last relation we have expanded the exponentials through first order in the small quantity $\frac{2}{3}\frac{\mathcal{J}_f}{\mathcal{J}_F} n_F \ll 1$. This result is practically identical to the result (3.17).

3.3 Relation of spin length to γ-multiplicity

The moments of the γ-multiplicity distribution give a fairly good measure of the moments of the spin distribution for nuclei with mass number larger than approximately 60. Below mass number 60, evaporation of α particles removes too much angular momentum, and this obscures the relation between angular momentum and γ-multiplicity.[15)]

The γ-lifetime is only short enough for multipolarity one and two, so an absolute maximum of the average spin can readily be inferred from the average γ-multiplicity

$$\langle S^A_{n_A}\rangle + \langle S^B_{n_B}\rangle \leq 2\langle M_\gamma\rangle \tag{3.27}$$

Since the γ-multiplicity may vary for different events starting at the same spin in the same nucleus, a similar relation does not exist for the second moments.

Empirically the unresolved γ-rays deexciting nuclei of high spin have been studied in considerable detail. For rotational nuclei, all except approximately three γ-rays are stretched E2 transitions,[16] so for these nuclei one has a firm basis for relating the average γ-multiplicity to the average spin. For other nuclei, the picture is not so clear, but still a lower limit to the proportionality between spin and multiplicity seems to be approximately 1.5 spin units per γ-ray.[17]

In our analysis of γ-multiplicity data we employ the relation between average multiplicity and spin when given in the experimental paper. Otherwise, we shall employ simple relationships in terms of proportionality factors and subtraction of a certain number of statistical γ-rays.

4. Angular correlations

Starting from the density operator for the primary reaction products, and employing the helicity representation for the final states, a general expression can be derived for the angular correlation between the direction of nuclear motion and the emission direction of sequential radiation.[12] This expression can be interpreted in terms of classical distributions of the angular momentum vector in the nuclei. Since so far all theories of damped rections addressing the angular momentum variances consider the angular momentum as a classical quantity, we shall here discuss the classical version of the angular correlation description.

4.1 Distribution function and statistical tensors

For a given energy loss, the normalized distribution of angular momentum $\vec{S}$ in one of the nuclei, as calculated by theory, is denoted by $f(\vec{S})$.

The decay width at a given excitation energy depends on the magnitude S but not the direction $\hat{S}$ of the angular momentum $\vec{S}$. In order to describe the angular properties of the sequential decays, it is useful to define for each magnitude S a normalized distribution function $f_S(\hat{S})$ of the directions $\hat{S}$,

$$f(\vec{S}) = f_0(S)\, f_S(\hat{S})$$
$$\int f_S(\hat{S})\, d\hat{S} = 1 \qquad (4.1)$$

The direction $\hat{S}$ is conveniently expressed in terms of the polar angles (ϑ_S, φ_S), using the reaction normal as the polar direction.

For each S, the associated directional distribution function $f_S(\hat{S})$ is characterized by the statistical tensor components

$$\rho_{\lambda\mu}(S) = \sqrt{\frac{4\pi}{2\lambda+1}}\,\langle Y_{\lambda\mu}\rangle$$
$$= \sqrt{\frac{4\pi}{2\lambda+1}}\int_{-1}^{1} d\cos\vartheta_S \int_0^{2\pi} d\varphi_S\, f_S(\vartheta_S,\varphi_S)\, Y_{\lambda\mu}(\vartheta_S,\varphi_S) \tag{4.2}$$

The reflection symmetry in the reaction plane ensures that $\rho_{\lambda\mu}(S)$ vanishes for odd values of μ.

4.2 Effects of unobserved intermediate decay

The directional distribution $f_S(\hat{S})$, as given by the statistical tensors (4.2), is affected by the unobserved intermediate decay. The angular momenta S_{i-1}, j, S_i, of the i-1'th daughter nucleus, the emitted particle, and the i'th daughter nucleus, determine the size of the angle between S_i and S_{i-1} by

$$\cos(\vartheta_{S_i S_{i-1}}) = \frac{\vec{S}_i \cdot \vec{S}_{i-1}}{S_i S_{i-1}} = \frac{S_i^2 + S_{i-1}^2 - j^2}{2 S_i S_{i-1}} \tag{4.3}$$

For the emission of an unobserved particle, all directions of $\vec{S}_i$ with this angle $\vartheta_{S_i S_{i-1}}$ between $\vec{S}_i$ and $\vec{S}_{i-1}$ are equally probable. Consequently, the angle χ shown on fig. 1 is uniformly distributed. For a definite set of angles $(\vartheta_{S_{i-1}}, \varphi_{S_{i-1}})$ and χ we have

$$Y_{\lambda\mu}(\vartheta_{S_i},\varphi_{S_i}) = \sum_{\mu'} \mathcal{D}^{\lambda}_{\mu\mu'}(-\varphi_{S_{i-1}}, \vartheta_{S_{i-1}}, \varphi_{S_{i-1}})\, Y_{\lambda\mu'}(\vartheta_{S_i S_{i-1}}, \chi) \tag{4.4}$$

Averaging over χ leaves only the terms with $\mu' = 0$. A final averaging over the distribution of directions of $\vec{S}_{i-1}$ described by the statistical tensors $\rho_{\lambda\mu}(S_{i-1})$, yields for the statistical tensors for $\vec{S}_i$:

$$\rho_{\lambda\mu}(S_i) = P_\lambda\left(\frac{\vec{S}_i \cdot \overleftarrow{S}_{i-1}}{S_i S_{i-1}}\right) \rho_{\lambda\mu}(S_{i-1}) \tag{4.5}$$

For an entire unobserved cascade, with angular momenta $S_0, S_1, \ldots, S_n$, this relation can be applied at each step, so we obtain for the final daughter nucleus

$$\rho_{\lambda\mu}(S_n) = \left\langle P_\lambda\left(\frac{\vec{S}_n \cdot \overleftarrow{S}_0}{S_n S_0}\right)\right\rangle \rho_{\lambda\mu}(S_0)$$

$$= \left\langle P_\lambda\left(\frac{\vec{S}_n \cdot \overleftarrow{S}_{n-1}}{S_n S_{n-1}}\right)\right\rangle \left\langle P_\lambda\left(\frac{\vec{S}_{n-1} \cdot \overleftarrow{S}_{n-2}}{S_{n-1} S_{n-2}}\right)\right\rangle \cdots \left\langle P_\lambda\left(\frac{\vec{S}_1 \cdot \overleftarrow{S}_0}{S_1 S_0}\right)\right\rangle \rho_{\lambda\mu}(S_0) \tag{4.6}$$

For a statistical cascade of neutrons, analytic expressions for these factors are derived in Appendix A.

4.3 Expression for the angular correlation

By S_n we denote the angular momentum magnitude of that nucleus which emits the sequential decay product being observed, after n unobserved intermediate emissions.

For a fixed direction and size of $\vec{S}_n$, the angular distribution of the momentum $\vec{p}$ of the sequential decay product is only a function of the angle between $\vec{S}_n$ and $\vec{p}$, and so can be expanded on Legendre polynomials

$$\mathcal{W}(\vartheta_{S_n p}) = \frac{1}{4\pi} \sum_{\lambda} B_\lambda(S_n)\, P_\lambda(\cos\vartheta_{S_n p}) \tag{4.7}$$

The angular distribution coefficients $B_\lambda(S_n)$ are then given by

$$B_\lambda(S_n) = (2\lambda+1)\left\langle P_\lambda\left(\frac{\vec{S}_n \cdot \overleftarrow{p}}{S_n p}\right)\right\rangle \tag{4.8}$$

Here $\frac{\vec{S}_n \cdot \overleftarrow{p}}{S_n p}$ is the helicity of the emitted radiation. For a decay mode conserving parity B_λ is zero for odd λ.[12)]

For a fixed size of S_n the angular correlation of the sequential decay is obtained by folding the basic angular distribution (4.7) with the distribution function f_{S_n} of the directions of $\vec{S}_n$. Denoting by (ϑ,φ) the polar coordinates of the momentum $\vec{p}$ and applying again the relation between spherical harmonics and Legendre polynomials, we obtain

$$\mathcal{W}(\vartheta,\varphi) = \frac{1}{\sqrt{4\pi}} \sum_{\lambda\mu} \frac{B_\lambda(S_n)}{\sqrt{2\lambda+1}}\, \rho_{\lambda\mu}(S_n)\, Y^*_{\lambda\mu}(\vartheta,\varphi) \tag{4.9}$$

In principle, the observed sequential decay can be emitted at any step in a cascade of unobserved particles. By $N_{decay}(S_i)$ and $B_\lambda(S_i)$ we denote the decay probability and angular distribution coefficients along the chain of unobserved intermediate decay. The effective decay probability, $\mathcal{N}_{decay}$, and angular distribution coefficients for the entire cascade, $\mathcal{B}_\lambda$, are then

$$\mathcal{N}_{decay}(S_0) = \sum_{i=0,\dots} N_{decay}(S_i)$$

$$\mathcal{B}_\lambda(S_0) = \sum_{i=0,\dots} B_\lambda(S_i)\left\langle P_\lambda\left(\frac{\vec{S}_i \cdot \overleftarrow{S}_0}{S_i S_0}\right)\right\rangle \frac{N_{decay}(S_i)}{\mathcal{N}_{decay}(S_0)} \tag{4.10}$$

We shall later, in figs. 2 and 3, give examples of these functions.

Summing the angular correlation (4.9) over all angular momenta S of the primary reaction product, and over all decay steps (and keeping only terms with $\lambda = 0,2,4$), we can write the angular correlation as

$$4\pi\, \mathcal{W}(\vartheta,\varphi) = c_0 + c_2 P_2(\cos\vartheta) + c_{22} \sin^2\vartheta \cos 2\varphi$$

$$+ c_4 P_4(\cos\vartheta) + c_{42}(7\cos^2\vartheta - 1)\sin^2\vartheta\cos 2\varphi$$

$$+ c_{44} \sin^4\vartheta \cos 4\varphi \tag{4.11}$$

with the coefficients given by

$$c_0 = \int f(\vec{S})\, \mathcal{N}_{decay}(S)\, d\vec{S}$$

$$c_2 = \int f(\vec{S})\, \mathcal{N}_{decay}(S)\, \mathcal{B}_2(S)\, \frac{3S_Y^2 - S^2}{2S^2}\, d\vec{S}$$

$$c_{22} = \frac{3}{4}\int f(\vec{S})\, \mathcal{N}_{decay}(S)\, \mathcal{B}_2(S)\, \frac{S_Z^2 - S_X^2}{S^2}\, d\vec{S} \tag{4.12}$$

$$c_4 = \int f(\vec{S})\, \mathcal{N}_{decay}(S)\, \mathcal{B}_4(S)\, \frac{35S_Y^4 - 30S_Y^2S^2 + 3S^4}{8S^4}\, d\vec{S}$$

$$c_{42} = \frac{5}{16}\int f(\vec{S})\, \mathcal{N}_{decay}(S)\, \mathcal{B}_4(S)\, \frac{(7S_Y^2 - 1)(S_Z^2 - S_X^2)}{S^4}\, d\vec{S}$$

$$c_{44} = \frac{35}{64}\int f(\vec{S})\, \mathcal{N}_{decay}(S)\, \mathcal{B}_4(S)\, \frac{S_Z^4 + S_X^4 - 6S_Z^2S_X^2}{S^4}\, d\vec{S}$$

We have here employed a standard right-handed coordinate system with the

Y-axis (equal to the reaction normal) as the polar direction and the orientation of the Z-axis determined so as to yield an extremal value of $\langle S_Z^2 \rangle$. This choice ensures that the following moments vanish,

$$\langle S_X S_Z \rangle, \langle S_X S_Y^2 S_Z \rangle, \langle S_X^3 S_Z \rangle, \langle S_X S_Z^3 \rangle = 0 \tag{4.13}$$

for the entire distribution $f(\vec{S})$, as well as for each of the directional distributions $f_S(\hat{S})$.

For γ-decay of multipolarity L, the angular distribution coefficient B_λ vanishes for $\lambda > 2L$, so for multipolarity one and two, which are the only multipolarities of interest for angular correlation studies of damped reactions, the expression (4.11) is exact. For other decays, even fission, where the anisotropy of the angular correlation can be of the order of 20, angular distribution coefficients are generally small for $\lambda > 4$. In an actual application to a very anisotropic case, the expansion up to $\lambda = 4$ only failed for angles close to the polar direction, where the angular correlation has its minimum. Integral quantities of the angular correlation, as for example the dispersion in the polar angle, discussed in section 5, are extremely well determined by the coefficients (4.12) up to $\lambda = 4$.

4.4 Angular correlation parameters for bump region γ-rays

We consider the emission of a γ-ray of multipolarity L, transforming a state with spin magnitude S_0 to a state with spin magnitude S_1 in the same nucleus. For stretched transitions, i.e.

$L = |S_0 - S_1|$, the angular distribution coefficients are independent of S_0.[12] For stretched dipole and quadrupole γ-rays, the angular distribution coefficients are

$$L = 1: \qquad B_2 = \frac{1}{2}, \quad B_4 = 0$$

$$L = 2: \qquad B_2 = -\frac{5}{7}, \quad B_4 = -\frac{2}{7} \tag{4.14}$$

For damped reactions between heavy nuclei with mass numbers above 50 or so, many different nucleides emit γ-rays, and the intensity of any discrete γ-ray of known multipolarity is very weak. Consequently, angular correlation studies of heavy nuclei have been limited to unresolved γ-spectra.

Information about the multipolarity composition of continuum γ-rays has been gained from multi-γ-ray angular correlation studies with compound nuclei formed in fusion reactions. In a careful study,[16] these angular correlation data for many nuclei could to a high accuracy be accounted for by only stretched γ-rays of dipole and quadrupole multipolarity. For given compound reaction and γ-energy interval, only one parameter then need be specified, namely the ratio of stretched quadrupole γ-rays to the total number of γ-rays.

Especially the energy interval between 600 keV and 1200 keV, situated in the so-called rotational bump[4,17] for rotational nuclei in the middle of the rare earth region, has a very high percentage of stretched quadrupole γ-rays, between 90 and 97 percent[17,18]. γ-rays in this energy interval have been used[4] for the study of angular correlations in the collision of ^{165}Ho with ^{165}Ho.

To determine the angular distribution coefficients, we combine the information about the multipolarity composition with other experimental information. The lower limit of 600 keV γ-ray energy corresponds to an angular momentum of 17 $\hbar$, obtained as an average for all isotopes between Tb and Yb and with mass number between 156 and 164. The upper limit of 1200 keV γ-energy corresponds to an angular momentum of 45 $\hbar$, as determined on the basis of continuum spectroscopy.[19] For a feeding above angular momentum 45 $\hbar$, there will then on the average be 14 stretched quadrupole γ-rays within the interval. Considering the high multiplicity for the γ-rays in this interval[17] and the fact that the multiple correlation enhances the upper part of the multiplicity distribution, the average number of quadrupole γ-rays in the energy interval in the multicorrelation experiment will only be slightly lower than 14. With 14 stretched quadrupole γ-rays and purity percentage between 90 and 97, there will be between 0.4 and 1.6 stretched dipole γ-rays.

Except for an insignificant change of the $\mathcal{B}_4$ coefficient, the same angular correlation can be explained by 14 stretched quadrupole γ-rays and in addition 0.8 to 2.9 γ-rays with isotropic angular distribution. Above 2.5 MeV γ-ray energy, statistical γ-rays dominate, and the angular distribution is almost isotropic. For the statistical γ-rays the isotropic angular distribution is expected to arise from a mixture of stretched and unstretched γ-rays. For the lower energy interval we consider here, we also believe that the interpretation in terms of stretched quadrupole transitions and isotropic statistical transitions is the more correct one.

With this information, we can now define the number of decay products and the angular distribution coefficients (4.10) for γ-rays in the energy interval between 600 keV and 1200 keV in the decay of nuclei in the middle of the rare earth region.

Starting at spin magnitude S, let $\langle S_n \rangle$ denote the average spin-magnitude after emission of n neutrons (A.24). The average number of stretched E2 γ-rays within the energy interval between 600 keV and 1200 keV is then:

$$\mathcal{N}_{\gamma E2} = \begin{cases} 14 & \text{for } \langle S_n \rangle \geq 45\hbar \\ \dfrac{\langle S_n \rangle - 17}{2} & \text{for } 17\hbar \leq \langle S_n \rangle < 45\hbar \\ 0 & \text{for } \langle S_n \rangle < 17\hbar \end{cases} \tag{4.15}$$

This result is not rigorously correct since we have ignored the fact that the evaporation chain contributes to the variance of S_n. However, since there is already an appreciable variance in the injection spin magnitude S the committed error is negligible.

To the E2 γ-rays we add a number of isotropic γ-rays, and although there seems to be some increase in the number of statistical γ-rays with increasing angular momentum,[20] we use a constant number, $\mathcal{N}_{stat}$. For the isotropic part of the γ-rays, the angular distribution coefficients are zero. The resulting number of γ-rays within the interval and the corresponding angular distribution coefficients are then

$$\mathcal{N}_\gamma(S) = \mathcal{N}_{\gamma E2}(S) + \mathcal{N}_{stat}$$

$$\mathcal{B}_2(S) = -\frac{5}{7}\cdot\mathcal{N}_{\gamma E2}(S)\cdot\left\langle P_2\left(\frac{\vec{S}\cdot\overleftarrow{S}_n}{SS_n}\right)\right\rangle\cdot\mathcal{N}_\gamma(S)^{-1}$$

$$\mathcal{B}_4(S) = -\frac{2}{7}\cdot\mathcal{N}_{\gamma E2}(S)\cdot\left\langle P_4\left(\frac{\vec{S}\cdot\overleftarrow{S}_n}{SS_n}\right)\right\rangle\cdot\mathcal{N}_\gamma(S)^{-1} \tag{4.16}$$

where $\mathcal{N}_{stat}$ is between 0.8 and 2.9, $\mathcal{N}_{\gamma E2}(S)$ is defined in (4.15) and the average P_2 and P_4, factors are estimated in (A.24).

Figure 2 shows these coefficients as functions of spin magnitude for different excitation energies of ^{165}Ho.

The kinks on the curves in the figure would be smoothed out if one also took into account the evaporation-induced fluctuation in the magnitude of the angular momentum S_n. As mentioned above, for the quite broad primary spin distributions in question, the neglect of this fluctuation is of minor importance.

For large spins the angular distribution coefficients approach the asymptotic values obtained with 14 stretched E2 and 1.2 isotropic γ-rays and no dealignment due to neutrons. With the average spin typically around 35 $\hbar$ (cf. fig. 6), the coefficients are significantly different from these asymptotic values.

4.5 Angular correlation parameters for fission

In the standard theory of nuclear fission it is assumed that the angle between the nuclear symmetry axis, along which the collective separation proceeds, and the total angular momentum remains constant

beyond a certain transition configuration, usually identified with the fission saddle shape. This assumption is motivated by the expectation that the motion from the saddle region to the scission point is fast compared with the relaxation time for the K quantum number determining the tilting angle. The angular distribution of the fission fragments is then directly related to the distribution of saddle configuration orientations. This distribution, in turn, is assumed to be statistical, depending on the nuclear temperature at the saddle. A recent review of fission angular distributions, including a comprehensive analysis of data, is given in ref. [21].

Before proceeding to calculate the angular distribution parameters, we wish to point out certain problems concerning the fission of heavy nuclei which, if solved in some way, may modify our results significantly.

The first such problem concerns the role of the preceding reaction dynamics on the transition stage at which the helicity distribution is frozen out. [We prefer to discuss the angular distribution in terms of the helicity representation because of its generality and the maximal simplicity of the expressions for the angular distribution coefficients in this representation.] For sequential fission of very heavy nuclei following a damped nuclear reaction,[9] the width of the helicity distribution is approximately constant as a function of the nuclear charge all the way up to $Z = 115$, as evidenced by the nearly constant width of the out-of-plane fission fragment angular distribution. [In making such a direct connection between the angular distribution and the helicity distribution we assume that there is only a weak correlation between the mass number and the spin of the nucleus. This assumption is supported by

the fact that the out-of-plane angular distribution is practically independent of the mass of the reaction partner.] On the other hand, for fission of very heavy nuclei formed in fusion reactions,[8] the width of the helicity distribution, as given by K_0 in the standard parametrization, increases significantly with the nuclear charge, although K_0 is smaller than expected from rotating liquid drop estimates of the saddle shape for $K = 0$. Thus, for the heaviest nuclei, the angular distributions indicate that fission after fusion is quite different from fission after a damped reaction.

The second problem concerns the dependence of the saddle shape upon the orientation of the nuclear symmetry axis relative to the angular momentum vector. Until now, one common shape has been used for all values of K, namely the one determined by the rotating liquid drop model with $K = 0$. Generally, this is expected to underestimate the elongation of the saddle shape since a finite value of K will reduce the centrifugal force acting on the rotating nucleus.

The third problem concerns the calculation of the probability for fission relative to neutron evaporation. This quantity is determined by the ratio of level densities associated with the respective transition configurations (namely the fission saddle shape and the residual daughter nucleus with a neutron at the barrier).

It is not clear which degrees of freedom should be treated explicitly in the two decay modes, apart from the disintegration coordinate itself.[22] In the traditional approach, the two coordinates perpendicular to the disintegration coordinate for the free motion of the neutron at the barrier are treated explicitly whereas for fission only the

disintegration coordinate is considered. This leaves open the question which other degrees of freedom require different treatments in the two cases. In our calculations we shall take a Fermi gas level density of the same form for both the residual nucleus after neutron emission and for the fission saddle shape. This assumes that degrees of freedom not treated explicitly, such as for example collective vibrations, will give the same enhancement factors on the level densities for the (quite different) transition shapes associated with either fission or neutron emission.

4.5.1 Angular distribution coefficients for specified E and S

With an orientation-independent, axially symmetric saddle shape the distribution of helicities, in this case the distribution of K quantum numbers, will at medium and high excitation energies be gaussian-like:

$$\mathcal{P}(K) \propto \exp\left(-\frac{K^2}{2K_0^2}\right) \tag{4.17}$$

with K_0 given by

$$K_0^2 = \frac{\mathcal{J}_{eff}\,T}{\hbar^2}\,, \qquad \frac{1}{\mathcal{J}_{eff}} = \frac{1}{\mathcal{J}_{\parallel}^{(f)}} - \frac{1}{\mathcal{J}_{\perp}^{(f)}} \tag{4.18}$$

Here τ is the excitation temperature and $\mathcal{J}_{\parallel}^{(f)}$ and $\mathcal{J}_{\perp}^{(f)}$ the parallel and perpendicular moments of inertia of the fission saddle shape, respectively. For a given spin, the classical angular distribution coefficients (4.8) are given by

$$B_\lambda(S) = (2\lambda+1)\left\langle P_\lambda\left(\frac{K}{S}\right)\right\rangle \tag{4.19}$$

so, for example, $B_2(S) = 5(3\langle K^2\rangle - S^2)/2S^2$, where the average of K^2 is with respect to the distribution (4.17) with K within the interval between $-S$ and S.

4.5.2 Competition between fission and neutron evaporation

The fission of a highly excited heavy nucleus competes with light particle emission. Often this competition is important not only for the primary reaction product but also at later stages after emission of one or more neutrons. In a given nucleus with a definite spin S and excitation E, the ratio between the two decay widths is approximately given by the ratio of the level densities for the respective transition states,

$$\frac{\Gamma_n}{\Gamma_f} \approx \frac{\rho_n(E - B_n, S)}{\rho_f(E - B_f, S)} \quad \frac{2mR_n^2}{\hbar^2}\,\tau_n \tag{4.20}$$

Here ρ_f is the level density of the fission saddle configuration which has a barrier height equal to B_f, and ρ_n is the level density in the neutron evaporation daughter nucleus with B_n being the neutron separation energy. The effective barrier radius for the neutron is R_n and the temperature in the daughter nucleus is τ_n. The last factor is the contribution to the level density from the emitted neutron and its precise form depends on how the neutron's translational degrees of freedom are treated.

For the cases of present interest, Γ_n/Γ_f is of the order of unity so that delayed fission must be taken into account. In order to do that, we expand the level densities in (4.20) using the same nuclear temperature τ, which is a good approximation.

Including enhancements of the level density corresponding to an axially symmetric prolate shape,[23] and integrating over the K quantum number, we obtain

$$\frac{\Gamma_n}{\Gamma_f} \approx \sqrt{\frac{\mathcal{J}_\perp^{(n)}\,\mathcal{J}_\parallel^{(n)}}{\mathcal{J}_\perp^{(n)} - \mathcal{J}_\parallel^{(n)}}}\ \mathrm{erf}\left(\sqrt{\frac{\mathcal{J}_\perp^{(n)} - \mathcal{J}_\parallel^{(n)}}{2\tau\,\mathcal{J}_\perp^{(n)}\,\mathcal{J}_\parallel^{(n)}}}\ (S+\tfrac{1}{2})\right)$$

$$\times \left\{\sqrt{\frac{\mathcal{J}_\perp^{(f)}\,\mathcal{J}_\parallel^{(f)}}{\mathcal{J}_\perp^{f} - \mathcal{J}_\parallel^{f}}}\ \mathrm{erf}\left(\sqrt{\frac{\mathcal{J}_\perp^{(f)} - \mathcal{J}_\parallel^{(f)}}{2\tau\,\mathcal{J}_\perp^{(f)}\,\mathcal{J}_\parallel^{(f)}}}\ (S+\tfrac{1}{2})\right)\right\}^{-1}$$

$$\times \exp\left(\frac{B_f - B_n}{\tau} - \frac{S^2}{2\tau\,\mathcal{J}_e} + (a_n - a_f)\tau\right)\frac{2mR_n^2}{\hbar^2}\,\tau \tag{4.21}$$

Here a_n and a_f are the level density parameters for the daughter nucleus after neutron emission, and for the fission, respectively, and $\mathcal{J}_e = \mathcal{J}_\perp^{(f)}\mathcal{J}_\perp^{(n)}/(\mathcal{J}_\perp^{(f)} - \mathcal{J}_\perp^{(n)})$ is the effective moment of inertia for the neutron-to-fission competition. The perpendicular and parallel moments of inertia of the neutron emitting shape and of the fission shape are denoted $\mathcal{J}_\perp^{(n)}, \mathcal{J}_\parallel^{(n)}$ and $\mathcal{J}_\perp^{(f)}, \mathcal{J}_\parallel^{(f)}$, respectively. The neutron emitting shape is probably not much deformed, so, although this is not correct for the highest spins and lowest temperatures, we insert the limit of small arguments for the error function containing the neutron quantities to obtain:

$$\frac{\Gamma_n}{\Gamma_f} \approx \frac{2S+1}{\sqrt{2\pi}\,K_0}\,\mathrm{erf}\left(\frac{S+\frac{1}{2}}{\sqrt{2}\,K_0}\right)^{-1}\frac{2mR_n^2}{\hbar^2}\exp\left(\frac{B_f-B_n}{T}-\frac{S^2}{2\mathcal{J}_e T}+(a_n-a_f)T\right) \tag{4.22}$$

The most probable shape of the neutron emitting state will be oblate rather than prolate, but for the limiting case of small deformations, (4.22) is valid for both prolate and oblate deformations.

For small excitation energies it may be very crude to apply expressions for the level density not taking into account the shell structure of individual nuclei, but for the higher excitation energies and larger angular momenta we are interested in here it is well justified. The barrier heights and separation energies are then regarded as smooth quantities, derived from a macroscopic nuclear model (for example the liquid drop model), neglecting shell correction energies and odd-even mass differences.

The above result (4.20) can be used to follow the fission probability through an entire neutron cascade. Experimental evidence for fission in the later decay steps comes from lifetime measurements and detailed calculations have reproduced the observed fraction of slow fission.[24)]

4.5.3 Total fission probability and effective distribution coefficients

In the present study we shall content ourselves with a more schematic calculation of the total fission probability and the effective angular distribution coefficients associated with an entire neutron cascade.

Let $N_f^{(i)}$ be the probability that the nucleus fissions at the i'th stage in the cascade. We then have the equation

$$N_f^{(i)} = \frac{\Gamma_f(E_{i-1}, S_{i-1})}{\Gamma_f(E_{i-1}, S_{i-1}) + \Gamma_n(E_{i-1}, S_{i-1})} \left[1 - \sum_{j=1}^{i-1} N_f^{(j)} \right] \tag{4.23}$$

which can be solved iteratively to yield $N_f^{(i)}$.

In this calculation, the values of the excitation energy E_i^* and the angular momentum S_i along the decay chain are chosen randomly according to the statistical decay probabilities, given the approximations (A.7) and (A.8) to level densities and transmission coefficients. The fission probability and the angular distribution coefficients, taking into account the dealignment factors (A.20), are first calculated individually for each randomly selected decay chain, and finally averaged to obtain the quantities for the entire cascade.

A brief description of the calculated procedure is given in Appendix B together with a discussion of how important delayed fission is for the calculated quantities. Appendix B also contains a comparison between our calculations and the more detailed calculations of ref.[24] for the fission of ^{198}Pb, as well as a comparison of calculated angular distribution coefficients to data from the fission of compound nuclei formed in fusion reactions. The comparison shows that our calculation gives a reasonably good reproduction of the more refined calculation, and of data.

4.5.4 Fission parameters for nuclei in the vicinity of ^{208}Pb

The results for the fission probability depend sensitively on the fission barriers and neutron decay energies. In table 1 we show three different parameter sets derived from different prescriptions for the nucleus ^{208}Po. In fig. 3 is shown the fission probabilities and angular distribution coefficients following from the different prescriptions.

With the liquid drop model and the Lysekil parameters, the fission barrier rapidly decreases as the neutrons are evaporated and the fissility parameter x thus increases. Given enough excitation energy, all nuclei will then eventually fission, and the fission will occur after the evaporation of quite many neutrons. On the other hand, the droplet values for the parameters display a weak tendency in the opposite direction. For the highest excitation energy applied in fig. 3, there is therefore a very pronounced difference between the fission probabilities calculated with the two different parameter sets. The lower temperatures encountered at the later decay steps lead to larger values of the angular distribution coefficients, but those are, on the other hand, being counterbalanced to some extent by the dealignment accumulated during the preceding decay steps. So, although fission on the average occurs later in the decay for the liquid drop model and with the parameters from the folded Yukawa than for the droplet parameters the angular distribution coefficients are quite similar.

We shall apply the liquid drop model with the Lysekil parameters for our comparisons of fission probabilities and correlations to data in Section 5.

5. Comparison with data

In this section we compare calculated spin magnitude moments and angular correlations with experimental data on sequential decay. The calculated quantities are obtained by combining our theoretical primary spin distributions of nuclei leaving the reaction with the description of the sequential decay.

In some experiments, all scattering angles are covered, and our comparison is formally correct. For other experiments, only a certain range of scattering angles are investigated, and the spin distribution will be biased by the limitation to a particular interval of scattering angle. Some experimental results, however, indicate that this is not a strong bias. Furthermore, for the strongly focussed reactions which we are mostly concerned with, the angular range is often wide enough to encompass most of the distribution for the smaller energy losses. At present, we cannot include a scattering angle bias in our theoretical treatment, because we do not include any coupling between the size of the transport coefficients and the deviation of a given trajectory from the mean trajectory.

5.1 Mean value and variance of γ-multiplicity

5.1.a The reaction Kr + Sm

The most complete γ- multiplicity data exist for the collision of $^{86}Kr + ^{154}Sm$ at the two bombarding energies 490 MeV and 610 MeV.[2] The data are shown in fig. 4 together with our calculation of the mean values and variances of the spin. For the mean values we integrate over the distribution, using the full relations (A.24) for the neutron decay. For the variances we employ the approximate relations (3.5) and (3.8), modified by the neutron decay as in (3.17). For the highest TKEL, the relation (3.1) is

not fulfilled, and for TKEL > 80 MeV and 140 MeV for the two bombarding energies we just show the calculated values at TKEL = 80 MeV and 140 MeV, respectively.

For the small TKEL, the calculated mean value of the spin is rising too steeply by a factor of two, relative to the experimental results. For the higher TKEL, the experimental values reach a maximum and then stay almost constant, showing a very weak decrease towards the highest TKEL. The theoretical results reproduce these features and the maximum has approximately the correct size, but is reached at a too small TKEL, and the decrease for the highest TKEL is too pronounced.

The variances are in good agreement with the data. About 20 percent of the calculated variance is due to the correlation between the spins in the nuclei, especially the appreciable positive covariance σ_{YY}^{AB} along the reaction normal. The presence of this correlation explains in a natural way the rather large variance of the sum of spin magnitudes seen in the γ-multiplicity data.

5.1.b The reaction Ho + Ho

The mean γ-multiplicity has been measured as a function of TKEL for the reaction of 1400 MeV ^{165}Ho with ^{165}Ho, which we used as the example to illustrate the angular momentum transport in I (see figs. 2-3, 6-8 and 12-14 of I). The comparison between experimental and theoretical results for the spin magnitude after neutron decay is shown in fig. 5. The experimental result shows qualitatively the same behavior as for the reaction of ^{86}Kr with ^{154}Sm, except that the decrease toward the highest TKEL is significantly present for the Ho + Ho reaction. The calculated results deviate in the comparison with experiments for the lowest and highest TKEL in the same way as for the Kr + Sm reaction.

5.2 Angular correlation of bump-region γ-rays

The most detailed experiment on γ-ray angular correlations in coincidence with nuclei from damped nuclear reactions for sufficiently heavy systems has been performed for the $^{165}Ho + ^{165}Ho$ reaction.[4] Using the mean values and variances shown in I, figs. 12 and 14 and employing the angular distribution coefficients given in the equations (4.16), we arrive at the result shown in the lower part of fig. 5 for the out-of-plane anistropy as a function of TKEL.

Before discussing the dependence of the angular correlation on the polar angle ϑ (the out-of-plane angle), where there is a significant variation, we briefly discuss the dependence upon the azimuthal angle φ (the in-plane angle). For $\vartheta = 90^\circ$ (i.e. in the reaction plane), the variation of the experimental angular correlation as a function of φ is less than 10 percent. Although our calculated spin variances show a considerable asymmetry between the two in-plane directions, the angular distribution coefficients of stretched E2 γ-rays have such values that the two terms c_{22} and c_{42} of the angular correlation (4.11) almost cancel each other for $\vartheta = 90^\circ$. In the reaction plane our calculated angular correlation thus only has an anisotropy of less than 2 percent. Going to polar angles around $\vartheta \approx 45^\circ$, the two terms interfere constructively, and we have a 10 percent variation of the angular correlation as a function of azimuthal angle φ for TKEL = 150 MeV, dropping to around 4 percent when going to smaller or to larger TKEL. Generally in experiments on the angular correlation of stretched E2 γ-rays, the variation with azimuthal angle φ for the fixed polar angle $\vartheta \approx 45^\circ$ is expected to give the most sensitive information about the in-plane asymmetry of the spin variances.

The calculated out-of-plane anisotropies overshoot the experimental ones significantly. To produce a smaller anisotropy, the spin distribution has to be less aligned with the reaction normal. This can be achieved either by decreasing the size of the average spin vector or by increasing the in-plane variances, or both. Before reaching conclusions we shall obtain a more complete picture by considering also fission data.

5.3 Angular correlation of sequential fission

5.3.a The reactions Pb + Ni and Pb + Zn

Figure 6 shows the average and the dispersion of the magnitude of the angular momentum, together with the alignment and other tensor components of rank two and four, as calculated with our version of the Nucleon Exchange Transport Model for the reactions of ^{208}Pb at 7.5 MeV per nucleon with targets of ^{58}Ni and ^{90}Zr. The fourth order alignment is defined as

$$P_{YYYY} = \langle P_4(\hat{S}) \rangle = \left\langle \frac{35 S_Y^4 - 30 S^2 S_Y^2 + 3 S^4}{8 S^4} \right\rangle \qquad (5.1)$$

(in the classical limit). The angular correlation between the outgoing target-like fragments and fission fragments from the sequential fission of the lead-like nuclei has been measured by von Harrach et al.,[7] and the inverse reaction for the case of ^{58}Ni on ^{208}Pb at the same center-of-mass energy has been measured by Steckmeyer et al.[29] In fig. 7 we show the results by von Harrach et al. for the dispersion in the polar angle and the fission probability as functions of the total kinetic energy loss. By using angular distribution coefficients and fission probabilities equivalent to the ones shown in fig. 3, combined with our calculated spin distributions in the lead-like nuclei, we arrive at the results shown in fig. 7 for the dispersion

in the polar angle and for the fission probability. (In the calculation, the dissipated energy is divided between the reaction products in proportion to their mass.) With increasing TKEL, the charge and mass of the reaction products change. The different curves labelled a, b and c show calculations performed with the average value for the mass and charge as obtained with our model for different kinetic energy losses. Curve a corresponds to TKEL = 0, curve b to TKEL in the middle of the interval, and curve c corresponds to the highest calculated energy losses.

With the angular correlation written in the form (4.11) the variance in the polar angle is given by:

$$\sigma_\vartheta^2 \equiv \int (\vartheta - \tfrac{\pi}{2})^2 \, W(\vartheta,\varphi) \sin\vartheta \, d\vartheta \, d\varphi = \frac{\pi^2}{4} - 2 + \frac{2}{9}\frac{C_2}{C_0} + \frac{8}{225}\frac{C_4}{C_0} + \ldots \quad (5.2)$$

Since $(\vartheta - \frac{\pi}{2})^2$ is a smooth function of angle, it is well described by the expansion coefficients for the second and fourth Legendre polynomials. The coefficient for the 6'th order term will be around 0.01.

As shown in ref. [13], applying the absolute limitations to the $\mathcal{B}_2$ angular distribution coefficient makes it possible to derive an absolute lower limit to the alignment of the nuclei emitting the sequential decay product observed:

$$\langle P_{YY} \rangle_{decay} > -\frac{9}{5}\left(\sigma_\vartheta^2 - \frac{\pi^2}{4} + 2\right) \quad (5.3)$$

For TKEL above 140 MeV for the nickel collision and above 200 MeV for the zirconium collision, more than 90 percent of the heavy nuclei fission, and the relation (5.3) applies to the entire spin distribution to a good accuracy. The absolute limits derived on the basis of the polar angle dispersions are shown in fig. 6.

Following the full drawn parts of the curves a, b and c on fig. 7 within the intervals of TKEL where they should apply, we see that there is an interval around TKEL = 80 MeV for the nickel case and around TKEL = 110 MeV for the zirconium case, where we have a good agreement with the data. For the smaller TKEL, the statistics of the data is not so good, while for the larger TKEL there is a clear discrepancy between calculation and experiment.

5.3.b The reactions U + Ni and U + Zr.

Following the same procedure, we arrive at the results shown in figs. 8 and 9, equivalent to figs. 6 and 7, but now with ^{238}U as the heavy projectile. The uranium-like nuclei have larger fission probabilities and the saddle shapes are more compact than for the case of the lead-like nuclei. The dispersion in the polar angle is thus much larger in fig. 9 than in fig. 7. Our calculations show reasonable agreement with the data for TKEL smaller than 70 MeV for the nickel collisions and for TKEL smaller than 120 MeV for the zirconium collisions. For the higher TKEL, the calculated polar angle dispersion is far too large. With the present treatment of the sequential fission, a significant increase of the average spin vector is required to obtain agreement with the data for the highest TKEL. (However, see the further discussion in section 5.5.)

5.3.c In-plane angular correlation for the reactions Kr + Bi and Kr + U

The first experiment on sequential fission was performed by Vandenbosch *et al.* for the reaction of ^{86}Kr with ^{209}Bi, and then later with ^{238}U as the target.[6] These data are in good agreement with the results by von Harrach *et al*[7,9] concerning the variation of the angular correlation with the polar angle. Our comparison to the polar angle variance in figs. 7

and 9 thus addresses both sets of data, and, besides, a calculation of the angular correlation itself close to the pole will require terms beyond the 4'th order in (4.11), since the main 0'th, 2'nd and 4'th order terms tend to cancel each other.

The data sets are, however, in mutual disagreement concerning the dependence of the angular correlation with respect to the azimuthal angle. The Kr + Bi and Kr + U data show an appreciable in-plane anisotropy, up to a factor of two, whereas the Pb + Zr and U + Zr data display less than a 20 percent variation. For directions close to the reaction plane, $\vartheta \approx 90°$, the leading terms of the angular correlation (4.11) add up, and we only introduce a minor error by terminating at the 4'th order.

Figure 10 shows the experimental and calculated in-plane angular correlation for three different kinetic energy losses for each of the two reactions Kr + Bi and Kr + U. The data are summed over intervals of TKEL, and we calculate the angular correlation at the average TKEL in each case, except for the lowest TKEL, where we use the centroid of the interval, TKEL = 20 MeV instead of the average TKEL = 13 MeV, since both our model for the nucleon transfer and our description of sequential fission are not expected to be realistic at such low TKEL. For each TKEL we apply fission parameters for the average mass and charge of the heavy nucleus as calculated in the model. The data are taken for fixed detector positions, and this introduces a bias on the spin distribution relative to the spin distribution for fixed TKEL only and this additional bias we cannot take into account in the calculations. We have not included a fourth data set at the very highest TKEL in our comparison because of this bias, whereas the bias is less severe for the lower energy losses, where the reaction is quite focussed in scattering angle.

Our calculation agrees well with the experiment on the position of the maximum and minimum of the in-plane angular correlation, along the minor and major principal axes of the spin variance tensor, respectively. Only for TKEL = 170 MeV in the Kr + Bi reaction do we get a discrepancy here, but this TKEL is in our calculation located at the upper edge of the energy loss distribution and is not focussed in scattering angle, so the discrepancy is not so serious. The amplitude of the calculated variation is too small relative to the data by a factor of two.

5.4 Discussion

5.4.a Information on the spin moments from the combined data

In fig. 11 we show, as functions of the energy loss relative to the maximum energy loss for each reaction, the most important characteristics of the spin distribution in the heavy reaction partner for some of the collisions we are studying. The figure displays a strong similarity between the different spin distributions, although the basic parameters determining the dynamical evolution, such as for example the grazing orbital angular momentum in the reaction, the relaxation times, and the moments of inertia, do not scale in a simple way between the different collisions. The similarity of our results allows us to give a general discussion of the discrepancies between calculations and experiment, as functions of TKEL. One should be aware, though, that actual spin distributions may be more diverse, depending upon the specific reaction. Since the comparison to different kinds of data will lead to opposing conclusions in some cases, we must evaluate which kind of data has the most significance.

For small TKEL, the fission data with ^{238}U as a projectile are well reproduced by the calculation, whereas the γ-multiplicity data, on the other hand, indicate that the calculated average spin vector is too large. A

substantial part of this conflict between the two types of data may be due to the excitation energy ascribed to the heavy nucleus being too large. A more equal division of the dissipated energy (than in proportion to the mass) would leave the γ-multiplicity results almost unaffected, whereas the resulting lower temperature in the fissioning nucleus would reduce the width of the K distribution thus resulting in a smaller polar angle dispersion. Since the γ-multiplicity data give the more direct information, our conclusion for this interval of TKEL is based upon these data.

For medium TKEL all data sets are in agreement with our calculation, except for the angular correlation of bump region γ-rays. This may be due to the lack of precise knowledge of the structure of the γ-rays, with respect to the multipolarity and the average amount of angular momentum removed by each γ-ray. With increasing TKEL, the mass width becomes larger, and the nuclei emit more neutrons. Consequently, an increasing number of the γ-emitting nuclei will not have good bump spectra. Experiments utilizing known discrete γ-ray lines in damped nuclear reaction studies will be very valuable to check the continuum γ-ray data.

For the largest TKEL, the comparison to all data sets, except for the angular correlation of bump region γ-rays, indicate that the average spin vector decreases too much in the calculation. Again, we disregard the continuum γ-data because of the above mentioned difficulty.

Since our calculated spin distributions are dominated by the average spin vector, it is natural to point to this quantity as the source of the most pronounced discrepancies, as we are doing here. Indeed, it is not possible to turn the conclusions around, postulating that the average spin vector is in accordance with data and that the variances are the sources of the discrepancies. For small TKEL, the calculated average spin vector alone will

result in too large average γ-multiplicities, even with zero variances. For the largest TKEL, agreement with the γ-multiplicity data may be achieved by increasing the variances, especially the in-plane variances (cf. eq. (3.3)), but this would worsen the comparison to the fission data. Ascribing the disagreement at the largest TKEL to a too small value of the average spin vector, as we do, gives the right direction for both kinds of experiments.

Turning now to the spin variances, the variance along the reaction normal (the Y-axis) is rather directly related to the spin magnitude variance which in turn is related to the second moment of the γ-multiplicity distribution, and this quantity is well reproduced by our calculations.

The in-plane variances enter the results in two ways:

(i) The difference between the two principal in-plane variances, quantitatively expressed through the asymmetry P_{XZ} (2.7), is directly tested through the azimuthal angle variation of the angular correlations. The calculated directions of the principal axes of the in-plane covariance tensor are well in accordance with the data, and the calculated asymmetry is too small according to one data set and too high according to the other.

(ii) The two in-plane variances combine to give alignments and fourth order alignments smaller than the maximal value of 1. The alignment is the main quantity controlling the out-of-plane correlation, but the alignment is always multiplied by the second-order angular distribution coefficient, which is a function of the magnitude of the angular momentum. The average γ-multiplicity and the fission probaility give us a handle on the size of the angular momentum, and for medium TKEL the agreement of all data sets (except for the bump region continuum γ-ray angular correlation) supports the calculated values of the sum of in-plane spin variances.

5.4.b Sensitivity of results to the neck dynamics

Throughout the present study we have employed the standard implementation of the model, as described in detail in App. A of ref. [30]. In order to assess the significance of the disagreement with the data it is of interest to study the sensitivity of the central results to certain less well-founded details of the implementation. They all concern aspects of the neck dynamics about which we have little direct evidence.

In the standard version of the model, it is assumed that the neck contains nuclear matter at normal density ρ_0. Of course, it might well be that the density in the interaction zone is somewhat below normal. We have therefore made calculations with the (probably extreme) assumption that the neck density is only $\frac{1}{2}\rho_0$. This change reduces the Fermi momentum of the nucleons being transferred and thus inhibits their dissipative efficiency. The result of this modification is shown as the thin line on fig. 12. However, since the energy dissipation and the angular momentum transfer are both affected, the resulting effect is only moderate. As regards the rise of the spin magnitude with TKEL, there is about a 20 percent decrease, which is in the direction of the data but far short of the 50 percent reduction needed for agreement. It should be noted, though, that this change in S versus TKEL is produced without any noticable change in the NZ-distribution, so that the good agreement with the aspect of the data is not affected.

The second type of modificaton explored concerns the damping of the neck. In the standard implementation, the transfer of nucleons takes place partly though a (fully open) cylindrical neck of radius c and partly across the gap between the two juxtaposed nuclear surfaces outside the cylinder. Therefore one may introduce an effective neck radius c_{eff} which is the radius of that slightly larger uniform cylinder which would allow the same

total nucleon current. During the early approach phase, the cylinder radius is zero but c_{eff} is not. Since the overall form factor for nucleon transfer is governed by c_{eff} rather than c it may be more appropriate to use $\dot{c}_{eff}$ in the energy dissipation rate. This can be accomplished through suitable technical modifications. The main effect is an effective increase in the radial dissipation rate. In consequence, the two nulceides will not approach as closely and the form factor will remain smaller. Althogh the evolution of the nuclear shape, as given by $R(t)$ and $c(t)$, will thus be noticeably different, the resulting effect on the various observables as functions of TKEL will be only minor. For example, both σ_A^2 and S will decrease by about 10 percent for a given value of TKEL.

The third type of modification examined concerns the damping of the neck towards the end of the reaction. As argued in ref. [30], one would generally expect the one-body wall dissipation to be reduced for long narrow necks. Therefore, a reduction factor, $\exp(-d/(c + b))$, was introduced in the neck dissipation rate. (Here d is the neck length, c the neck radius, and $b = 1$ fm the nuclear surface diffuseness.) In order to explore the sensitivity to this somewhat arbitrary element in the model, we have made calcuations without the reduction factor. The neck then grows longer before rupture occurs, resulting in a somewhat larger energy loss for a given number of transferred nucleons. In order to get an impression of the maximum effect of such modifications we consider the results of making both the second and the third modification in the same calculation. The effect is then around 30 percent on the mass dispersion and around 50 percent on the mean spin magnitude. The effect on the spin magnitude is just what is needed to bring agreement with the data (cf. fig. 2) but at the same time the good agreement for the NZ-distribution is spoiled.

We thus find that while various modifications of the more uncertain details in the implementation of the model can produce substantial effects in some of the observables, no combination of the modifications considered appears able to achieve a substantial reduction in the slope of S versus TKEL without at the same time significantly affecting the behavior of the NZ-distribution. In view of this finding we consider the discrepancy in S versus TKEL to have some significance.

5.5 Prescession determined angular correlation for fission

For the angular correlation of fission fragments, the discrepancy between calculation and experiment is very pronounced for the largest TKEL, and it would require a much larger adjustment of the average spin vector to obtain agreement with these data points than with the γ-multiplicity data.

Part of this problem may be that the fission of the heaviest nuclei following damped nuclear reactions is not a truly sequential process, since the time scale associated with a full equilibration of the nuclear orientation may be comparable to a typical fission life time. In order to examine this possibility, we explore below an idealized situtaion in which the fission angular distribution is determined by the prescession of the fission precusor around its spin vector.

When the two nuclear fragments lose contact at the end of the damped reaction, the heavy nucleide is likely to be deformed with its largest principal axis lying close to the reaction plane. [The occurrence of large deformations at the scission stage is indicated by calculations within the TDHF and the Coherent Surface Excitation models which both include the deformation degrees of freedom. However, so far no calculation has been made to study the out-of-plane orientation of the fragments at scission so our

assumption that the major axis lies near the reaction plane is guided by intuition.] After scission this deformed fragment will start precessing around its angular momentum vector. At the same time, its intrinsic excitations will couple to its orientation, and the distribution in orientations relative to the spin vector will tend to relax towards the standard statistical distribution. In analogy to what happens during the reaction phase, the diffusion in orientation is accompanied by the excitation of the tilting mode in the deformed fragment. If the time for fission is shorter than the tilting relaxation time, but on the other hand larger than the time for a full prescession revolution, each orientation on the prescession circles described by the poles of the deformed shape will become an equally probable emission direction for the fission fragments. Denoting by ϑ_S the angle between the reaction normal and the spin vector, the angle between the spin vector and the emission direction of fission fragments will be either $\pi/2 - \vartheta_S$ or $\pi/2 + \vartheta_S$. Expanded on Legendre polynomials, the angular distribution of the momentum $\vec{p}$ of the fission fragments will depend upon ϑ_S and is

$$4\pi\, W(\vartheta_{Sp}) = \sum_{\text{even}\,\lambda} (2\lambda+1)\, P_\lambda(\sin\vartheta_S)\, P_\lambda(\cos\vartheta_{Sp}) \tag{5.4}$$

Applying the addition theorem for the spherical harmonics, the angular correlation for an entire distribution of magnitudes and orientations of the spin can be written

$$4\pi\, W(\vartheta,\varphi) = \sum_{\text{even}\,\lambda\mu} c_{\lambda\mu}\, Y^*_{\lambda\mu}(\vartheta,\varphi) \tag{5.5}$$

and the expansion coefficients are

$$c_{\lambda\mu} = \int f(\vec{S})\, \mathcal{N}_{fission}(S)\, Y_{\lambda\mu}(\vartheta_S, \varphi_S)\, P_\lambda(\sin\vartheta_S)\, d\vec{S} \qquad (5.6)$$

Evaluating the terms, as it was done for the standard case (4.11-12), we obtain for the second-order Legendre term:

$$\frac{c_2}{c_0} = -1 + \frac{15}{14}\langle P_{YY}\rangle_{fission} - \frac{18}{7}\langle P_{YYYY}\rangle_{fission} \qquad (5.7)$$

where the subscript indicates the restriction to the part of the distribution undergoing fission. Cutting off at the 4'th order term, the variance in the out-of-plane angle is

$$\sigma_\vartheta^2 = 0.2807 + 0.2081\langle P_{YY}\rangle_{fission} - 0.5222\langle P_{YYYY}\rangle_{fission} \qquad (5.8)$$

The cut-off at the 4'th order term is less justified in this case than for the standard fission decay, but still this expression is expected to be accurate within a few percent for our calculated spin distributions.

To illustrate the angular correlations resulting from this picture, we show (by crosses) on fig. 9 the polar angle dispersions calculated on the basis of expression (5.8) for the U + Zr reaction. For the largest TKEL,

where the present picture is expected to be most relevant, the prescession determined angular correlation is in better agreement with the data. The remaining discrepancy in the polar angle dispersion at high TKEL may be remedied by increasing the aligned spin component; such a modification would also improve the agreement with the γ-multiplicity data, as discussed earlier.

The prescession angular correlation picture outlined here will also be able in part to resolve the discrepancy (mentioned in section 4) between the fission data for fused compound nuclei and nuclei having undergone damped nuclear reactions. In the present context we have found it sufficient to just sketch the main idea of this picture; a proper treatment would require not only a refined treatment of the reaction dynamics, so that the orientations of the deformed fragments can be better ascertained, but also a careful consideration of the fission dynamics, so that the relevant time scales can be estimated.

6. Correlated fission angular distributions

In this chapter we derive simple approximate expressions for the correlated angular distributions of fission fragments from the damped reaction products.

6.2 Definitions

The normalized correlated spin distribution for the spins $\vec{S}^A$ and $\vec{S}^B$ of the two reaction products A and B is given by $f_{AB}(\vec{S}^A,\vec{S}^B)$ with $\int d\vec{S}^A \int d\vec{S}^B f_{AB}(\vec{S}^A,\vec{S}^B) = 1$. The normalized spin distributions for the nuclei separately are given by

$$f_A(\vec{S}^A) = \int d\vec{S}^B \, f_{AB}(\vec{S}^A, \vec{S}^B)$$
$$f_B(\vec{S}^B) = \int d\vec{S}^A \, f_{AB}(\vec{S}^A, \vec{S}^B) \tag{6.1}$$

We now assume that the reaction products A and B may undergo fission after their mutual interaction has ceased. Let the corresponding probabilities be given by $P_A(\vec{\alpha},\vec{S}^A)$ and $P_B(\vec{\beta},\vec{S}^B)$ where $\vec{S}^A$ and $\vec{S}^B$ are the spins of the fissioning nuclei and $\vec{\alpha}$ and $\vec{\beta}$ are unit vectors indicating the fission directions, as seen in the respective CM frames of the fissioning nuclei. Taking into account the distribution of spins in the fissioning nuclei, we find for the corresponding angular distributions of fission products

$$P_A(\vec{\alpha}) = \int d\vec{S}^A \, f_A(\vec{S}^A) \, P_A(\vec{\alpha}, \vec{S}^A)$$
$$P_B(\vec{\beta}) = \int d\vec{S}^B \, f_B(\vec{S}^B) \, P_B(\vec{\beta}, \vec{S}^B) \tag{6.2}$$

respectively. The joint probability for A fissioning in the direction $\vec{\alpha}$ and B fissioning in the direction $\vec{\beta}$ is

$$P_{AB}(\vec{\alpha},\vec{\beta}) = \int d\vec{S}_A \int d\vec{S}^B \, f_{AB}(\vec{S}^A, \vec{S}^B)\, P_A(\vec{\alpha}, \vec{S}^A)\, P_B(\vec{\beta}, \vec{S}^B) \quad (6.3)$$

Since the two nuclear spins are correlated, the detection of a fission product from one of the nuclei introduces a bias on the spin distribution of the other. These biased spin distributions are given by

$$\begin{aligned} \tilde{f}_A(\vec{S}^A;\vec{\beta}) &= \int d\vec{S}^B \, f_{AB}(\vec{S}^A, \vec{S}^B)\, P_B(\vec{\beta}, \vec{S}^B)/P_B(\vec{\beta}) \\ \tilde{f}_B(\vec{S}^B;\vec{\alpha}) &= \int d\vec{S}^A \, f_{AB}(\vec{S}^A, \vec{S}^B)\, P_A(\vec{\alpha}, \vec{S}^A)/P_A(\vec{\alpha}) \end{aligned} \quad (6.4)$$

where $\tilde{f}_A(\vec{S}^A,\vec{\beta})$ is the probability that the nucleus A has the spin $\vec{S}^A$ when its reaction partner B is known to fission in the direction $\vec{\beta}$; analogously for $\tilde{f}_B(\vec{S}^B;\vec{\alpha})$; they are thus normalized to unity when integrated over the spin variable. It is clear that we have $\int d\vec{S}^A \tilde{f}_A(\vec{S}^A;\vec{\beta}) = P_B(\vec{\beta})$ and $\int d\vec{S}^B \tilde{f}_B(\vec{S}^B;\vec{\alpha}) = P_A(\vec{\alpha})$.

6.2 The basic fission probabilities

We shall assume that the nuclei A and B always fission, regardless of the magnitudes of their spins. We then have

$$\begin{aligned} P_A(\vec{\alpha}, \vec{S}^A) &= \left[(2\pi)^{3/2} \frac{K_A}{S^A} \operatorname{erf}\left(\frac{S^A}{\sqrt{2}\,K_A}\right)\right]^{-1} e^{-(\vec{S}^A \cdot \overleftarrow{\alpha})^2/2K_A^2} \\ P_B(\vec{\beta}, \vec{S}^B) &= \left[(2\pi)^{3/2} \frac{K_B}{S^B} \operatorname{erf}\left(\frac{S^B}{\sqrt{2}\,K_B}\right)\right]^{-1} e^{-(\vec{S}^B \cdot \overleftarrow{\beta})^2/2K_B^2} \end{aligned} \quad (6.5)$$

where K_A and K_B are the mean K-values associated with A and B; they depend on the nuclear temperatures but need not be further discussed here. If the spin distribution is fairly narrow the spins in the preexponential factor may be replaced by an appropriate mean value:

$$
\begin{aligned}
S^A &\rightarrow S_A \equiv \langle S_Y^A \rangle \left(1 + \frac{\sigma_{xx}^{AA} + \sigma_{zz}^{AA}}{2\langle S_Y^A \rangle^2} \right) \\
S^B &\rightarrow S_B \equiv \langle S_Y^B \rangle \left(1 + \frac{\sigma_{xx}^{BB} + \sigma_{zz}^{BB}}{2\langle S_Y^B \rangle^2} \right)
\end{aligned}
\tag{6.6}
$$

Furthermore, if these mean values are large in comparison with the respective K-values the error functions are nearly unity and may be ignored. With these assumptions we arrive at the simple approximate expressions

$$
\begin{aligned}
P_A(\vec{\alpha}, \vec{S}^A) &\approx (2\pi)^{-3/2} \frac{S_A}{K_A} e^{-(\vec{S}^A \cdot \overleftarrow{\alpha})^2/2K_A^2} \\
P_B(\vec{\beta}, \vec{S}^B) &\approx (2\pi)^{-3/2} \frac{S_B}{K_B} e^{-(\vec{S}^B \cdot \overleftarrow{\beta})^2/2K_B^2}
\end{aligned}
\tag{6.7}
$$

6.3 Notational tools

Throughout our discussion of the fragment spin correlations two different spaces are intertwined: 1) the three-dimensional space associated with the nuclear spins and 2) the two-dimensional space

associated with the fragment labels A and B. It is therefore useful to introduce a six-dimensional superspace in which both of those spaces are embedded. In analogy with our notation in three-dimensional space, we shall use double arrows over quantities associated with the superspace. Thus, we introduce the superspin

$$\overset{\Rightarrow}{S} \equiv (\vec{S}^A, \vec{S}^B) \tag{6.8}$$

and the associated covariance matrix

$$\overset{\Leftrightarrow}{\sigma} \equiv \begin{pmatrix} \overset{\leftrightarrow}{\sigma}^{AA} & \overset{\leftrightarrow}{\sigma}^{AB} \\ \overset{\leftrightarrow}{\sigma}^{BA} & \overset{\leftrightarrow}{\sigma}^{BB} \end{pmatrix} \tag{6.9}$$

It is also natural to imbed the individual fragment spins as

$$\begin{aligned} \overset{\Rightarrow}{S}^A &\equiv (\vec{S}^A, \vec{0}) \\ \overset{\Rightarrow}{S}^B &\equiv (\vec{0}, \vec{S}^B) \end{aligned} \tag{6.10}$$

For pedagogical reasons we adopt the symbol $*$ to denote multiplication of supervariables. Thus, for example, we have $\overset{\Rightarrow}{S}^A * \overset{\Leftarrow}{S}^B = \vec{S}^A \cdot \overset{\leftarrow}{0} + \vec{0} \cdot \overset{\leftarrow}{S}^B = 0$.

With this notation the gaussian approximation to the spin-spin distribution can be written

$$f_{AB}(\overset{\Rightarrow}{S}) = (2\pi)^{-3} |\overset{\Leftrightarrow}{\sigma}|^{-\frac{1}{2}} \, e^{-\frac{1}{2}(\overset{\Rightarrow}{S} - \langle \overset{\Rightarrow}{S} \rangle) * (\overset{\Leftrightarrow}{\sigma})^{-1} * (\overset{\Leftarrow}{S} - \langle \overset{\Leftarrow}{S} \rangle)} \tag{6.11}$$

It is helpful to introduce the reduced directional vectors

$$\vec{a} \equiv \frac{\vec{\alpha}}{K_A} \quad , \qquad \vec{b} \equiv \frac{\vec{\beta}}{K_B} \tag{6.12}$$

and the associated tensors

$$\overleftrightarrow{A} \equiv \overleftarrow{a}\,\vec{a} = \frac{\overleftarrow{\alpha}\,\vec{\alpha}}{K_A^2} \quad , \qquad \overleftrightarrow{B} \equiv \overleftarrow{b}\,\vec{b} = \frac{\overleftarrow{\beta}\,\vec{\beta}}{K_B^2} \tag{6.13}$$

These quantities are imbedded in superspace as

$$\begin{aligned} \vec{\vec{a}} &\equiv (\vec{a}, \vec{0}) \quad , \qquad \vec{\vec{b}} \equiv (\vec{0}, \vec{b}) \\ \overleftrightarrow{\overleftrightarrow{A}} &\equiv \overleftarrow{\overleftarrow{a}}\,\vec{\vec{a}} \quad , \qquad \overleftrightarrow{\overleftrightarrow{B}} \equiv \overleftarrow{\overleftarrow{b}}\,\vec{\vec{b}} \end{aligned} \tag{6.14}$$

Finally, for calculating the joint fission angular distributions, the following supertensor is of interest,

$$\overleftrightarrow{\overleftrightarrow{C}} = \overleftrightarrow{\overleftrightarrow{A}} + \overleftrightarrow{\overleftrightarrow{B}} = \begin{pmatrix} \dfrac{\overleftarrow{\alpha}\,\vec{\alpha}}{K_A^2} & \overleftrightarrow{0} \\ \overleftrightarrow{0} & \dfrac{\overleftarrow{\beta}\,\vec{\beta}}{K_B^2} \end{pmatrix} \tag{6.15}$$

With this notation the basic fission angular distributions (6.7) can be written

$$\begin{aligned} P_A(\vec{\alpha}, \vec{S}^A) &= (2\pi)^{-3/2} \frac{S_A}{K_A} e^{-\frac{1}{2} \vec{S}^A \cdot \overleftrightarrow{A} \cdot \overleftarrow{S}^A} = (2\pi)^{-3/2} \frac{S_A}{K_A} e^{-\frac{1}{2} \vec{\vec{S}}^A * \overleftrightarrow{\overleftrightarrow{A}} * \overleftarrow{\overleftarrow{S}}^A} \\ P_B(\vec{\beta}, \vec{S}^B) &= (2\pi)^{-3/2} \frac{S_B}{K_B} e^{-\frac{1}{2} \vec{S}^B \cdot \overleftrightarrow{B} \cdot \overleftarrow{S}^B} = (2\pi)^{-3/2} \frac{S_B}{K_B} e^{-\frac{1}{2} \vec{\vec{S}}^B * \overleftrightarrow{\overleftrightarrow{B}} * \overleftarrow{\overleftarrow{S}}^B} \end{aligned} \tag{6.16}$$

and their product can be written as

$$P_A(\vec{\alpha}, \vec{S}^A)\, P_B(\vec{\beta}, \vec{S}^B) = (2\pi)^{-3} \frac{S_A}{K_A} \frac{S_B}{K_B} e^{-\frac{1}{2} \vec{\vec{S}} * \overleftrightarrow{C} * \overleftarrow{\overleftarrow{S}}} \tag{6.17}$$

It is also useful to introduce the reduced spins $s_\alpha \equiv \vec{S}^A \cdot \overleftarrow{a} = \vec{S}^A \cdot \overleftarrow{\alpha}/K_A$ and $s_\beta \equiv \vec{S}^B \cdot \overleftarrow{b} = \vec{S}^B \cdot \overleftarrow{\beta}/K_B$ which are dimensionless measures of the alignment of the fragment spins with the respective fission directions. For this we introduce the operator

$$\underset{\leftarrow}{\overset{\Rightarrow}{T}} \equiv \begin{pmatrix} \vec{a} \\ \vec{b} \end{pmatrix} = \begin{pmatrix} \vec{\alpha}/K_A & \vec{0} \\ \vec{0} & \vec{\beta}/K_B \end{pmatrix} \tag{6.18}$$

which transforms supervectors into vectors in label space. We shall adopt the use of arrows under quantities associated with label space and the symbol $\circ$ for the multiplication in label space. (Again, the explicit use of multiplication symbols is redundant since the dimensionality of the matrices involved automatically indicates the type of multiplication involved.) We then have for the reduced spin

$$\underset{\rightarrow}{s} \equiv (s_\alpha, s_\beta) = \vec{\vec{S}} * \underset{\rightarrow}{\overset{\Leftarrow}{T}} \tag{6.19}$$

The associated reduced covariance matrix is

$$\underset{\leftrightarrow}{\sigma} \equiv \underset{\leftarrow}{\overset{\Rightarrow}{T}} * \overleftrightarrow{\sigma} * \underset{\rightarrow}{\overset{\Leftarrow}{T}} = \begin{pmatrix} \sigma_{\alpha\alpha} & \sigma_{\alpha\beta} \\ \sigma_{\beta\alpha} & \sigma_{\beta\beta} \end{pmatrix} \tag{6.20}$$

where, for example, $\sigma_{\alpha\beta} = \frac{\vec{\alpha}}{K_B} \cdot \overleftrightarrow{\sigma}^{AB} \cdot \frac{\vec{\beta}}{K_B}$. We note that $\underset{\leftrightarrow}{\sigma}$ is symmetric, $\sigma_{\alpha\beta} = \sigma_{\beta\alpha}$. We also note that

$$\overleftrightarrow{C} = \underset{\rightarrow}{\overset{\Leftarrow}{T}} \circ \underset{\leftarrow}{\overset{\Rightarrow}{T}} \tag{6.21}$$

6.4 The fission-fission angular distribution

We first consider the joint fission-fission angular distribution. This is the most complicated case and the other cases can readily be obtained subsequently by appropriate specializations.

Combining eqs. (6.3), (6.11) and (6.16) we have

$$P_{AB}(\vec{\alpha},\vec{\beta}) = (2\pi)^{-6}\frac{S_A}{K_A}\frac{S_B}{K_B}|\overleftrightarrow{\sigma}|^{-1}\int d\vec{S}\, e^{-\frac{1}{2}[(\vec{S}-\langle\vec{S}\rangle)*\overleftrightarrow{\sigma}^{-1}*(\overleftarrow{S}-\langle\overleftarrow{S}\rangle)+\vec{S}*\overleftrightarrow{C}*\overleftarrow{S}]} \tag{6.22}$$

Since the exponent is of second order in the integration variable it is possible to evaluate the integral by bringing the integrand on quadratic form ("completing the square"). The integrand is of the form

$$\begin{aligned}[\cdot] &= (\vec{S}-\langle\vec{S}\rangle-\vec{\Delta}_c)*(\overleftrightarrow{\sigma}^{-1}+\overleftrightarrow{C})*(\overleftarrow{S}-\langle\overleftarrow{S}\rangle-\overleftarrow{\Delta}_c) \\ &\quad + \langle\vec{S}\rangle*\overleftrightarrow{C}*(\overleftrightarrow{I}+\overleftrightarrow{\sigma}*\overleftrightarrow{C})^{-1}*\langle\overleftarrow{S}\rangle\end{aligned} \tag{6.23}$$

provided that the induced shift is given by

$$\vec{\Delta}_c = -\langle\vec{S}\rangle*\overleftrightarrow{C}*\overleftrightarrow{\sigma}*(\overleftrightarrow{I}+\overleftrightarrow{C}*\overleftrightarrow{\sigma})^{-1} \tag{6.24}$$

It expresses the bias introduced in the mean spins as a result of the joint detection of the two fission fragments at $\vec{\alpha}$ and $\vec{\beta}$. After carrying out the $\vec{S}$-integration we are left with

$$P_{AB}(\vec{\alpha},\vec{\beta}) = (2\pi)^{-3}\frac{S_A}{K_A}\frac{S_B}{K_B}|\overleftrightarrow{I}+\overleftrightarrow{\sigma}*\overleftrightarrow{C}|^{-\frac{1}{2}}\, e^{-\frac{1}{2}\langle\vec{S}\rangle*\overleftrightarrow{C}*(\overleftrightarrow{I}+\overleftrightarrow{\sigma}*\overleftrightarrow{C})^{-1}*\langle\overleftarrow{S}\rangle} \tag{6.25}$$

The rank of $\overset{\Leftrightarrow}{C}$ is only two, and therefore it is possible to reduce the six-dimensional determinant and exponent to quantities in the two-dimensional label space. We first note the following identity:

$$\begin{aligned}
\overset{\Leftrightarrow}{C} * (\overset{\Leftrightarrow}{I} + \overset{\Leftrightarrow}{\sigma} * \overset{\Leftrightarrow}{C})^{-1} &= \overset{\Leftarrow}{T}_{\rightarrow} \circ \overset{\Rightarrow}{T}_{\leftarrow} * (\overset{\Leftrightarrow}{I} + \overset{\Leftrightarrow}{\sigma} * \overset{\Leftarrow}{T}_{\rightarrow} \circ \overset{\Rightarrow}{T}_{\leftarrow})^{-1} \\
&= \overset{\Leftarrow}{T}_{\rightarrow} \circ \overset{\Rightarrow}{T}_{\leftarrow} * \sum_{n \geq 0} (-\overset{\Leftrightarrow}{\sigma} * \overset{\Leftarrow}{T}_{\rightarrow} \circ \overset{\Rightarrow}{T}_{\leftarrow})^{n} \\
&= \overset{\Leftarrow}{T}_{\rightarrow} \circ \sum_{n \geq 0} (-\overset{\Rightarrow}{T}_{\leftarrow} * \overset{\Leftrightarrow}{\sigma} * \overset{\Leftarrow}{T}_{\rightarrow})^{n} \circ \overset{\Rightarrow}{T}_{\leftarrow} \\
&= \overset{\Leftarrow}{T}_{\rightarrow} \circ (\underset{\leftrightarrow}{I} + \underset{\leftrightarrow}{\sigma})^{-1} \circ \overset{\Rightarrow}{T}_{\leftarrow}
\end{aligned} \tag{6.26}$$

where $\underset{\leftrightarrow}{I}$ is the identity in label space. The inverse matrix is readily calculated,

$$(\underset{\leftrightarrow}{I} + \underset{\leftrightarrow}{\sigma})^{-1} = \begin{pmatrix} 1+\sigma_{\alpha\alpha} & \sigma_{\alpha\beta} \\ \sigma_{\beta\alpha} & 1+\sigma_{\beta\beta} \end{pmatrix}^{-1} = \frac{1}{d} \begin{pmatrix} 1+\sigma_{\beta\beta} & -\sigma_{\alpha\beta} \\ -\sigma_{\beta\alpha} & 1+\sigma_{\alpha\alpha} \end{pmatrix} \tag{6.27}$$

where $d = |\underset{\leftrightarrow}{I} + \underset{\leftrightarrow}{\sigma}| = (1 + \sigma_{\alpha\alpha})(1 + \sigma_{\beta\beta}) - \sigma_{\alpha\beta}\sigma_{\beta\alpha}$. Thus the exponent in (6.25) is

$$\begin{aligned}
&-\tfrac{1}{2} \langle \overset{\Rightarrow}{S} \rangle * \overset{\Leftrightarrow}{C} * (\overset{\Leftrightarrow}{I} + \overset{\Leftrightarrow}{\sigma} * \overset{\Leftrightarrow}{C})^{-1} * \langle \overset{\Leftarrow}{S} \rangle \\
&= -\tfrac{1}{2} \langle \underset{\rightarrow}{s} \rangle \circ (\underset{\leftrightarrow}{I} + \underset{\leftrightarrow}{\sigma})^{-1} \circ \langle \underset{\leftarrow}{s} \rangle
\end{aligned} \tag{6.28}$$

In order to calculate the preexponential factor we make use of the identity

$$|\overset{\Leftrightarrow}{I} + \overset{\Leftrightarrow}{\sigma} * \overset{\Leftrightarrow}{C}| = |\overset{\Leftrightarrow}{I} + \overset{\Leftrightarrow}{C} * \overset{\Leftrightarrow}{\sigma}| \tag{6.29}$$

$$= |\overset{\Leftrightarrow}{I} + \overset{\Rightarrow}{\underset{\Leftrightarrow}{I}} * \overset{\Leftrightarrow}{\sigma} * \overset{\Leftarrow}{T}| = |\underset{\Leftrightarrow}{I} + \underset{\Leftrightarrow}{\sigma}| = d$$

We thus arrive at the following expression for the joint angular distribution

$$P_{AB}(\vec{\alpha},\vec{\beta}) = (2\pi)^{-3} \frac{S_A}{K_A}\frac{S_B}{K_B} |\underset{\Leftrightarrow}{I} + \underset{\Leftrightarrow}{\sigma}|^{-\frac{1}{2}} e^{-\frac{1}{2}\langle \underset{\Rightarrow}{s}\rangle \circ (\underset{\Leftrightarrow}{I} + \underset{\Leftrightarrow}{\sigma})^{-1} \circ \langle \underset{\Leftarrow}{s}\rangle} \tag{6.30}$$

6.5 The individual fission angular distributions

The individual angular distributions of the fission fragments from one of the reaction products are given by eqs. (6.2). Due to the results (6.16), these expressions are of the same form as the expression (6.17) for the joint angular distribution, the only difference being the replacement of the supertensor $\overset{\Leftrightarrow}{C}$ of rank two by either of the rank one tensors $\overset{\Leftrightarrow}{A}$ or $\overset{\Leftrightarrow}{B}$. The result (6.25) can then immediately be taken over for $P_A(\vec{\alpha})$ and $P_B(\vec{\beta})$ with the appropriate replacements of $\overset{\Leftrightarrow}{C}$. By proceeding in an analogous manner we then arrive at the results

$$P_A(\vec{\alpha}) = (2\pi)^{-3/2} \frac{S_A}{K_A} (1+\sigma_{\alpha\alpha})^{-\frac{1}{2}} e^{-\frac{1}{2}\langle S_\alpha\rangle (1+\sigma_{\alpha\alpha})^{-1} \langle S_\alpha\rangle}$$

$$P_B(\vec{\beta}) = (2\pi)^{-3/2} \frac{S_B}{K_B} (1+\sigma_{\beta\beta})^{-\frac{1}{2}} e^{-\frac{1}{2}\langle S_\beta\rangle (1+\sigma_{\beta\beta})^{-1} \langle S_\beta\rangle} \tag{6.31}$$

With these results we can derive an expression for the enhancement factor

$$F(\vec{\alpha},\vec{\beta}) \equiv \frac{P_{AB}(\vec{\alpha},\vec{\beta})}{P_A(\vec{\alpha})\, P_B(\vec{\beta})} \tag{6.32}$$

$$= \left(1 - \frac{\sigma_{\alpha\beta}\,\sigma_{\beta\alpha}}{(1+\sigma_{\alpha\alpha})(1+\sigma_{\beta\beta})}\right)^{-\frac{1}{2}} e^{-\frac{1}{2}\left[\sigma_{\alpha\beta}\sigma_{\beta\alpha}\left(\frac{S_\alpha^2}{1+\sigma_{\alpha\alpha}} + \frac{S_\beta^2}{1+\sigma_{\beta\beta}}\right) - (\sigma_{\alpha\beta}+\sigma_{\beta\alpha}) S_\alpha S_\beta\right]} \frac{1}{d}$$

6.6 Biased spin distributions

The biased spin distributions can also be derived in a manner analogous to the one used for obtaining the joint angular distribution. Let us consider the biased distribution for the spin of nucleus A; the other one follows analogously. Using (6.4), (6.7) and (6.11) we have

$$P_B(\vec{\beta})\,\tilde{f}_A(\vec{S}_A^A;\vec{\beta}) = (2\pi)^{-9/2}\,\frac{S_B}{K_B}\,|\overleftrightarrow{\sigma}|^{-1/2}\int d\vec{S}^B\, e^{-\frac{1}{2}[(\vec{S}-\langle\vec{S}\rangle)*\overleftrightarrow{\sigma}^{-1}*(\overleftarrow{S}-\langle\overleftarrow{S}\rangle)+\vec{S}*\overleftrightarrow{B}*\overleftarrow{S}]} \tag{6.33}$$

In analogy to (6.23) we find for the exponent

$$\begin{aligned}[\cdot] &= (\vec{S}-\langle\vec{S}\rangle-\vec{\Delta}_\beta)*(\overleftrightarrow{\sigma}^{-1}+\overleftrightarrow{B})*(\overleftarrow{S}-\langle\overleftarrow{S}\rangle-\overleftarrow{\Delta}_\beta)\\ &\quad+\langle\vec{S}\rangle*\overleftrightarrow{B}*(\overleftrightarrow{I}+\overleftrightarrow{\sigma}*\overleftrightarrow{B})^{-1}*\langle\overleftarrow{S}\rangle\end{aligned} \tag{6.34}$$

Here the biased shift is given by

$$\vec{\Delta}_\beta = -\langle\vec{S}\rangle*\overleftrightarrow{B}*\overleftrightarrow{\sigma}*(\overleftrightarrow{I}+\overleftrightarrow{B}*\overleftrightarrow{\sigma})^{-1} \tag{6.35}$$

The integrand in the above expression for $\tilde{f}_A$ is thus a six-dimensional gaussian centered at $\vec{S} = \langle\vec{S}\rangle + \vec{\Delta}_\beta$ and with covariance tensor $(\overleftrightarrow{\sigma}^{-1} + \overleftrightarrow{B})^{-1}$. The integration over $\vec{S}^B$ then leaves a distribution in $\vec{S}^A$ which is a three-dimensional gaussian centered at $\tilde{\vec{S}}^A = \langle\vec{S}^A\rangle + \vec{\Delta}_\beta^A$ where $\vec{\Delta}_\beta^A \equiv (\vec{\Delta}_\beta)^A$ is the A-part of the supervector $\vec{\Delta}_\beta$. Furthermore, the corresponding biased covariance tensor $\tilde{\overleftrightarrow{\sigma}}^{AA}$ is the AA-part of $(\overleftrightarrow{\sigma}^{-1} + \overleftrightarrow{B})^{-1}$.

We now make use of the following relations

$$
\begin{aligned}
|\overleftrightarrow{I} + \overleftrightarrow{B} * \overleftrightarrow{\sigma}| &= |\overleftrightarrow{I} + \overleftrightarrow{\sigma} * \overleftrightarrow{B}| \\
&= |\overleftrightarrow{I} + \overleftrightarrow{B} \cdot \overleftrightarrow{\sigma}^{BB}| = |\overleftrightarrow{I} + \overleftrightarrow{\sigma}^{BB} \cdot \overleftrightarrow{B}| \\
&= 1 + \frac{\vec{\beta}}{K_B} \cdot \overleftrightarrow{\sigma}^{BB} \cdot \frac{\overleftarrow{\beta}}{K_B} = 1 + \sigma_{\beta\beta} \equiv d_\beta
\end{aligned}
\tag{6.36}
$$

and

$$
(\overleftrightarrow{I} + \overleftrightarrow{B} * \overleftrightarrow{\sigma})^{-1} = \overleftrightarrow{I} - \frac{1}{d_\beta} \overleftrightarrow{B} * \overleftrightarrow{\sigma} \tag{6.37}
$$

It is then readily found that

$$
\begin{aligned}
\vec{\Delta}_\beta &= -\langle \vec{S} \rangle * \overleftrightarrow{B} * \overleftrightarrow{\sigma} \frac{1}{d_\beta} \\
&= \left(-\frac{S_\beta}{d_\beta} \frac{\vec{\beta}}{K_B} \cdot \overleftrightarrow{\sigma}^{BA}, -\frac{S_\beta}{d_\beta} \frac{\vec{\beta}}{K_B} \cdot \overleftrightarrow{\sigma}^{BB} \right) = (\vec{\Delta}^A_\beta, \vec{\Delta}^B_\beta)
\end{aligned}
\tag{6.38}
$$

Thus, the detection of a fission fragment from B in the direction $\vec{\beta}$ shifts the mean spin of A to

$$
\begin{aligned}
\tilde{\vec{S}}^A_\beta &= \langle \vec{S}^A \rangle - \vec{\Delta}^A_\beta \\
&= \langle \vec{S}^A \rangle - \langle \vec{S}^B \rangle \cdot \frac{\overleftarrow{\beta}\vec{\beta}}{K_B^2} \cdot \overleftrightarrow{\sigma}^{BA} \left(1 + \frac{\vec{\beta}}{K_B} \cdot \overleftrightarrow{\sigma}^{BB} \cdot \frac{\overleftarrow{\beta}}{K_B} \right)^{-1}
\end{aligned}
\tag{6.39}
$$

Furthermore, the mean spin of those target-like nuclei which fission in the direction of $\vec{\beta}$ is given by

$$\tilde{\vec{S}}^B_\beta = \langle \vec{S}^B \rangle - \vec{\Delta}^B_\beta$$

$$= \langle \vec{S}^B \rangle \left[\overleftrightarrow{I} - \frac{\overleftarrow{\beta}\vec{\beta}}{K_B^2} \cdot \overleftrightarrow{\sigma}^{BB} \left(1 + \frac{\vec{\beta}}{K_B} \cdot \overleftrightarrow{\sigma}^{BB} \cdot \frac{\overleftarrow{\beta}}{K_B} \right)^{-1} \right] \tag{6.40}$$

It also readily follows that

$$\left(\overleftrightarrow{\sigma}^{-1} + \overleftrightarrow{B} \right)^{-1} = \overleftrightarrow{\sigma} * \left(\overleftrightarrow{I} + \overleftrightarrow{B} * \overleftrightarrow{\sigma} \right)^{-1}$$

$$= \overleftrightarrow{\sigma} - \frac{1}{d_\beta} \overleftrightarrow{\sigma} * \overleftrightarrow{B} * \overleftrightarrow{\sigma} \tag{6.41}$$

so that the biased covariance for the $\vec{S}^A$-distribution is given by

$$\tilde{\overleftrightarrow{\sigma}}^{AA}_\beta = \overleftrightarrow{\sigma}^{AA} - \frac{1}{d_\beta} \overleftrightarrow{\sigma}^{AB} \cdot \overleftrightarrow{B} \cdot \overleftrightarrow{\sigma}^{BA}$$

$$= \overleftrightarrow{\sigma}^{AA} - \overleftrightarrow{\sigma}^{AB} \cdot \frac{\overleftarrow{\beta}\vec{\beta}}{K_B^2} \cdot \overleftrightarrow{\sigma}^{BA} \left(1 + \frac{\vec{\beta}}{K_B} \cdot \overleftrightarrow{\sigma}^{BB} \cdot \frac{\overleftarrow{\beta}}{K_B} \right)^{-1} \tag{6.42}$$

The biased spin distribution can therefore be written

$$\tilde{f}_A(\vec{S}^A; \vec{\beta})$$

$$= (2\pi)^{-3/2} \left| \tilde{\overleftrightarrow{\sigma}}^{AA}_\beta \right|^{-1/2} e^{-\frac{1}{2}\left[\left(\vec{S}^A - \tilde{\vec{S}}^A_\beta \right) \cdot \left(\tilde{\overleftrightarrow{\sigma}}^{AA}_\beta \right)^{-1} \cdot \left(\overleftarrow{S}^A - \tilde{\overleftarrow{S}}^A_\beta \right) \right]} \tag{6.43}$$

6.7 Illustration: 8.5 MeV/n U + Pb

We now wish to illustrate the theory by considerng the reaction 8.5 MeV/n $^{238}U + ^{208}Pb$ which is of actual experimental interest.[32] We have carried out dynamical trajectory calculations for specified J-values and subsequently integrated over those to obtain the final spin distribution as a function of the kinetic energy loss TKEL. We consider in some detail the results for a moderate energy loss, TKEL = 140 MeV, and a large one, TKEL = 280 MeV. For a specified energy loss, the joint fission-fission angular distribution $P_{AB}(\vec{\alpha},\vec{\beta})$ is a function of the four angles $\vec{\alpha} = (\vartheta_A,\varphi_A)$ and $\vec{\beta} = (\vartheta_B,\varphi_B)$ and thus not easy to display. We therefore choose to fix the direction $\vec{\beta}$ at a specified value and then study P_{AB} as a function of $\vec{\alpha}$. We wish to recall that $\vec{\alpha}$ denotes the fission direction for the projectile-like reaction fragment A as seen in its rest frame while $\vec{\beta}$ denotes the fission direction for the target-like reaction fragment B as seen in its rest frame; thus the two directions $\vec{\alpha}$ and $\vec{\beta}$ do not refer to the same inertial frame, and the appropriate transformations need be carried out to relate $P_{AB}(\vec{\alpha},\vec{\beta})$ to angular distributions obtained in the laboratory system. Our particular choice of frames is made in order to best bring out the physical effects of the correlation between the fragment spins.

In order to give a global impression of the effect of the correlation of the two fragment spins $\vec{S}^A$ and $\vec{S}^B$ on the joint fission-fission angular distribution we show in fig. 13 contour plots of the quantity $P_{AB}(\vec{\alpha},\vec{\beta})/P_A(\vec{\alpha})P_B(\vec{\beta})$. The fission direction of the target-like reaction product has been fixed at either $\vec{\beta} = (\vartheta_\beta = 45°, \varphi_\beta = 60°)$ or $\vec{\beta} = (\vartheta_\beta = 45°, \varphi_\beta = -30°)$. The directions $\varphi_\beta = 60, -30°$

correspond to the major and minor in-plane principal directions, respectively, at the specified energy loss of TKEL=140 MeV. [At both energy losses considered, the calculated scattering angle is $\theta_{CM} \approx 70^\circ$ so that the major in-plane principal direction is expected to form an angle of approximately 35° ($\approx \theta_{CM}/2$) with the beam direction. In actuality this angle is close to 30°. Consequently in the adopted coordinate system, which has the Z-axis perpendicular to the beam and the X-axis along the beam, the major in-plane direction has $\theta_0 \approx 60^\circ$.] When $\vec{\beta}$ is taken to be out of (but not perpendicular to) the reaction plane (i.e. when $\vartheta_\beta \neq 90^\circ$ and $\vartheta_\beta \neq 0^\circ$) the distribution of fission fragments from the projectile-like reaction product is no longer reflection symmetric with respect to the reaction plane (nor with respect to any other plane, as we shall discuss later). This is clearly seen from the figure. It is also noted that the effect is considerably larger when $\vec{\beta}$ is chosen in the major principal direction ($\varphi_\beta = 60^\circ$) than when $\vec{\beta}$ is chosen in the minor principal direction ($\varphi_\beta = -30^\circ$), as is to be expected since it is easiest to tilt the spin in the major principal direction.

The division by the product of the individual distributions $P_A(\vec{\alpha})$ and $P_B(\vec{\beta})$ of course enhances the effect in the polar regions where the absolute yields are the smallest. In order to gain an impression of the absolute size of the effect we show in fig. 14 the absolute yield $P_{AB}(\vec{\alpha},\vec{\beta})$ as a function of a single angular variable, namely the polar angle ϑ_α, with φ_α fixed to be the same value as φ_β (since the largest effect is expected when $\vec{\alpha} \approx \vec{\beta}$). Figure 14a corresponds to $\vec{\beta} = (45^\circ, 60^\circ)$ while fig. 14b has $\vec{\beta} = (45^\circ, -30^\circ)$. The upper portions are for a moderate energy loss of TKEL = 140 MeV while the lower portions are for a large energy loss of TKEL = 280 MeV.

We note that the distribution in fig. 14 is biased towards $\vec{\beta}$, particularly at the moderate energy loss. This is expected since this particular angular selection will probe the major in-plane components of the spin distribution which arises predominantly from the in-plane wriggling mode and consequently has positive signature. Towards the largest energy losses the distribution will relax more towards equilibrium which is characterized by a slightly positive covariance for the in-plane wriggling mode (c.f. fig. 14 of I). Thus, the correlated fission distribution P_{AB} is significantly different from the uncorrelated product $P_A P_B$ at the moderate energy loss, whereas, for the larger energy loss, the difference is less pronounced.

In fig. 14b, where $\vec{\beta}$ is in the minor principal direction, we probe mainly the twisting and tilting modes. Generally, the tilting mode dominates at the small TKEL, leading to small positive σ^{AB} along the minor princpal axis. For larger TKEL, the tilting relaxation time becomes very long, whereas the twisting relaxation time decreases, and σ_{AB} along the minor principal axis decreases at some point and ultimately turns negative with increasing TKEL (c.f. fig. 14 of I). Thus, at the moderate TKEL, where σ^{AB} is still positive along the minor principal axis, the maximum of P_{AB} is shifted slightly towards the direction $\vec{\beta}$, whereas the negative value σ^{AB} at the large TKEL induces a shift of the maximum in the opposite direction.

The fact that the location of the maximum of P_{AB}, as a function of the direction $\vec{\alpha}$ for fixed $\vec{\beta}$, moves toward $\vec{\beta}$ for positive σ^{AB} and away from $\vec{\beta}$ for negative σ^{AB} can qualitatively be understood as a three-step process: (i) Fission into the direction $\vec{\beta}$ imposes a strong bias of the spin $\vec{S}_B$ of nucleus B towards directions perpendicular

to $\vec{\beta}$ (c.f. eq. (6.40)). (ii) For positive σ^{AB}, this bias of $\vec{S}_B$ induces a bias of $\vec{S}_A$ in the same direction and in the opposite direction for negative σ^{AB}. (iii) The fission fragments emitted from nucleus A will preferably be emitted perpendicular to the spins $\vec{S}_A$ biased in this way, and this favours the direction $\vec{\beta}$ over directions perpendicular to $\vec{\beta}$ for positive σ^{AB} and disfavors it for negative σ^{AB}.

Figure 15 shows the average spin and contours for the variance in the two planes containing the Y-axis and, respectively, the minor and major principal axes for the unbiased spin distribution in nucleus A, and for the distribution biased by a detection of fission fragments from nucleus B. The angles of maximum P_{AB} restricted to the planes shown correspond roughly to the directions perpendicular to the biased average spin $\tilde{\vec{S}}^A_\beta$ in the two cases. Since the biased variance tensor does not have the biased average spin direction as a principal axis, P_{AB} is not reflection symmetric with respect to the plane perpendicular to $\tilde{\vec{S}}^A_\beta$, or any other plane.

It is instructive to contrast the above results with the expectations of a statistical model. For this purpose we assume that all spin modes are fully relaxed at the time of neck snapping, as already discussed in I. As already pointed out there, the resulting principal system is rotated approximately -45° relative to the dynamically calculated distribution. In order to maximize the effect we therefore choose either $\beta = (45°, 0°)$ or $\beta = (45°, 90°)$, corresponding approximately to the major and minor principal directions of the statistical spin distribution.

The results are shown in fig. 16. It is clearly seen that the effect is much smaller (nearly an order of magnitude) and probably hardly experimentally detectable. The results exhibit the qualitative feature of

a slight positive shift when biasing along the major principal detection and a slight negative shift when biasing along the minor principal direction, as specified.

In summary, we wish to state the following. Our calculations indicate that the dynamically accumulated correlated structure in the spin-spin distribution of the reaction products gives rise to significant effects in the joint fission-fission angular distribution. Moving one fission detector out of the reaction plane breaks the symmetry with respect to reflections in that plane. The resulting reflection asymmetry of the fission distribution from the other reaction product is fairly sizeable and shows a characteristic variation with direction and energy loss. In contrast, calculations based on the assumption of full statistical relaxation of the spin modes yield very little effect. It would be of great interest to observe such structure. Given sufficient data quality, it should be possible to determine the principal directions and, from the character of the correlations, obtain an indication of the relaxation times for the various dinuclear spin modes.

7. Concluding Remarks

Theories of damped nuclear reactions are often expressed in terms of degrees of freedom which are familiar from simpler nuclear reactions, such as surface vibrations and nucleon transfer. However, the clean characteristics of such elementary nuclear excitations are largely washed out due to the complexity of a damped reaction where high temperatures and large distortions occur. [One exception may be the substantial overall deformations of the reaction products at the time of scission, as suggested by the fact that the nuclei often emerge with relative energies well below the exit channel Coulomb barrier. Another exception may be the (still conjectured) Fermi jets, which are transferred nucleons directly transmitted through the recipient.] The experimental study of damped reactions is therefore practically limited to observables subject to overall conservation after the reaction: the mass and charge numbers, the momentum and energy, and the angular momentum. (Parity is also conserved, prior to sequential decays, but is of little use.)

Observables related to the mass and charge partition, for example as expressed in terms of the mean neutron and proton numbers of the projectile-like reaction product and the associated three second moments, can be obtained experimentally in a fairly direct manner and have been studied thoroughly in the past. The present series of two papers has focussed on the angular momentum observables. Being vectors, the angular momenta enrich the description considerably, adding two first moments and thirteen second moments as functions of the kinetic energy loss, but the experimental methods for obtaining this information are less direct.

The most direct experiments so far are γ-multiplicity experiments, which probe the spin magnitude distribution. The mean multiplicity of γ-rays is closely related to the mean spin component along the reaction normal while the γ-multiplicity variance is mostly determined by the spin variance in that direction.

An ideal experiment for probing the directional distribution of the spin would be the measurement of angular correlations of γ-rays associated with known discrete rather low-lying E2 transitions, through which most of the intensity passes. This would permit the determination of the reflection symmetric moments of the spin directional distribution, i.e., the statistical tensors of even rank. (Of course the dealigning effect of sequential decays preceding the particular transition studied must be incorporated in the analysis.) In this way the tensors of rank two and four could be determined fairly unambiguously. Ideally the entire 4π angular region would have to be covered, or, exploiting the symmetries, one quarter thereof. Recent improvements in discrete γ-ray detection techniques may soon make such an experiment possible.

At present, angular correlation experiments are using less perfect sequential decay modes. They introduce a bias on the spin distribution which must be taken into account in terms of decay probabilities and angular distribution coefficients. The variation of the angular correlation with respect to the polar angle (using the reaction normal as the polar axis) is primarily determined by the magnitude and alignment of the spin relative to the reaction normal. Sometimes fission data directly yield a lower bound on the spin alignment for large TKEL. Since most theories do not conflict with such absolute bounds, it is necessary to perform detailed calculations to compare theory and data. The variation

of the angular correlation with azimuthal angle yields, to the extent it is statistically significant, information about the direction of the principal in-plane axes for the spin variance tensor. This is important since different theories predict quite different results for this quantity. The amplitude of the variation with azimuthal angle depends on the spin magnitude and the difference between the major and minor in-plane variances, and again the comparison between theory and experiment requires detailed calculations.

Of particular interest is the correlation between the spins in the two product nuclei, since different assumptions about the reaction dynamics yield quite different results for this quantity. The spin-spin covariances can be probed in a double angular correlation experiment. Again, discrete γ-rays would be ideally suited to obtain precise information on the correlation coefficients. However, for the time being, a more practical method is offered by the double fission process. On the basis of our approximate analytical analysis of the double fission angular correlations, it appears that this type of experiment should suffice to give a rough indicator of the sign and size of the spin-spin correlation.

The present study is carried out within the framework of the nucleon exchange transport model. This model has arisen as a natural consequence of our general understanding of low-energy nuclear dynamics in terms of nearly independent nucleons moving in a time-dependent effective one-body field. In this picture the dissipation of the macroscopic motion is caused by the inelastic interactions of the individual nucleons with the mean field. In the case of a binary system, as is temporarily created during a damped reaction, this mechanism appears as the transfer of individual nucleons between the two reaction partners. The strong

spin-spin correlations predicted directly reflects this character of the angular momentum exchange in the reaction and thus appear to be an important test case for the theory.

In the present paper we have compared theory and experiment for a number of angular-momentum related observables. [Data[33)] on the correlation between angular momentum and charge partition have not been considered since the theory has not yet been developed sufficiently regarding this type of observable.] Throughout our studies we have kept the various model parameters fixed at their standard values and no attempts have been made at fitting the data. On the whole, the theory is supported as far as the variances of the spin are concerned, but the situation is less favorable for the mean spin. For small TKEL the calculated mean spin increases to rapidly, reaches a maximum for intermediate TKEL in accordance with the data, and proceeds to decrease at higher TKEL somewhat too markedly. [However, the picture is somewhat obscured by the fact that the different sets of data are not in mutual accordance.]

As we have discussed, the disagreement for small TKEL can be reduced by more refined treatment of the neck dynamics but only at the cost of affecting the behavior of other observables. We therefore attach some significance to this discrepancy. The cause of this failure is not clear to us at this point but the problem might be helped by an improved treatment of the nucleon transfer process and future studies may be focussed in this direction.

The disagreement for large TKEL is probably caused by the mean trajectory method of solution, which prevents dynamical fluctuations, for example in the nuclear separation, from coupling back into the mobility

coefficients. If the fluctuations were allowed to accentuate themselves through the induced changes in mobility coefficients, potentials, etc, the highest TKEL-values might receive contributions from a wider range of impact parameters, in turn giving rise to a larger mean spin.

The present study has developed the description of angular momentum in damped reactions to a considerable detail, within the nucleon exchange transport model, and has carried out a fairly broad confrontation with data. It would be very helpful to our assessment of the situation if other models would be subjected to an equally complete treatment. This would amount to determining the characteristics of the spin evolution implied by the degrees of freedom considered, as well as comparing to data in order to test the qualitative and more quantitative predictions.

Acknowledgement

During part of this work, one of us (TD) was supported by a Niels Bohr Fellowship granted by the Royal Danish Academy of Science.

This work was supported by the Director, Office of Energy Research Division of Nuclear Physics of the Office of High Energy and Nuclear Physics of the U.S. Department of Energy under Contract DE-AC03-76SF00098.

Appendix A.

In this appendix we derive expressions for the changes in magnitude and statistical tensors for the spin in a nucleus caused by a statistical cascade of unobserved neutrons.

By S_0 we denote the spin magnitude in the nucleus leaving the damped reaction and by S_i, $i = 1,\ldots,n$ we denote the spin magnitudes in the first, second, etc. daughter nucleus after neutron emission. Then S_n is the spin of the n'th daughter nucleus, which finally emits the decay product being observed, whether a γ-ray or a fission fragment.

At each step in the cascade we imagine (for the time being) that the mother nucleus has a definite spin magnitude S_{i-1}. We then wish to determine the distribution of the spin magnitude S_i in the daughter nucleus, as characterized by the average change

$$\langle \Delta_i \rangle \equiv \langle S_i - S_{i-1} \rangle \tag{A.1}$$

and the incurred variance

$$\sigma_i^2 \equiv \langle (S_i - S_{i-1})^2 \rangle - \langle S_i - S_{i-1} \rangle^2 \tag{A.2}$$

For the statistical tensors we are interested in the average values of the factors (4.5) relating the statistical tensors of rank $\lambda = 2,4$ at the i'th step,

$$\left\langle P_\lambda \left(\frac{\vec{S}_i \cdot \overleftarrow{S}_{i-1}}{S_i S_{i-1}} \right) \right\rangle$$

to those at the previous step.

Denoting by j the angular momentum of the evaporated neutron, we obtain

$$P_2\left(\frac{\vec{S}_i \cdot \overleftarrow{S}_{i-1}}{S_i S_{i-1}}\right) = P_2\left(\frac{S_i^2 + S_{i-1}^2 - j^2}{2 S_i S_{i-1}}\right) \approx 1 - \frac{3}{2}\,\frac{j^2 - (S_i - S_{i-1})^2}{S_{i-1}^2} \qquad (A.3)$$

and

$$P_4\left(\frac{\vec{S}_i \cdot \overleftarrow{S}_{i-1}}{S_i S_{i-1}}\right) \approx 1 - 5\,\frac{j^2 - (S_i - S_{i-1})^2}{S_{i-1}^2} \qquad (A.4)$$

where we have kept leading order terms in j/S_i and $(S_i - S_{i-1})/S_i$.

For one step in a statistical cascade, starting from definite values of the angular momentum S_{i-1} and the excitation energy E_{i-1}, the relative probability for the angular momentum sequence S_{i-1}, j, S_i is given by

$$R(S_{i-1}, j, S_i) = \sum_{\ell} \int d\varepsilon\; T_\ell(\varepsilon)\, \rho(E_{i-1} - B - \varepsilon, S_i) \qquad (A.5)$$

where the summation runs over the orbital angular momentum of the neutron and its kinetic energy ε. $T_l(\varepsilon)$ is the transmission coefficient. $\rho = \rho(E_i, S_i)$ is the level density in the i'th daughter nucleus, evaluated at the angular momentum S_i and the energy $E_{i-1} - B - \varepsilon$ after neutron emission, where B is the binding energy.

To obtain the changes in the magnitude of the angular momentum (A.1) and the factors for the tensors, we must evaluate the averages

$$\langle F \rangle = \sum_{S_i} \sum_{j} F \cdot R(S_{i-1}, j, S_i) \Big/ \sum_{S_i} \sum_{j} R(S_{i-1}, j, S_i) \qquad (A.6)$$

of the quantities $F = S_i - S_{i-1}$, $(S_i - S_{i-1})^2$ and j^2.

In order to obtain analytic expressions we apply the two standard approximations: (i) Sharp cut-off transmission coefficients with effective barrier radius R:

$$T_\ell(\varepsilon) = \begin{cases} 1 & \text{if} \quad \varepsilon > \dfrac{\ell^2}{2mR^2} \\ 0 & \text{otherwise} \end{cases} \tag{A.7}$$

Here m is the mass of the neutron. (ii) Approximation of the level density around some set of arguments E',S':

$$\rho(E,S) = \rho(E',S') \exp\left[\frac{1}{T}(E-E')\right] \frac{2S+1}{2S'+1} \exp\left[\frac{-1}{2T\mathcal{J}}(S^2-S'^2)\right] \tag{A.8}$$

In this expression $\mathcal{J}$ is the moment of inertia of the i'th daughter nucleus and T is the temperature at E',S', given by

$$T = \sqrt{\frac{E' - \frac{S'^2}{2\mathcal{J}}}{a}} \tag{A.9}$$

where a is the level density parameter. We choose the values $E' = E_{i-1} - B$ and $S' = S_{i-1}$. The level density $\rho(E',S')$ is common to all the terms of the summations in both numerator and denominator of expression (A.6), and therefore cancels.

The integral over the kinetic energy of the neutron, entering into the first exponential factor of the expression (A.8), yields:

$$\int d\varepsilon\, T_\ell(\varepsilon) \exp\left[\frac{1}{T}(E_{i-1}-B-\varepsilon) - \frac{1}{T}(E_{i-1}-B)\right] = T \exp\left(-\frac{\ell^2}{2TmR^2}\right) \tag{A.10}$$

For particles of spin $\frac{1}{2}$, the sums in the expressions (A.5) and (A.6) are:

$$\sum_{S_i = \begin{cases} 0 \text{ for even nuclei} \\ 1/2 \text{ for odd nuclei} \end{cases}} \sum_{j=|S_i - S_{i-1}|}^{S_i + S_{i+1}} \sum_{\ell = j-\frac{1}{2}}^{j+\frac{1}{2}}$$

For each j the l summation yields

$$\sum_{\ell = j-\frac{1}{2}}^{j+\frac{1}{2}} \exp\left(-\frac{\ell^2}{2\tau m R^2}\right) = \exp\left(-\frac{(j-\frac{1}{2})^2}{2\tau m R^2}\right) + \exp\left(-\frac{(j+\frac{1}{2})^2}{2\tau m R^2}\right)$$

$$= \exp\left(-\frac{1}{8\tau m R^2}\right) \exp\left(-\frac{j^2}{2\tau m R^2}\right) 2\cosh\left(\frac{j}{2\tau m R^2}\right)$$

$$= \exp\left(-\frac{1}{8\tau m R^2}\right) \exp\left(-\frac{j^2}{2\tau m R^2}\right) \left[2 + \frac{j^2}{(2\tau m R^2)^2} + \dots\right] \qquad \text{(A.11)}$$

Finally, the factors containing the spin magnitude S_i in (A.8) are approximated:

$$\frac{2S_i+1}{2S_{i-1}+1} \exp\left(-\frac{(S_{i-1}+\Delta_i)^2 - S_{i-1}^2}{2\tau J}\right) \approx \left(1 + \frac{\Delta_i}{S_{i-1}}\right) \exp\left(-\frac{2S_{i-1}\Delta_i + \Delta_i^2}{2\tau J}\right)$$

$$= 1 - \left(\frac{S_{i-1}}{\tau J} - \frac{1}{S_{i-1}}\right)\Delta_i + \frac{1}{2}\left(\frac{S_{i-1}^2}{\tau^2 J^2} - \frac{3}{\tau J}\right)\Delta_i^2$$

$$- \frac{1}{6}\left(\frac{S_{i-1}^3}{\tau^3 J^3} - \frac{6S_{i-1}}{\tau^2 J^2} + \frac{3}{\tau J S_{i-1}}\right)\Delta_i^3 + \dots \qquad \text{(A.12)}$$

The summations over S_i and j can be interchanged:

$$\sum_{S_i = \begin{cases} 0 \\ 1/2 \end{cases}} \sum_{j=|S_i - S_{i-1}|}^{S_i + S_{i+1}} = \sum_{j=1/2}^{\infty} \sum_{\Delta_i = \max(-j, -S_{i-1})}^{j} \approx \sum_{j=\frac{1}{2}}^{\infty} \sum_{\Delta_i = -j}^{j} \qquad \text{(A.13)}$$

Defining the following variables and constants

$$x \equiv j\,, \quad y \equiv \Delta_i\,, \quad b_0 \equiv \frac{1}{2\tau m R^2}\,, \quad b_1 \equiv -\left(\frac{S_{i-1}}{\tau j} - \frac{1}{S_{i-1}}\right),$$
$$b_2 \equiv \frac{1}{2}\left(\frac{S_{i-1}}{\tau^2 j^2} - \frac{3}{\tau j}\right), \quad b_3 \equiv -\frac{1}{6}\left(\frac{S_{i-1}^3}{\tau^3 j^3} - \frac{6\,S_{i-1}}{\tau j} + \frac{3}{\tau j S_{i-1}}\right) \tag{A.14}$$

we replace the sums over j and Δ_i by integrals, and combining the factors (A.11) and (A.12), except for common factors, we then obtain:

$$\left\{\begin{array}{l} \text{norm} \\ \text{norm} * \langle S_i - S_{i-1} \rangle \\ \text{norm} * \langle (S_i - S_{i-1})^2 \rangle \\ \text{norm} * \langle j^2 \rangle \end{array}\right\}$$

$$= \int_{\frac{1}{2}}^{\infty} dx\, \exp(-b_0 x^2)(2 + b_0^2 x^2 + \cdots) \int_{-x}^{x} dy \left\{\begin{array}{c} 1 \\ y \\ y^2 \\ x^2 \end{array}\right\} (1 + b_1 y + b_2 y^2 + b_3 y^3 + \ldots) \tag{A.15}$$

where norm (the normalisation) represents the numerator in expression (A.6). The integrals are elementary:

$$\left\{\begin{array}{l} \text{norm} \\ \text{norm} * \langle S_i - S_{i-1} \rangle \\ \text{norm} * \langle (S_i - S_{i-1})^2 \rangle \\ \text{norm} * \langle j^2 \rangle \end{array}\right\} = \frac{2}{b_0} \left\{\begin{array}{l} 1 + \frac{b_0}{2} + \frac{b_2}{3b_0} + \frac{b_2}{3} + \cdots \\ \frac{b_1}{3b_0} + \frac{b_1}{3} + \frac{2b_3}{5b_0^2} + \cdots \\ \frac{1}{3b_0} + \frac{1}{3} + \frac{2b_2}{5b_0^2} + \cdots \\ \frac{1}{b_0} + 1 + \frac{2b_2}{3b_0^2} + \cdots \end{array}\right\} - \left\{\begin{array}{l} \frac{1}{2} + \cdots \\ \cdots \\ \cdots \\ \cdots \end{array}\right\} \tag{A.16}$$

Here the last column is due to the lower integration limit being $\frac{1}{2}$ instead of 0.

Keeping the main terms plus the first order terms in the small parameters b_o, $\frac{b_2}{b_o}$, and $\left(\frac{S_{i-1}^2}{\tau \mathfrak{J}}\right)^{-1}$, we obtain

$$\langle \Delta_i \rangle = \langle S_i - S_{i-1} \rangle = -\frac{2}{3}\frac{mR^2}{\mathfrak{J}} S_{i-1}\left(1 + \frac{1}{15}\frac{S_{i-1}^2}{\tau \mathfrak{J}}\frac{mR^2}{\mathfrak{J}}\right) + \frac{2}{3}\frac{\tau m R^2}{S_{i-1}} - \frac{S_{i-1}}{4\tau \mathfrak{J}}$$

$$\langle (S_i - S_{i-1})^2 \rangle = \frac{2}{3}\tau m R^2\left(1 + \frac{13}{15}\frac{S_{i-1}^2}{\tau \mathfrak{J}}\frac{mR^2}{\mathfrak{J}}\right) + \frac{1}{4}$$

$$\langle j^2 - (S_i - S_{i-1})^2 \rangle = \frac{4}{3}\tau m R^2\left(1 + \frac{1}{15}\frac{S_{i-1}^2}{\tau \mathfrak{J}}\frac{mR^2}{\mathfrak{J}}\right) + \frac{1}{2}$$

$$\begin{aligned} \sigma_i^2 &= \langle (S_i - S_{i-1})^2 \rangle - \langle S_i - S_{i-1} \rangle^2 \\ &= \frac{2}{3}\tau m R^2\left(1 + \frac{1}{5}\frac{S_{i-1}^2}{\tau \mathfrak{J}}\frac{mR^2}{\mathfrak{J}}\right) + \frac{1}{4} \end{aligned} \tag{A.17}$$

In these expressions, the second terms in the parentheses are of the order $\frac{b_2}{b_o}$. The expansion of the result as a power series in this parameter, assuming

$$\frac{b_2}{b_o} \approx \frac{S_{i-1}^2}{\tau \mathfrak{J}}\frac{mR^2}{\mathfrak{J}} < 1 \tag{A.18}$$

is the most severe approximation done. For a heavy nucleus, $A > 100$, the relation (A.18) is valid, except at the last few steps of a neutron cascade at the highest angular momenta.

Looking in more detail at the change in the angular momentum $\langle S_i - S_{i-1} \rangle$, the first term (except for the above mentioned corrections of the order b_2/b_o) comes from the orbital motion of the neutron. It can be

interpreted classically as the average angular momentum of a neutron placed randomly on the surface of the nucleus at the effective barrier radius and following the overall classical rotation of the nucleus. The second term, which diverges for $S_{i-1} = 0$, comes from the factor $2S_i + 1$ in the level density. The last term is due to the spin $\frac{1}{2}$ of the neutron. Relative to emission of a spinless particle with the angular momentum sequence $S_{i-1}, 1, S_i$, the spin $\frac{1}{2}$ gives two possibilities of the daughter nucleus angular momentum, adding or subtracting $\frac{1}{2}$. The relative probability for addition or subtraction is given by the different level densities at $S_i - \frac{1}{2}$ and $S_i + \frac{1}{2}$. Expanding the level density around S_i, the average change in the angular momentum introduced by the spin is then

$$\left[-\frac{1}{2}\exp\left(-\frac{(S_i-\frac{1}{2})^2}{2\tau\mathcal{J}}\right) + \frac{1}{2}\exp\left(-\frac{(S_i+\frac{1}{2})^2}{2\tau\mathcal{J}}\right)\right]\left[\exp\left(-\frac{(S_i-\frac{1}{2})^2}{2\tau\mathcal{J}}\right) + \exp\left(-\frac{(S_i+\frac{1}{2})^2}{2\tau\mathcal{J}}\right)\right]^{-1}$$

$$= -\frac{1}{2}\tanh\left(\frac{S_i}{2\tau\mathcal{J}}\right) \approx -\frac{1}{4}\frac{S_i}{\tau\mathcal{J}} \approx -\frac{1}{4}\frac{S_{i-1}}{\tau\mathcal{J}} \qquad \text{(A.19)}$$

Inserting the results (A.17) into expressions (A.3) and (A.4), and keeping the main terms, we obtain for the changes in the average spin magnitude and of the tensors:

$$\langle S_i \rangle \approx S_{i-1}\left(1 - \frac{2}{3}\frac{mR^2}{\mathcal{J}} - \frac{1}{4\tau\mathcal{J}} + \frac{2}{3}\frac{\tau mR^2}{S_{i-1}^2}\right)$$

$$\left\langle P_2\left(\frac{\vec{S}_i \cdot \overleftarrow{S}_{i-1}}{S_i S_{i-1}}\right)\right\rangle \approx 1 - \frac{2\tau mR^2}{S_{i-1}^2} - \frac{3}{4S_{i-1}^2}$$

$$\left\langle P_4\left(\frac{\vec{S}_i \cdot \overleftarrow{S}_{i-1}}{S_i S_{i-1}}\right)\right\rangle \approx 1 - \frac{20}{3}\frac{\tau mR^2}{S_{i-1}^2} - \frac{5}{2S_{i-1}^2} \qquad \text{(A.20)}$$

The change in angular momentum due to the evaporation of neutrons has also been considered by Blau and Moretto.[34] When the condition (A.18) is fulfilled, the first two terms of their expression read

$$\langle S_i \rangle \approx S_{i-1} \left[1 - \frac{2}{3} \frac{mR^2}{\mathfrak{J} + mR^2} \left(1 + \frac{1}{15} \frac{S_{i-1}^2}{\tau(\mathfrak{J} + mR^2)} \frac{mR^2}{\mathfrak{J} + mR^2} \right) \right] \quad \text{(A.21)}$$

which is very similar to our result. Also our expression for the change in the tensors of second order can be related to their expressions in the same way.

One advantage of the present derivation relative to the derivation by Blau and Moretto is that it is more direct and compact. Another advantage is that it rests upon the traditional detailed balance principle, which has been implemented in statistical decay codes and used to discuss data and determine parameters for level densities.[35] This permits a direct comparison between our expressions and the results of statistical decay code calculations, as we will show below.

The treatment by Blau and Moretto, on the other hand, is more general and can be applied for the emission of large fragments also. The occurrence of the moment of inertia of $\mathfrak{J} + mR^2$ of the transition shape instead of just the moment of inertia of the daughter nucleus, is thus more correct.

The temperature changes down a decay chain. Assuming that each neutron roughly takes away the same amount of energy, a summation over decay steps can be replaced by an integral over the excitation energy of the daughter nuclei. The highest excitation energy is the one in the first daughter nucleus, E_1, and by τ_1 we denote the corresponding temperature. For a complete neutron decay chain down to the entry line for γ- decay, the lowest excitation energy above the yrast line in the daughter nucleus is zero. Inserting these limits, we obtain for a complete decay chain:

$$\langle \tau \rangle_{\text{decay chain}} \cong \int_0^{E_1} \sqrt{\frac{E}{a}}\, dE \Big/ \int_0^{E_1} dE = \frac{2}{3}\sqrt{\frac{E_1}{a}} = \frac{2}{3}\tau_1$$

$$\left\langle \frac{1}{\tau} \right\rangle_{\text{decay chain}} \cong \int_0^{E_1} \sqrt{\frac{a}{E}}\, dE \Big/ \int_0^{E_1} dE = \frac{2}{\tau_1} \tag{A.22}$$

By repeated use of the addition theorem for spherical harmonics, we obtain the following approximate result, for $\lambda = 2,4$

$$\left\langle P_\lambda\left(\frac{\vec{S}_0 \cdot \overleftarrow{S}_n}{S_0 S_n}\right)\right\rangle$$

$$\approx \left\langle P_\lambda\left(\frac{\vec{S}_0 \cdot \overleftarrow{S}_1}{S_0 S_1}\right)\right\rangle \left\langle P_\lambda\left(\frac{\langle \vec{S}_1 \rangle \cdot \overleftarrow{S}_2}{\langle S_1 \rangle S_2}\right)\right\rangle \cdots \left\langle P_\lambda\left(\frac{\langle \vec{S}_{n-1} \rangle \cdot \overleftarrow{S}_n}{\langle S_{n-1} \rangle S_n}\right)\right\rangle \tag{A.23}$$

Products of the above type, where the factors differ little from unity, may to a good approximation be replaced by exponential functions. Therefore,

$$\langle S_n \rangle \approx S_0 \exp\left[-n\left(\frac{2}{3}\frac{mR^2}{\mathfrak{J}} + \frac{\hbar^2}{2\mathfrak{J}\tau_1} - \frac{4}{9}\frac{mR^2\tau_1}{S_0^2}\right)\right]$$

$$\left\langle P_2\left(\frac{\vec{S}_0 \cdot \overleftarrow{S}_n}{S_0 S_n}\right)\right\rangle \approx \exp\left[-n\left(\frac{4}{3}\frac{mR^2\tau_1}{S_0\langle S_n \rangle} + \frac{3\hbar^2}{4 S_0 \langle S_n \rangle}\right)\right]$$

$$\left\langle P_4\left(\frac{\vec{S}_0 \cdot \overleftarrow{S}_n}{S_0 S_n}\right)\right\rangle \approx \exp\left[-n\left(\frac{40}{9}\frac{mR^2\tau_1}{S_0\langle S_n \rangle} + \frac{5\hbar^2}{2 S_0 \langle S_n \rangle}\right)\right] \tag{A.24}$$

The amount of excitation energy removed by neutrons is equal to the original excitation energy minus the entry energy in the last daughter nucleus. The average entry energy is approximately equal to the yrast energy plus half a neutron binding energy. The average excitation energy taken away by the i'th neutron is equal to $B + 2\tau_i$, B being the neutron binding energy and τ_i being the temperature in the i'th daughter nucleus. So the average number of neutrons emitted is

$$n \approx \left(E_0 - \frac{S_0^2}{2\mathfrak{J}} - \frac{B}{2}\right)\left(B + \frac{4}{3}\tau_1\right)^{-1} \tag{A.25}$$

where the temperature in the first daughter nucleus is given by

$$\tau_1 \approx \sqrt{\frac{E_0 - \frac{S_0^2}{2\mathfrak{J}} - B}{a}} \tag{A.26}$$

In accordance with the approximative treatment of level densities and transmission coefficients some approximations have been made for the calculation of n and τ_1. Thus the yrast energies in both (A.25) and (A.26) are just represented by the original yrast energy at spin S_0 in the nucleus leaving the collision, and the average energy removed by the first neutron in (A.26) is just represented by B instead of $B - 2\tau_1$.

The application of the expressions (A.24) to (A.26) requires four parameters to be inserted, B, mR^2, $\mathfrak{J}$, a. Of these, the binding energy B can be taken directly from tables.

The level density constant a and the moment of inertia $\mathfrak{J}$ enter the expressions through the approximation (A.8) to the level density around some set of values. For energies not too close to the yrast line, the approximation is very accurate over a quite wide range of energies and angular momenta, both for numerically calculated level densities on the basis of independent particle levels, and for standard analytic expressions for the level density. Often the effect of shell structure in the single particle levels and the pairing energy are taken into account in terms of one additional parameter besides a and $\mathfrak{J}$ for calculating the analytic level density, namely the back shift energy. For the high exictation energies and angular momenta we are mainly interested in here, the back shift should just

be subtracted from the energy E_0 in the calculating of the temperature, and this does not affect the quality of the approximation (A.8).

The effective barrier radius R enters the expressions (A.24) to (A.26) through the sharp cut-off approximation to the transmission coefficient. The calculation of optical potential transmission coefficients is, in contrast to the calculation of level densities, rather involved, and the sharp cut-off approximation is crude.

To be able to use the analytic expressions (A.24) to (A.26), we therefore determine the effective barrier radius R by fitting the values of $\langle\Delta_1\rangle$ and σ_1^2 (A.17) to calculations by a statistical decay code.

We use the statistical decay code GROGI 2, and perform the calculation for nuclei with mass number $A = 50, 100, 150, 200$ and with various excitation energies and angular momenta. In the calculation we apply the level density constant as A/(9 MeV) and the moment of inertia for rigid rotation of a spherically symmetric mass distribution with rms radius $1.25\ A^{1/3}$fm. These values are in accordance with experiments for nuclei in the mass range around 60.[35] The optical potential for neutrons is, apart from inessential details, the one used in the newly developed code MBII.[36] Table A.1 gives the parameters for the optical potential.

Figure A.1 shows the result of the statistical decay code calculation together with the results of expressions (A.17) for $\langle\Delta_1\rangle$ and σ_1^2, using the value $R = 1.95\ A^{1/3}$ for the effective barrier radius. For the neutron binding energy a common value was inserted in (A.25) and (A.26). So, the four parameters are:

$$a = \frac{A}{9}\ \mathrm{MeV}^{-1}$$

$$\mathcal{J} = 0.015\ A^{5/3}\ \mathrm{MeV}\cdot\hbar^2$$

$$mR^2 = 0.091\ A^{2/3}\ \mathrm{MeV}\cdot\hbar^2$$

$$B = 8\ \mathrm{MeV} \qquad \text{(A.27)}$$

The figure displays a consistency beeween the two analytic expressions for $\langle\Delta_1\rangle$ and σ_1^2, and shows that the analytic expressions with an overall common value for R proportional to $A^{1/3}$ accounts well for the result of the statistical calculation.

By enforcing a common value proportional to $A^{1/3}$ for the barrier radius, we neglect some dependencies upon the excitation energy and the mass number. With individual fits of R to the statistical code calculation, the coefficient in front of $A^{1/3}$ in the effective barrier radius will show a decrease with increasing excitation energy and a slight decrease with increasing mass number.

Appendix B.

In this appendix we discuss the fission decay probabilities and angular distribution coefficients, taking into account fission in competition with neutron emission in all decay steps.

First we give a description of our schematic calculation scheme. For given excitation energy and spin E_{i-1}, S_{i-1} in the i'th decay step, the temperature τ is calculated at energy and angular momentum $E_{i-1} - B_n$, S_{i-1} according to the expression (A.9). Next, the ratio between the fission probability and the neutron decay probability is calculated according to (4.22). For fission the angular distribution coefficients (4.19) are calculated, multiplied by the dealignment factors, (A.20) accumulated along the previous decay steps. The angular momentum in the i'th daughter nucleus is picked at random from a gaussian distribution with first and second moments given by the main terms of (A.17). The kinetic energy of the neutron ε is then calculated in two steps. First the orbital angular momentum l of the neutron is picked randomly according to the distribution $\exp(-l^2/2\,\tau m R^2)$ and with lower limit $|S_i - S_{i-1}|$. This neglects the spin 1/2 of the neutron. Secondly the energy is picked according to the distribution $\exp(-\frac{\varepsilon}{\tau})$, with a lower limit given by $l^2/2\,mR^2$. In this way it is assured that the average neutron kinetic energy is approximately twice the temperature. Each particular decay chain simulation is stopped at the i-1'th step if the average excitation energy in the i'th nucleus, $E_i - B_n - 2\tau$ would drop below the yrast energy in the i'th nucleus for spin S_{i-1}. This is a crude way of taking into account the takeover of the decay by γ-rays close to the yrast line.

The total fission probability and angular distribution coefficients for given excitation energy and spin E , S_0 is found by averaging over the accumulated simulations of decay chains.

The parameters entering the calculations are of three types. First we need the level density parameters a_n and a_f, which we typically take as A/10 MeV^{-1}, A being the mass number. Secondly, we need the smooth neutron binding energy B_n and fission barrier B_f, together with their variation down the neutron decay steps for which we just include a linear dependence with the derivatives $\frac{dB_n}{d(-N)}$, $\frac{dB_f}{d(-N)}$. Finally the effective moments of inertia must be specified, $\mathcal{J}_e$ for the neutron-to-fission competition, $\mathcal{J}_{eff}$ for the fission saddle shapes and mR^2 for the neutron at the barrier radius. For mR^2 we use the parameter (A.27) determined in Appendix A.

The parameter values not already specified are derived from the liquid drop model, with the Lysekil parameters. This readily yields the neutron separation energies, and the fission barriers and moments of inertia of the saddle shapes are calculated by using figures from ref. [10]. The moments of inertia change with increasing spin, and we use the average of the two values obtained at spin 20 and 50. For the moment of inertia of the daughter nucleus after neutron emission, we use the value (A.27) for spherical nuclei.

To test the calculation against more complete calculations, which include barrier penetration and which do not approximate the level densities as crudely as we do, we apply the present calculation scheme to the well studied case of fission of the nucleus ^{198}Pb as formed in fusion reactions of ^{182}W with ^{16}O at various bombarding energies. Taking into account the shell correction energy of ^{198}Pb, which is approximately -5 MeV, we obtain the

values $E^* = 50$ MeV and 73 MeV for the excitation energy above the liquid drop model ground state for the lowest and highest bombarding energies of 90 MeV and 117 MeV, respectively.

Figure B1 shows the fission probability and angular distribution coefficients for these two extreme values of the excitation energy as function of angular momentum for the whole cascade and for the first decay step only. It is apparent from the figure that it is important to take into account fission at all decay steps, especially for the fission probability. The angular distribution coefficients obtained for the first stop only, on the other hand, deviate from those obtained for an entire cascade by less than 25 percent in most cases.

The fission probabilities display an almost step-like behavior, being small and almost constant for the small spins and rising sharply within a rather narrow interval towards the asymptotic value of one. For an entire angular momentum distribution corresponding to a compound nucleus formed in a fusion reaction, almost all the angular momenta above a certain value will go to fission. The properties of the fission probability for the case of a fusion reaction is then best characterized by the average maximum spin S_{ER} remaining in evaporation residues, defined by

$$(S_{ER} + 1)^2 = \sigma_{ER}/\pi\lambda\!\!\!^{-2} = (S_{max} + 1)^2 (1 - P_f)$$

Here σ_{ER} is the evaporation residue cross section, $\lambda\!\!\!^{-}$ is the reduced wavelength in the entrance channel, S_{max} is the maximum angular momentum for fusion, and P_f is the fission probability for the whole distribution.

Figure B2 shows the S_{max} value put into the calculation together with S_{ER} as calculated with our schematic calculation together with the results

of the calculation of ref. [24]. Also shown are the angular distribution coefficients for fission of the entire distribution, defined as

$$\mathcal{B}_\lambda(\text{total}) = \frac{\sum_{S=0}^{S_{max}} (2S+1)\, \mathcal{N}_{fission}(S)\, \mathcal{B}_\lambda(S)}{\sum_{S=0}^{S_{max}} (2S+1)\, \mathcal{N}_{fission}(S)} \tag{B.1}$$

For compound nuclei formed in a fusion reaction between spinless nuclei, the statistical tensors in the classical interpretation (4.2) are independent of the size of the angular momentum and are equal to $\rho_{\lambda\mu}(S) = P_\lambda(0)\delta_{\mu 0}$, and the angular distribution as function of the angle to the beam axis will be

$$\mathcal{W}(\vartheta) = \frac{1}{4\pi} \sum_\lambda \mathcal{B}_\lambda(\text{total})\, P_\lambda(0)\, P_\lambda(\cos\vartheta) \tag{B.2}$$

from which $\mathcal{B}_\lambda$(total) can be extracted from experimental or calculated angular distributions. Taking into account that the scales are quite expanded, our calculation gives a good account of the more detailed calculation.

Our angular distribution coefficients have slightly larger absolute values than those extracted from ref. [24]. This may be related to the neglect of the quite pronounced shell energy in lead-nuclei which, when included, probably would suppress the fission relative to the neutron emission during the latest decay stops.

In ref. [24] the dealignment due to neutrons is not taken into account, and fig. B2 shows that inclusion of the dealignment produces variations of the same order as the deviations between the different parameter sets.

To test the calculation against data, we calculate total angular distribution coefficients for the decay of the nucleus ^{211}Rn, as formed in

fusion of ^{14}N with ^{197}Au[37]. Although these nuclei are not spinless their spins are very small compared to the angular momentum in the compound nucleus, so the relation (B.2) can be applied with good accuracy. Figure B3 shows the angular distribution coefficients extracted from the data of ref. [7] together with our calculated values. The maximum spins for the various excitation energies entering our calculation are taken from ref. [21].

The first chance fission makes a stronger selection of the highest spins than fission including neutron delayed fission. So, although the angular distribution for a definite value of the spin becomes more anisotropic when neutron delayed fission is included, the angular distribution integrated over spin becomes less anisotropic, except for the lowest excitation energy.

Apart from the excitation energy 80 MeV, the calculated values of the total angular distribution coefficients are in very good agreement with data. (The level of agreement may be somewhat fortuitous since the parameters entering the calculation are not that well defined.)

References:

1) R. Albrecht, W. Dünnweber, G. Graw, H. Ho, S. G. Steadman and J. P. Wurm, Phys. Rev. lett. 34 (1975) 1400

2) P. R. Christensen, F. Folkmann, O. Hansen, O. Nathan, N. Trautner. F. Videbaek, S. Y. van der Werf, H. C. Britt, R. P. Chestnut, H. Freiesleben and F. Pühlhofer, Nucl. Phys. A349 (1980) 217;
P. R. Christensen, O. Hansen, O. Nathan, F. Videbaek, H. Freiesleben, H. C. Britt and S. Y. van der Werf, Nucl. Phys. A390 (1982) 336; and references therein

3) A. Olmi, H. Sann, D. Pelte, Y. Eyal, A. Gobbi, W. Kohl, U. Lynen, G. Rudolf, M. Stelzer, and R. Bock, Phys. Rev. Lett 41 (1978) 688

4) R. J. McDonald, A. J. Pacheco, G. J. Wozniak, H. H. Bolotin, L. G. Moretto, C. Schuck, S. Shih, R. M. Diamond and F. S. Stephens, Nucl. Phys A373 (1982)54, and references therein

5) W. Trautmann, J. de Boer, W. Dünnweber, G. Graw, R. Kopp, C. Lauterbach, H. Puchta, and U. Lynen, Phys. Rev. Lett. 39 (1977) 1062

6) P. Dyer, R. J. Puigh, R. Vandenbosch, T. D. Thomas, M. S. Zisman and L. Nunnelly, Nucl. Phys. A322 (1979) 205;

R. J. Puigh, P. Dyer, R. Vandenbosch, T. D. Thomas, L. Nunnelley and M. S. Zisman, Phys. lett. 86B (1979) 24

7) D. von Harrach, P. Glässel, Y. Civelekoglu, R. Männer and H.J. Specht, Phys. Rev. lett. 42 (1979) 1728

8) B. B. Back, H.-G. Clerc, R. R. Betts, B. G. Glagola and B. D. Wilkins, Phys. Rev. Lett. 46 (1981) 1068

9) P. Glässel, D. von Harrach, Y. Civelekoglu, R. Männer, H. J. Specht, J. B. Wilhelmy, H. Freiesleben and K. D. Hildenbrand, Phys. Rev. Lett. 43 (1979) 1783

10) S. Cohen, F. Plasil and W. J. Swiatecki, Ann. of Phys. 82 (1974)557

11) L. G. Moretto, S. Blau and A. Pacheco, Nucl. Phys. A364 (1981) 125

12) T. Døssing, Nucl. Phys. A357 (1981) 488

13) T. Døssing, in Proc. Nucl. Phys. Workshop, held at the ICTP, Trieste, Eds. C. H. Dasso, R. A. Broglia, and A. Winther, (North-Holland, Amsterdam, 1982)

14) J. Randrup, Nucl. Phys. A383 (1983) 468, Appendix B

15) J. B. Natowitz, M.N. Namboodiri, P. Kasiraj, R. Eggers, L. Adler, P. Gonthier, C. Cerruti, and T. Alleman, Phys. Rev. Lett 40 (1978) 751

16) M. A. Deleplanque, Th. Byrski, R. M. Diamond, H. Hubel, F. S. Stephens, B. Herskind, and R. Bauer, Phys. Rev. Lett. 41 (1978) 1105

17) M. A. Deleplanque, I. Y. Lee, F. S. Stephens, R. M. Diamond and M. M. Aleonard, Phys. Rev. Lett. 40 (1978) 629

18) B. Herskind (1982) private communication

19) M. A. Deleplanque, H. J. Korner, H. Kluge, A. O Machiavelli, N. Bendjaballah, R. M. Diamond and F. S. Stephens, Phys. Rev. Lett 50 (1983) 409

20) H. J. Körner, D. L. Hillis, C. P. Roulet, P. Aguer, C. Ellegaard, D. B. Fossan, D. Habs, M. Neiman, F. S. Stephens and R. M. Diamond, Phys. Rev. Lett. 43 (1979) 490

21) L. C. Vaz and J. M. Alexander, Phys. Reports 97 (1983) 1

22) W. Swiatecki, Aust. J. Phys. 36 (1983) 641

23) S. Bjørnholm, A. Bohr and B. R. Mottelson, Proc. Int. Symp. on Physics and Chemistry of Fission (IAEA, Vienna, 1974), Vol. I, p. 373

24) J. U. Andersen, A. S. Jensen, K. Jørgensen, E. Laegsgaard, K. O. Nielsen, J. S. Forster, J. V. Mitchell, D. Ward, W. M. Gibson and J. J. Cuomo, Kgl. Dan. Vid. Selsk. Mat. Fys. Medd. 40, No. 7 (1980)

25) W. D. Myers and W. J. Swiatecki, Ark. Fys. 36 (1967) 343

26) W. D. Myers, Droplet Model of Atomic Nuclei (Plenum, New York, 1977)

27) P. Möller and J. R. Nix, Atomic Data and Nucl. Data Tab. 26 (1981) 165

28) A. J. Sierk, (1983) private communication

29) C. Le Brun, J. F. Lecolley, F. Lefebures, M. L' Haridon, A. Osmont, J. P. Patry and J. C. Steckmeyer, in Proc. XX Int. Winter Meeting on Nucl. Phys. Bornio, Italy, January 1982 (University of Milano, 1982)

30) J. Randrup, Nucl. Phys. A383 (1983) 468

31) R. Vandenbosch, (1983) private communication

32) A. Lazzarini, (1983) private communication

33) L. G. Moretto et al., to be published

34) S. K. Blau and L. G. Moretto, Nucl. Phys. A359 (1981) 477

35) C. C. Lu, L. C. Vaz and J. R. Huizenga, Nucl. Phys. A190 (1972) 229; ibid. A197 (1972) 321

36) B. Sikora, W. Scobel, M. Beckerman and M. Blann, Phys. Rev. C25 (1982) 1446; and references therein

37) V. E. Viola, Jr., T. D. Thomas and G. T. Seaborg, Phys. Rev. 129 (1963) 2710

Table Caption

Table 1 a_n and a_f denote the level density constants the for first decay step for the fission and neutron decay, respectively. $\tilde{B}_n$ and $\tilde{B}_f$ denote the smooth (excluding shell energies and odd-even mass differences) neutron separation energy and fission barrier, respectively, and $\frac{d\tilde{B}_n}{d(-N)}$ and $\frac{d\tilde{B}_f}{d(-N)}$ denote their changes per step in a neutron cascade. $\mathcal{J}_\perp/\mathcal{J}_{sph}$ and $\mathcal{J}_\parallel/\mathcal{J}_{sph}$ denote the moments of inertia of the saddle shape relative to a spherical nucleus. The moment of inertia for a spherical nucleus is $\mathcal{J}_{sph}$ and mR^2 is the effective moment of inertia of a neutron at the barrier radius for the first step of the decay. The parameters a_n, a_f, $\mathcal{J}_{sph}$ and mR^2 are chosen according to standard prescriptions identical for all parameter sets, and they scale slightly with the decreasing mass along the neutron decay cascade. The parameters are extracted from refs. [10,25-28]. The authors are grateful to Arnold J. Sierk for providing the fission barriers and moments of inertia shown in the third column.

Table 1

Fission parameters for ^{208}Po

Parameter	Liquid drop model Lysekil parameters	Droplet model	Yukawa plus Exponential
$a_n (MeV^{-1})$	20.7	20.7	20.7
$a_f (MeV^{-1})$	20.8	20.8	20.8
$\tilde{B}_n$ (MeV)	7.10	6.98	6.81
$\frac{d\tilde{B}_n}{d(-N)}$ (MeV)	0.15	0.14	0.15
$\tilde{B}_f$ (MeV)	11.3	11.06	10.2
$\frac{d\tilde{B}_f}{d(-N)}$ (MeV)	-0.19	0.05	-0.14
$\frac{\mathcal{J}_\perp}{\mathcal{J}_{sph}}$	2.34	2.4	2.39
$\frac{\mathcal{J}_\parallel}{\mathcal{J}_{sph}}$	0.52	0.5	0.55
$\mathcal{J}_{sph}$ $(MeV \cdot \hbar^2)$	109.5	109.5	109.5
mR_n^2 $(MeV \cdot \hbar^2)$	3.19	3.19	3.19

Table A 1 Optical potential parameters for neutrons employed in the calculations with the statistical decay code GROGI2. The parameters are essentially the same as those employed in the code MBII[36]. The depth of the central potential is obtained by inserting a neutron kinetic energy ε_n = 4 MeV into the energy dependent potential depth $V = 47.01 - 0.267\ \varepsilon_n$, employed in MBII, and similarly for the depth of the imaginary potential.

Table A 1

Optical potential parameters for neutrons

Mass	Real Potential			Imaginary Potential			Spin-Orbit Potential		
	V	r_V	a_V	W	r_W	a_W	V_{so}	r_{so}	a_{so}
A = 50	46.00	1.293	0.66	9.30	1.252	0.48	7.00	1.252	0.48
A = 100	46.00	1.278	0.66	9.30	1.245	0.48	7.00	1.245	0.48
A = 150	46.00	1.271	0.66	9.30	1.242	0.48	7.00	1.242	0.48
A = 200	46.00	1.266	0.66	9.30	1.240	0.48	7.00	1.240	0.48

Table B 1 See caption to Table 1 for the definitions of symbols. Parameter set II and the level density constants for both parameter sets are taken from ref.[24].

Table B 1

Fission parameters for ^{198}Pb

Parameter	Liquid drop model Lysekil parameters	Parameter set II
$a_n(MeV^{-1})$	20.74	20.74
$a_f(MeV^{-1})$	20.84	20.84
$\tilde{B}_n(MeV)$	8.00	8.00
$\frac{d\tilde{B}_n}{d(-N)}$ (MeV)	0.19	0.19
$\tilde{B}_f$ (MeV)	12.30	11.30
$\frac{d\tilde{B}_f}{d(-N)}$ (MeV)	0.26	0.00
$\frac{\mathcal{J}_\perp}{\mathcal{J}_{sph}}$	2.66	3.13
$\frac{\mathcal{J}_\parallel}{\mathcal{J}_{sph}}$	0.525	0.49
$\mathcal{J}_{sph}$ $(MeV\cdot\hbar^2)$	100.9	93.4
mR^2 $(MeV\cdot\hbar^2)$	3.09	3.09

Figure Captions

Fig. 1 Illustration of the spherical geometry relevant for describing the change in the directional distribution of the spin caused by the emission of the i'th unobserved decay product.

Fig. 2 Number of decay products and the angular distribution coefficients for bump region γ-rays (full curves, left hand scale) shown together with the averge angular momentum left in the nucleus after neutron evaporation (dashed curves, right hand scale), calculated as function of angular momentum for the deformed nucleus ^{165}Ho at three different exictation energies. The value 1.2 is used for the parameter $\mathcal{N}_{stat}$, denoting the number of isotropic statistical γ-rays within the bump region (cf. eq. (4.16)).

Fig. 3 Decay probability and angular distribution coefficients calculated as functions of angular momentum for fission of the nucleus ^{208}Po at three different excitation energies. The parameters from the three columns of table 1 were applied in the calculation for the three columns of the figure.

Fig. 4a Average spin magnitude $\langle S \rangle$ and dispersion σ_S as functions of TKEL for the reaction 610 MeV $^{86}Kr + ^{154}Sm$. The dashed lines correspond to calculated spin distributions right after the collision, and the full curves include the correction for neutron emission prior to the emission of γ-rays. The data points are extracted from the

γ-multiplicity data of ref.[2] using the following relations between spin magnitude moments and γ multiplicity moments: $\langle S \rangle = 2(\langle M_\gamma \rangle - 3)$ (open circles), $\langle S \rangle = 1.6 \langle M_\gamma \rangle$ (solid circles), $\sigma_S = 2\sigma_{M_\gamma}$ (open triangles), $\sigma_S = 1.6\ \sigma_{M_\gamma}$ (solid triangles). The TKEL of the data points has been corrected for neutron evaporation, which decreases the kinetic energy of the krypton-like nucleus prior to its measurement.

Fig. 4b Same as fig. 4a, for the smaller bombarding energy 490 MeV.

Fig. 5 Average spin magnitude (top) and out of plane anisotropy of bump region γ-rays with energies between 600 and 1200 keV (bottom), shown as functions of TKEL for the reaction 1400 MeV $^{165}Ho + ^{165}Ho$. The dashed curves correspond to calculated spin distributions right after the collision, and the full curves include a correction for neutron evaporation prior to the γ-ray emission. The data points are taken directly from ref. [4].

Fig. 6 Average value and dispersion of the spin magnitude (top) shown together with the values of statistical tensors (bottom), calculated for the heavy nucleus as functions of TKEL for the reactions 7.5 MeV/n $^{208}Pb + ^{58}Ni$, ^{90}Zr. The data points and arrows denote absolute lower limits to the alignment P_{YY} extracted from data as described in the text.

Fig. 7 Polar angle dispersion (top) and fission probability (bottom) as functions of TKEL for fission of the heavy nucleus produced in the reactions 7.5 MeV/n ^{208}Pb + ^{58}Ni, ^{90}Zr. The curves labelled a, b and c are calculated with the theoretical values for the averge mass and charge of the heavy nucleus, corresponding to small, medium and maximum TKEL, respectively, and the curves are fully drawn in that region of TKEL where they apply. The data are from ref.[7].

Fig. 8 Same as fig. 6, but now with ^{238}U as the projectile.

Fig. 9 Same as fig. 7, but now with ^{238}U as the projectile. The crosses show polar angle dispersions as obtained with the precession determined angular correlation (see section 5.5).

Fig. 10 Angular correlation in the reaction plane for fission of the heavy nucleus produced in the reactions 610 MeV ^{86}Kr + ^{209}Bi and 730 MeV ^{86}Kr + ^{238}U. $\varphi = 90°$ corresponds to the beam axis. The open arrow for each TKEL shows the target recoil direction in the lab-frame and the solid arrows point to the directions of principal axes of the in-plane components of the spin variance tenser. The data points are taken from refs. [6,31], and they cover an interval 40 MeV wide in TKEL for each data set. Some of the error bars in the left hand part of the figure correspond to the size of the dots in the figure in ref. [6], and should thus actually be somewhat smaller.

Fig. 11 Average value and dispersion of the spin magnitude (top) and alignment (bottom), calculated for the heavy nucleus as function of TKEL for the reactions 1400 MeV $^{165}Ho + ^{165}Ho$, 610 MeV $^{86}Kr + ^{154}Sm$, 7.5 MeV/n $^{238}U + ^{90}Zr$. The maximal TKEL, used to define the relative scale for the energy loss, is picked as 200 MeV for the Kr + Sm and U + Zr reactions and as 340 MeV for the Ho + Ho reaction.

Fig. 12 Average spin magnitude $\langle S \rangle$ and dispersion σ_S as functions of TKEL for the reaction 610 MeV $^{86}Kr + ^{154}Sm$. The data points and the thick full curves are identical to those shown in fig. 4a. The thick full curves show the results of the calculation with the standard prescription for the neck dynamics, and the thin full curves are obtained with the density in the neck equal to half its standard value. Dashed and dot-dashed curves show results obtained with a neck wall dissipation rate determined by the motion of the effective neck radius (instead of the geometric neck radius); the dashed curves are obtained including the standard reduction factor of the neck wall dissipation for elongated neck shapes, whereas this reduction is removed for the results denoted by the dot-dashed curves.

Fig. 13 Contour plots of the ratio between the joint fission angular distribution $P_A(\hat{\alpha},\hat{\beta})$ and the product of the two individual fission angular distributions $p_A(\hat{\alpha})$ and $P_B(\hat{\beta})$, for the reaction 8.5 MeV/n $^{238}U + ^{238}Pb$ at an energy loss of TKEL = 140 MeV. The fission direction $\hat{\beta}$ of the target-like reaction product B has been fixed at either $(\vartheta_\beta = 45^\circ, \varphi_\beta = 60^\circ)$ (a) or $(\vartheta_\beta = 45^\circ, \varphi_\beta = -30^\circ)$ (b) and the ratio is displayed as a function of the fission direction $\hat{\alpha} = (\vartheta_\alpha, \varphi_\alpha)$ for the reaction partner A.

Fig. 14 The absolute joint fission probability $P_{AB}(\hat{\alpha},\hat{\beta})$ for the U + Pb reaction. The direction $\hat{\beta}$ has been fixed at either ($\vartheta_\beta = 45°$, $\varphi_\beta = 60°$) (a) or ($\vartheta_\beta = 45°$, $\varphi_\beta = -30°$) (b), while the direction $\hat{\alpha}$ is moved from the north pole, through the point $\hat{\alpha} = \hat{\beta}$, and down to the south pole. Two energy losses have been considered, TKEL = 140 MeV and 280 Mev. The dashed curves indicate the product of the individual fission probabilities, $P_A(\hat{\alpha})P_B(\hat{\beta})$. The curves have been normalized so that isotropy would yield the value one for all $\hat{\alpha},\hat{\beta}$.

Fig. 15 Effect on the projectile-like fragment spin $\vec{S}^A$ of the bias introduced by detection on target fission fragment in the direction $\hat{\beta}$. The figure shows the distribution of $\vec{S}^A$ projected onto the plane containing the reaction normal (the Y-axis) and fission direction $\hat{\beta}$, which in turn has been chosen as either ($\vartheta_\beta = 45°$, $\varphi_\beta = 60°$) (a) or ($\vartheta_\beta = 45°$, $\varphi_\beta = -30°$) (b), corresponding to the directions considered in figs. 13, 14. The LHS shows the unbiased mean spins and the one-sigma contour for $\vec{S}^A$ while the RHS shows the biased mean spins (6.39) and (6.40) and the associated one-sigma contour (as determined from (6.42)).

Fig. 16 Similar to fig. 14 but calculated with a statistical model. The settings of the fission direction $\hat{\beta}$ correspond approximately to the associated major and minor principal directions and are ($\vartheta_\beta = 45°$, $\varphi_\beta = 0°$) (a) and ($\vartheta_\beta = 45°$, $\varphi_\beta = 90°$) (b).

Fig. A1a Change in average spin magnitude and dispersion caused by the emission of one neutron from typical nuclei of mass number $A = 50$ (left) and $A = 100$ (right), with a sharply defined spin value S_0, shown as function of S_0 for two values of the excitation energy E^*. The full curves result from a calculation with the statistical decay code GROGI 2 with standard parameters, and the dashed and dot-dashed curves result from analytical approximations as developed in the text. The dot-dashed curves present the full result (A.17), whereas the dashed curves present the result without terms of the order of the parameter (A.18).

Fig. A1b Same as fig. A1a, but now for typical nuclei with mass numbers $A = 150$ and $A = 200$.

Fig. B1 Decay probability and angular distribution coefficients calculated as functions of angular momentum for fission of the nucleus ^{198}Pb at two different excitation energies. The dashed curves show the values for the first chance fission and the full curves include also fission delayed by the evaporation of one or more neutrons. The left-hand part of the figure is calculated with the parameters given by the liquid drop model with the Lysekil parameters, whereas the right hand part of the figure is calculated with the parameters used in ref. [24] (cf. Table B.1).

Fig. B2 Upper spin limits (top) and angular distribution coefficients shown as function of the excitation energy in the compound nucleus ^{198}Pb as formed by fusion of ^{182}W with ^{16}O. S_{max} denotes the maximal spin entering the calculation, and S_{ER} denotes the average maximum spin leading to evaporation residues. Circles denote results extracted

from the calculation presented in ref. [24], triangles denote results of the present approximate treatment of the fission, applying the same parameters as in ref. [24], and squares denote results obtained with the parameters given by the liquid drop model with the Lysekil parameters. For the open triangles the dealignment of the spin direction due to neutrons is taken into account, whereas this is ignored for filled symbols.

Fig. B3 Angular distribution coefficients shown as function of the excitation energy in the compound nucleus ^{211}Rn as formed by fusion of ^{197}Au with ^{14}N. Circles show results extracted from the data shown in fig. 4 of ref. [37] Squares denote calculated results obtained by restriction to first chance fission only, whereas fission delayed by neutron evaporation is included in the calculated results denoted by triangles. The dealignment caused by the neutrons is included in the calculation leading to the closed triangles and neglected for the open triangles.

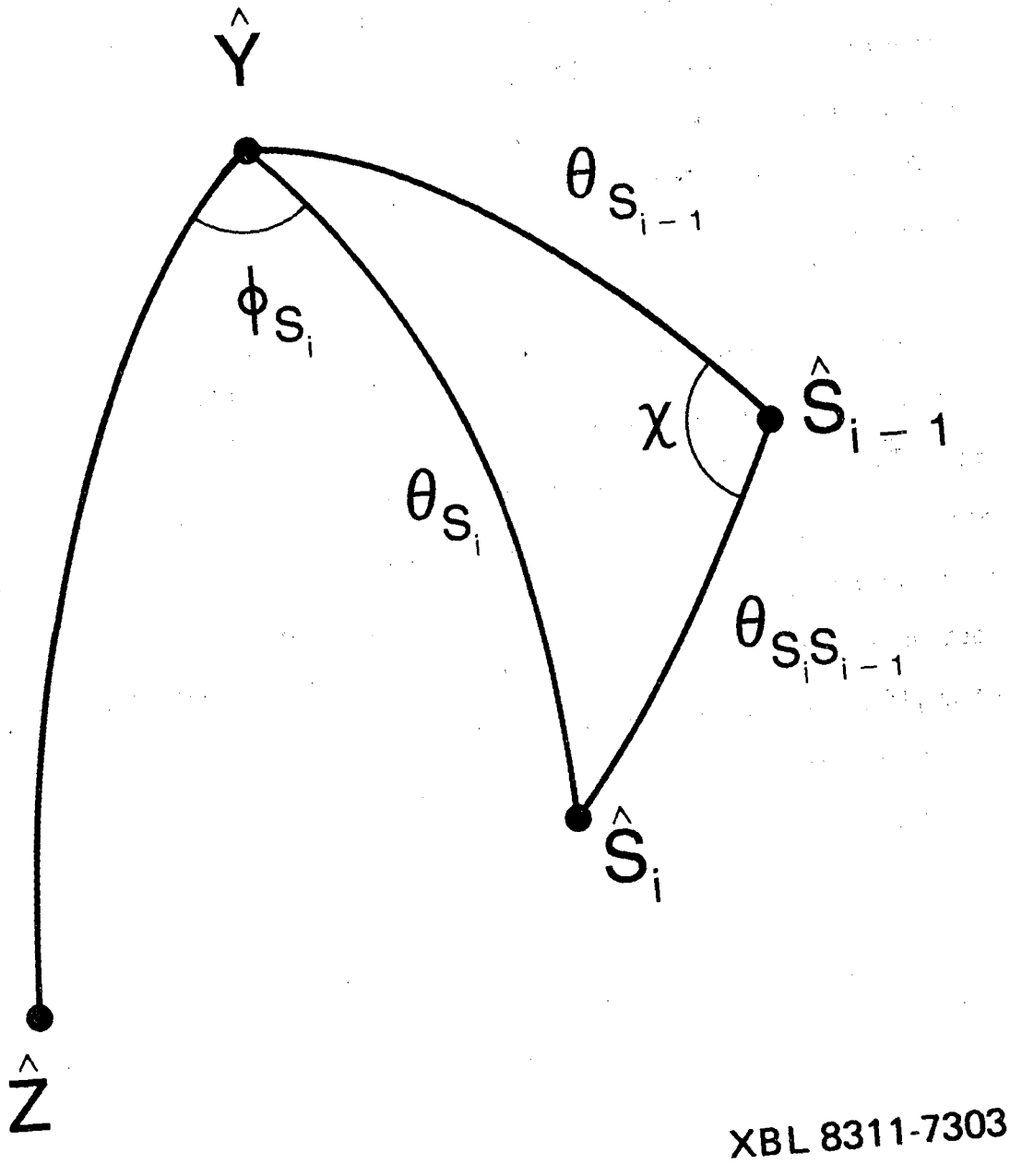
$\hat{Y}$
$\theta_{S_{i-1}}$
ϕ_{S_i}
χ
$\hat{S}_{i-1}$
θ_{S_i}
$\theta_{S_iS_{i-1}}$
$\hat{S}_i$
$\hat{Z}$
XBL 8311-7303

Fig. 1

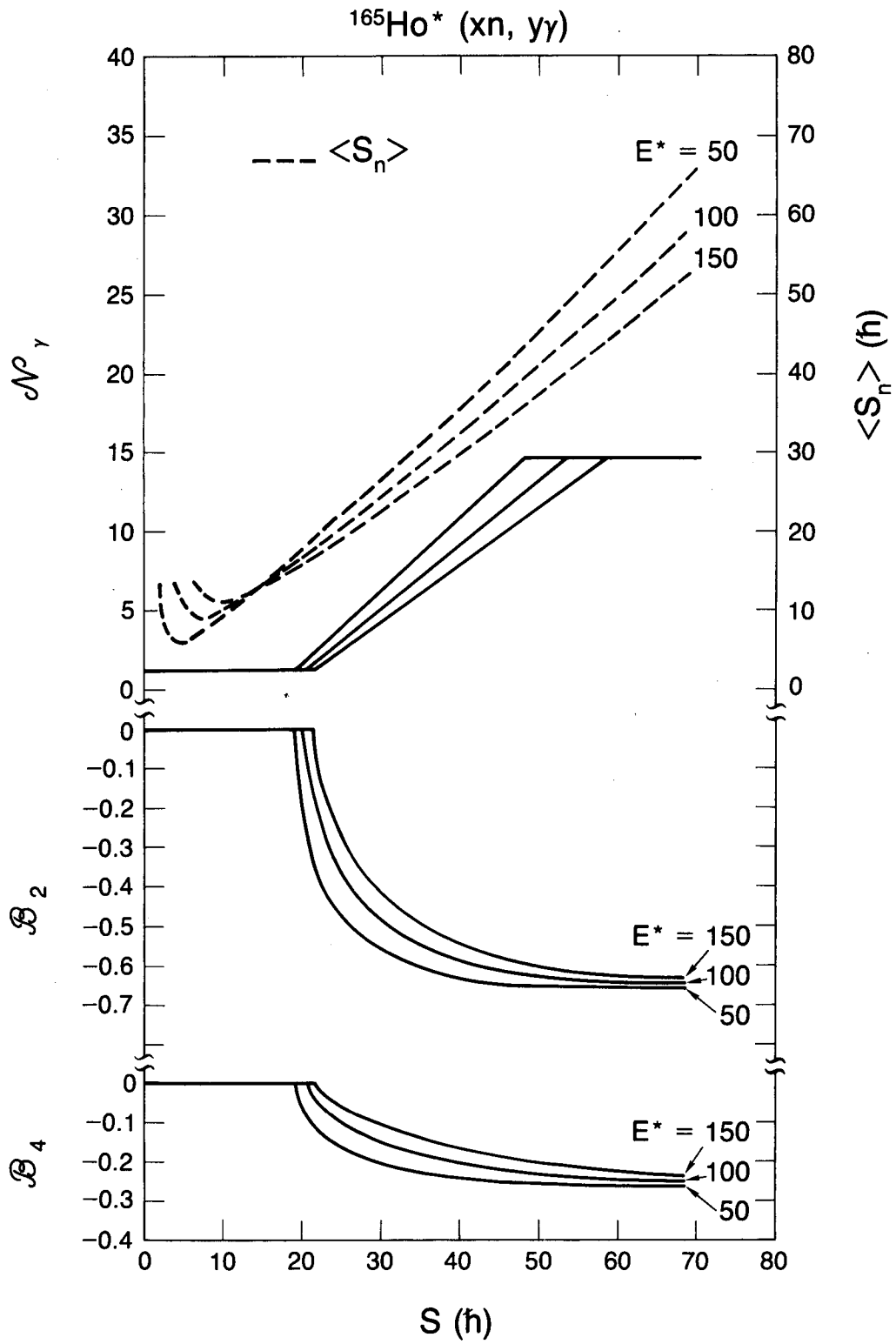

XBL 8311-7309

Fig. 2

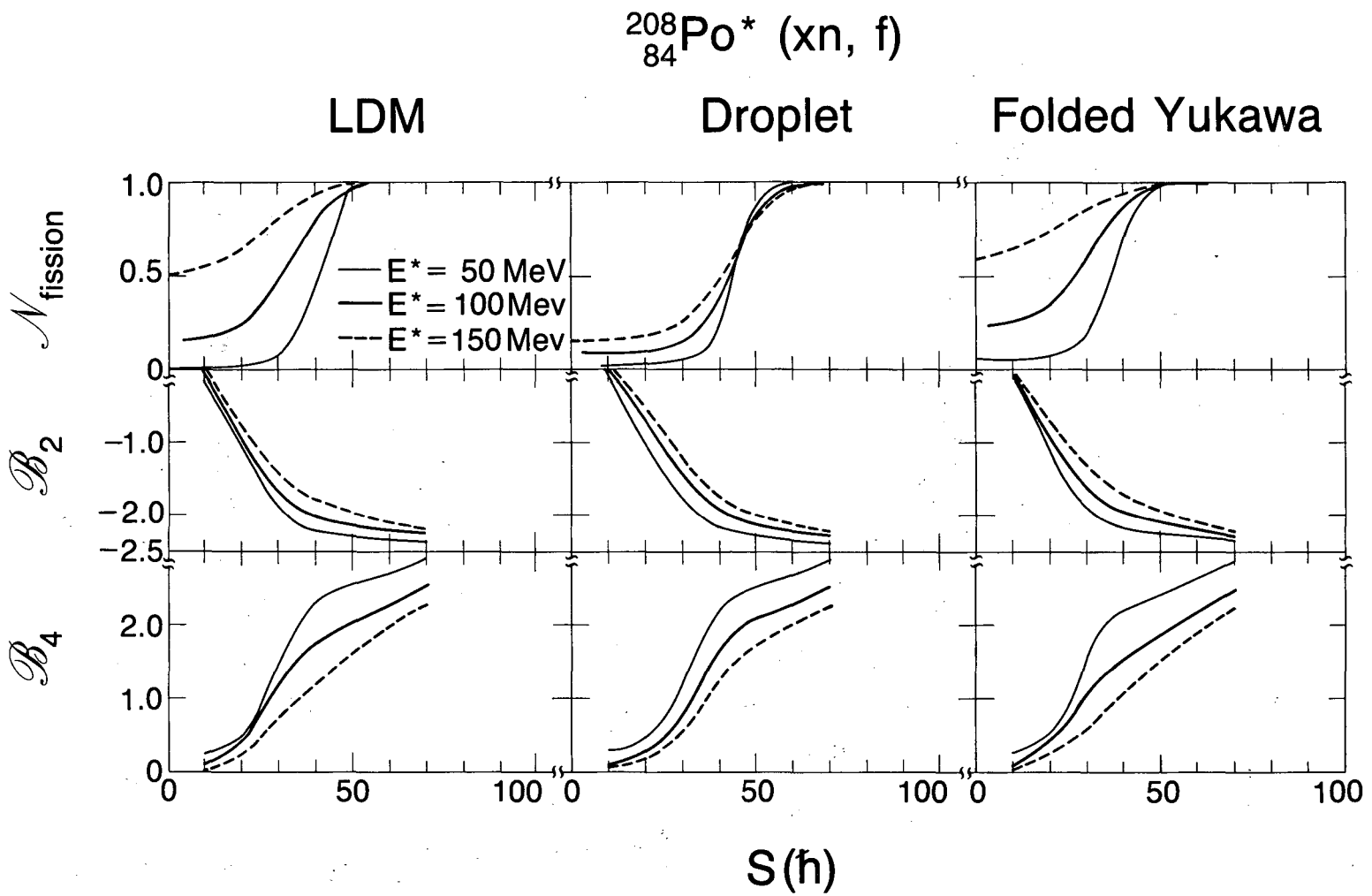
$^{208}_{84}$Po* (xn, f)
LDM
Droplet
Folded Yukawa
$\mathcal{N}_{fission}$
$\mathcal{B}_2$
$\mathcal{B}_4$
E* = 50 MeV
E* = 100 Mev
E* = 150 Mev
1.0
0.5
0
−1.0
−2.0
−2.5
2.0
1.0
0
0
50
100
S(ħ)
XBL 841-95

Fig. 3

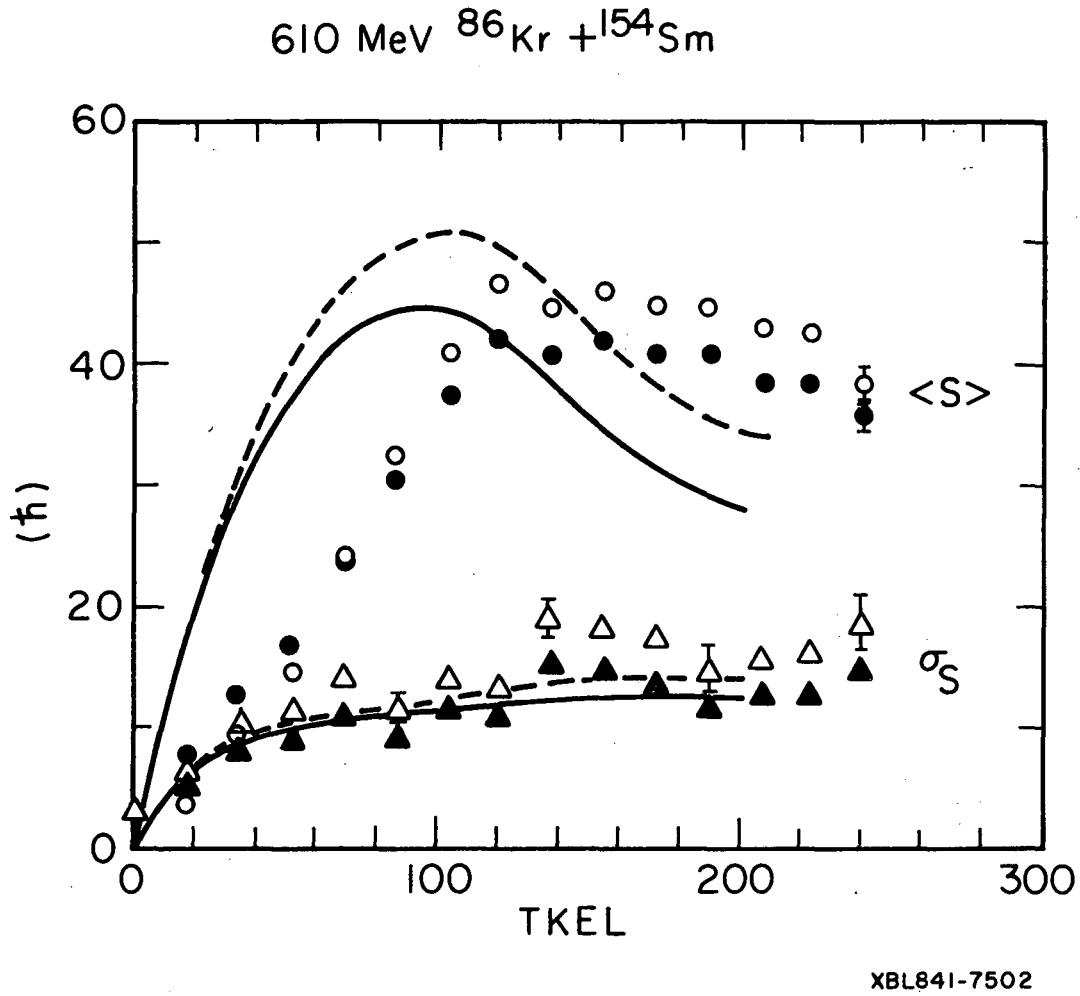
610 MeV 86Kr +154Sm
60
40
20
0
(ħ)
0
100
200
300
TKEL
<S>
σS
XBL841-7502

Fig. 4a

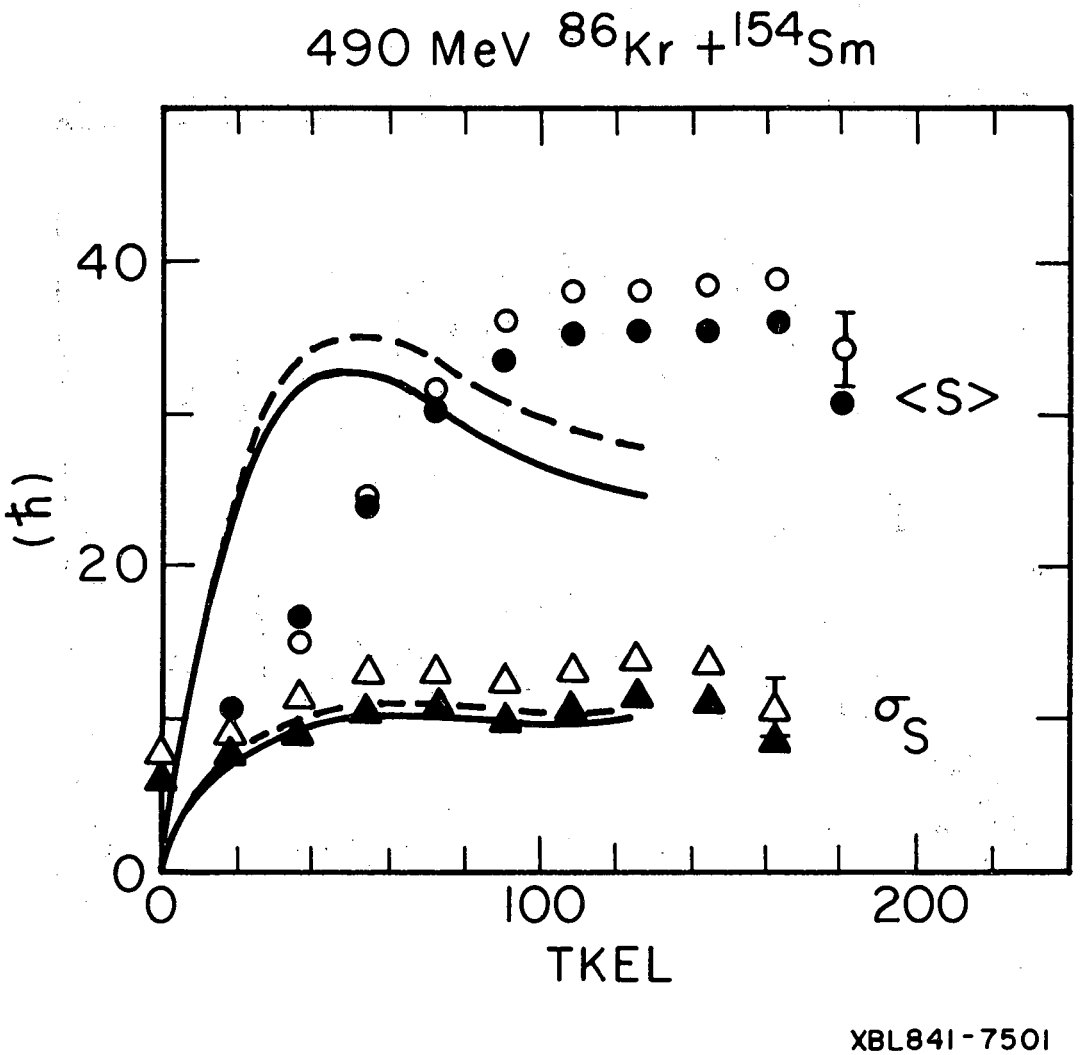

Fig. 4b

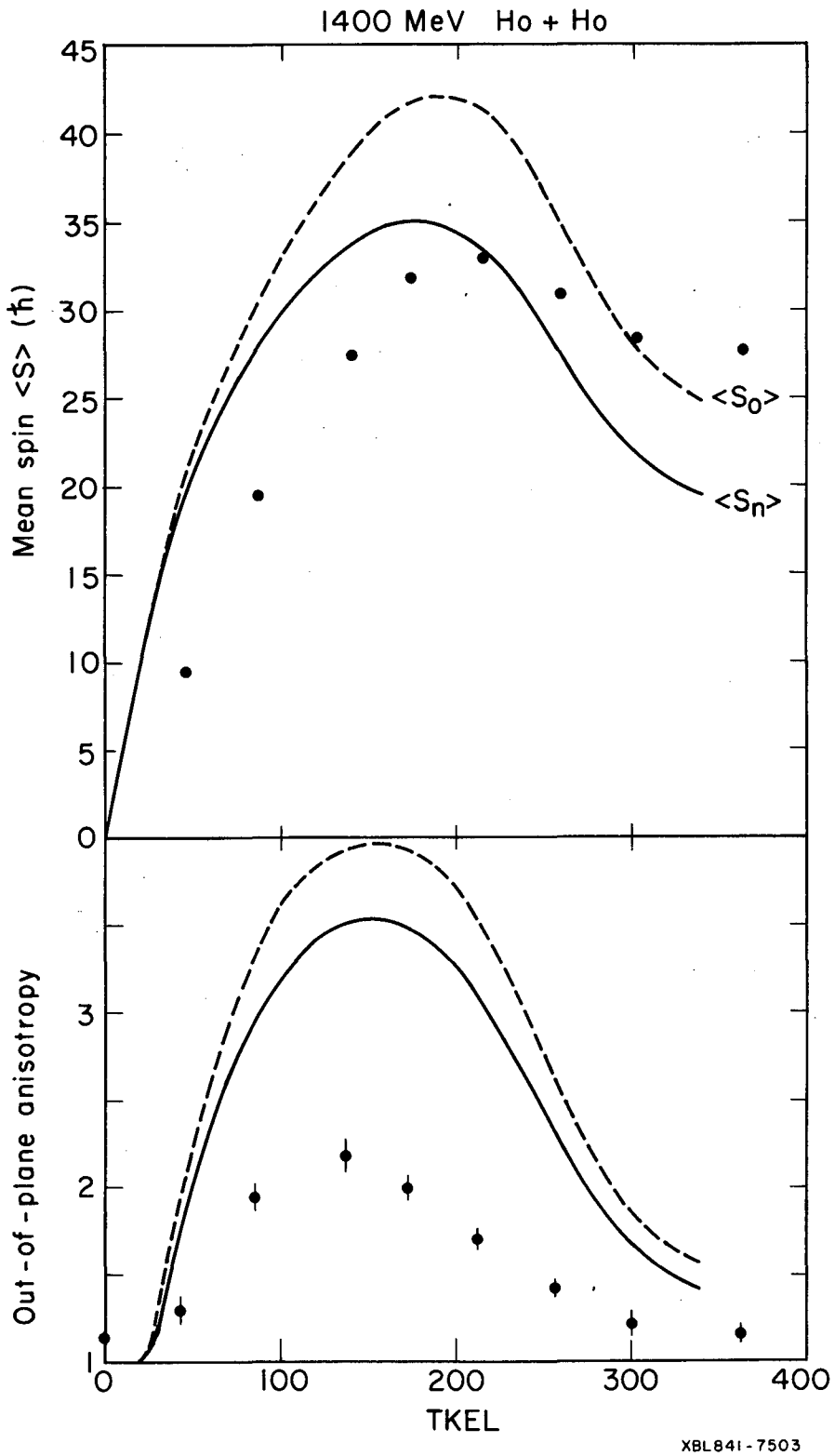
1400 MeV Ho + Ho
Mean spin <S> (ħ)
45
40
35
30
25
20
15
10
5
0
<S0>
<Sn>
Out-of-plane anisotropy
3
2
1
0
100
200
300
400
TKEL
XBL841-7503

Fig. 5

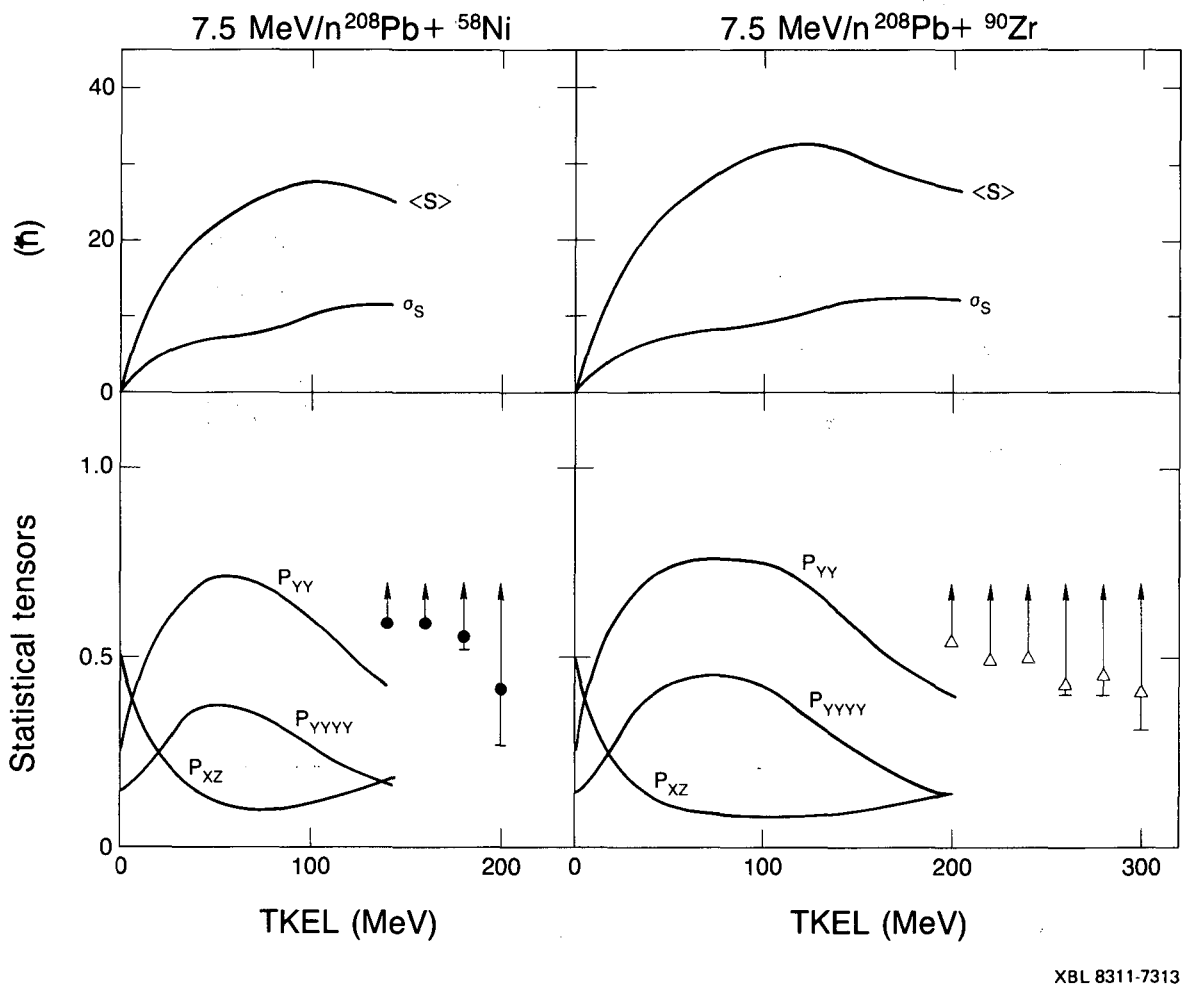
7.5 MeV/n 208Pb+ 58Ni
7.5 MeV/n 208Pb+ 90Zr
(ħ)
40
20
0
<S>
σS
1.0
0.5
0
Statistical tensors
PYY
PYYYY
PXZ
0
100
200
300
TKEL (MeV)
XBL 8311-7313

Fig. 6

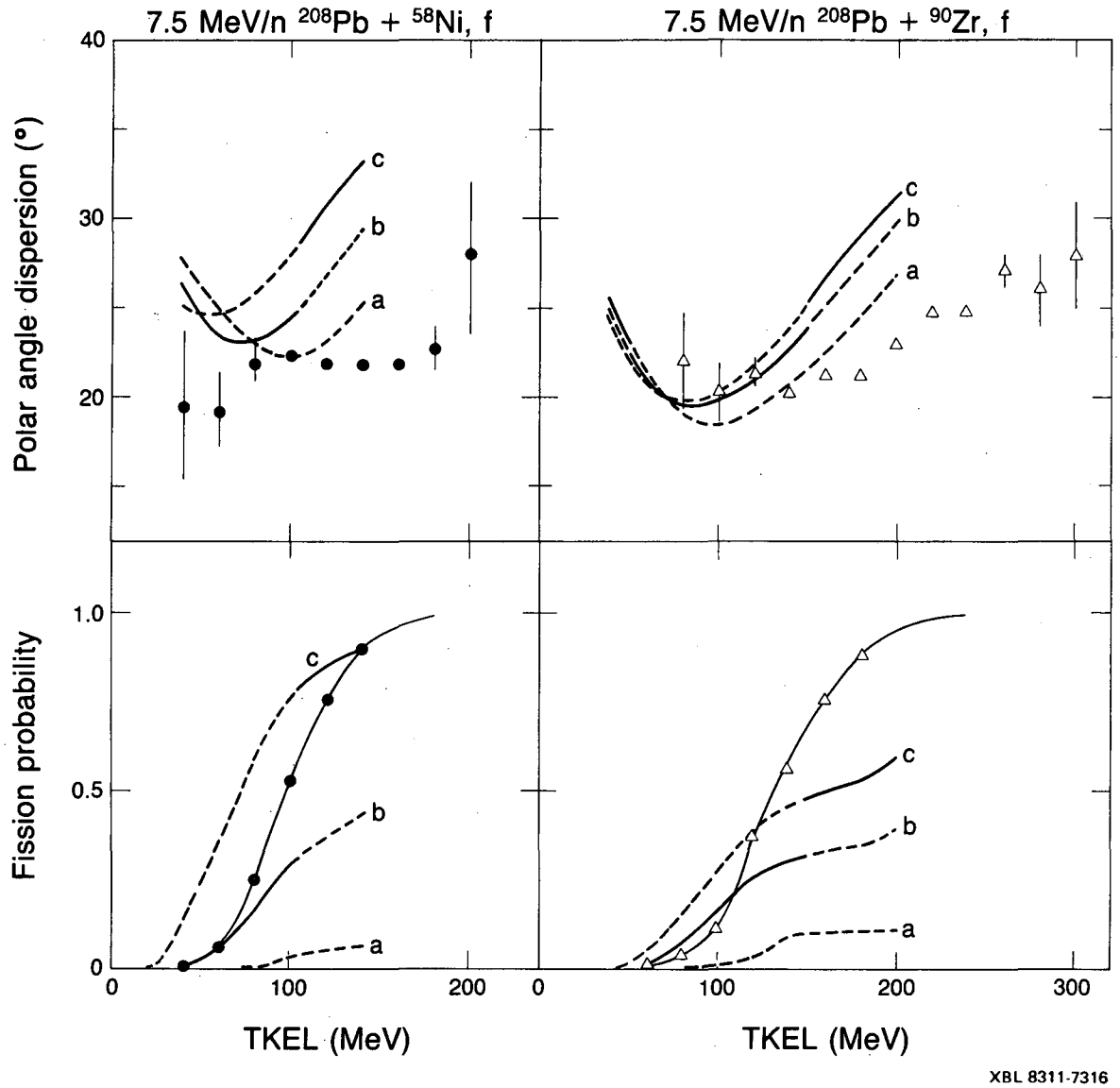
7.5 MeV/n 208Pb + 58Ni, f
7.5 MeV/n 208Pb + 90Zr, f
Polar angle dispersion (°)
Fission probability
TKEL (MeV)
TKEL (MeV)
a
b
c
XBL 8311-7316

Fig. 7

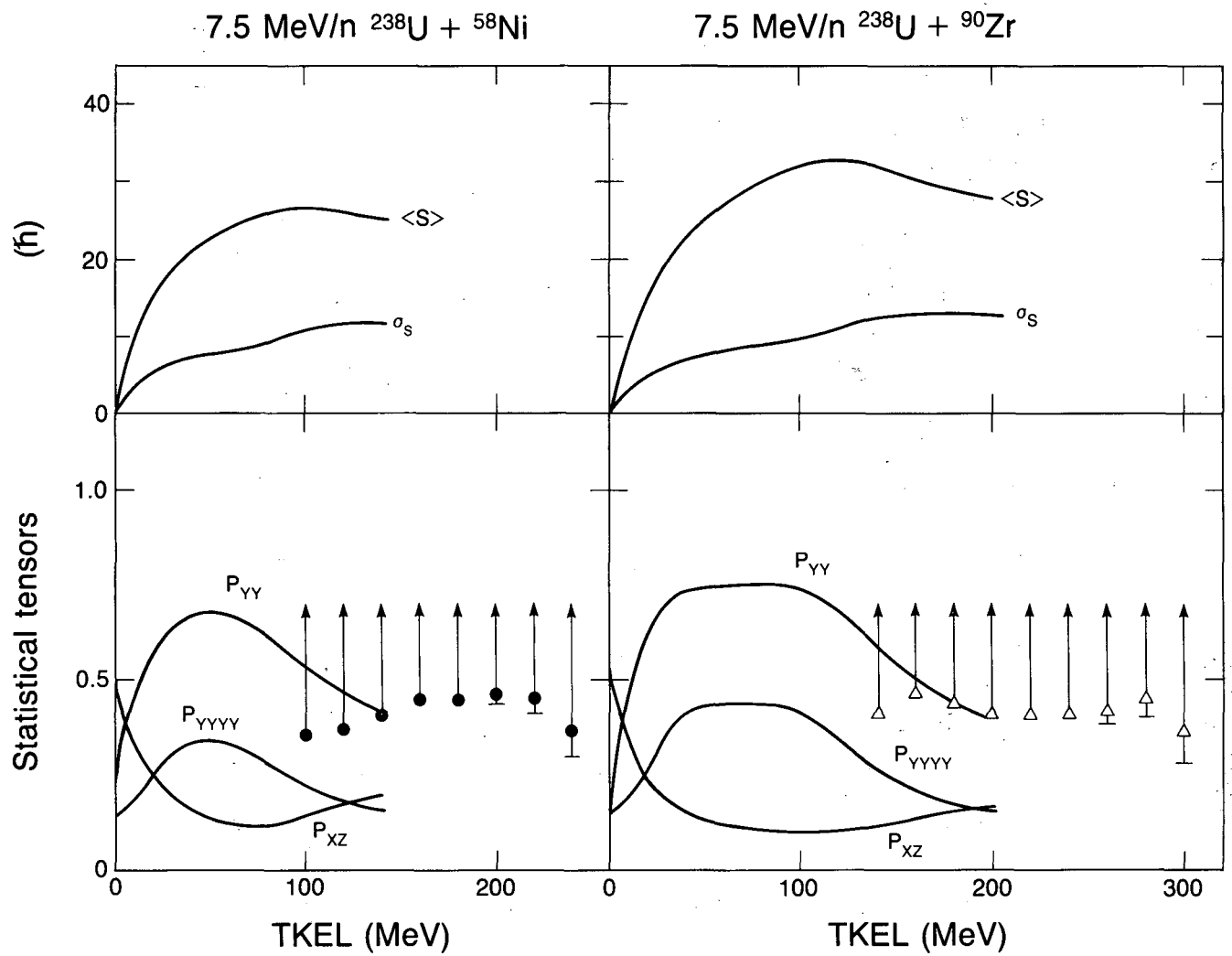
7.5 MeV/n ^{238}U + ^{58}Ni
7.5 MeV/n ^{238}U + ^{90}Zr
(ħ)
40
20
0
<S>
σ_S
Statistical tensors
1.0
0.5
0
P_{YY}
P_{YYYY}
P_{XZ}
0
100
200
300
TKEL (MeV)
XBL 8311-7314

Fig. 8

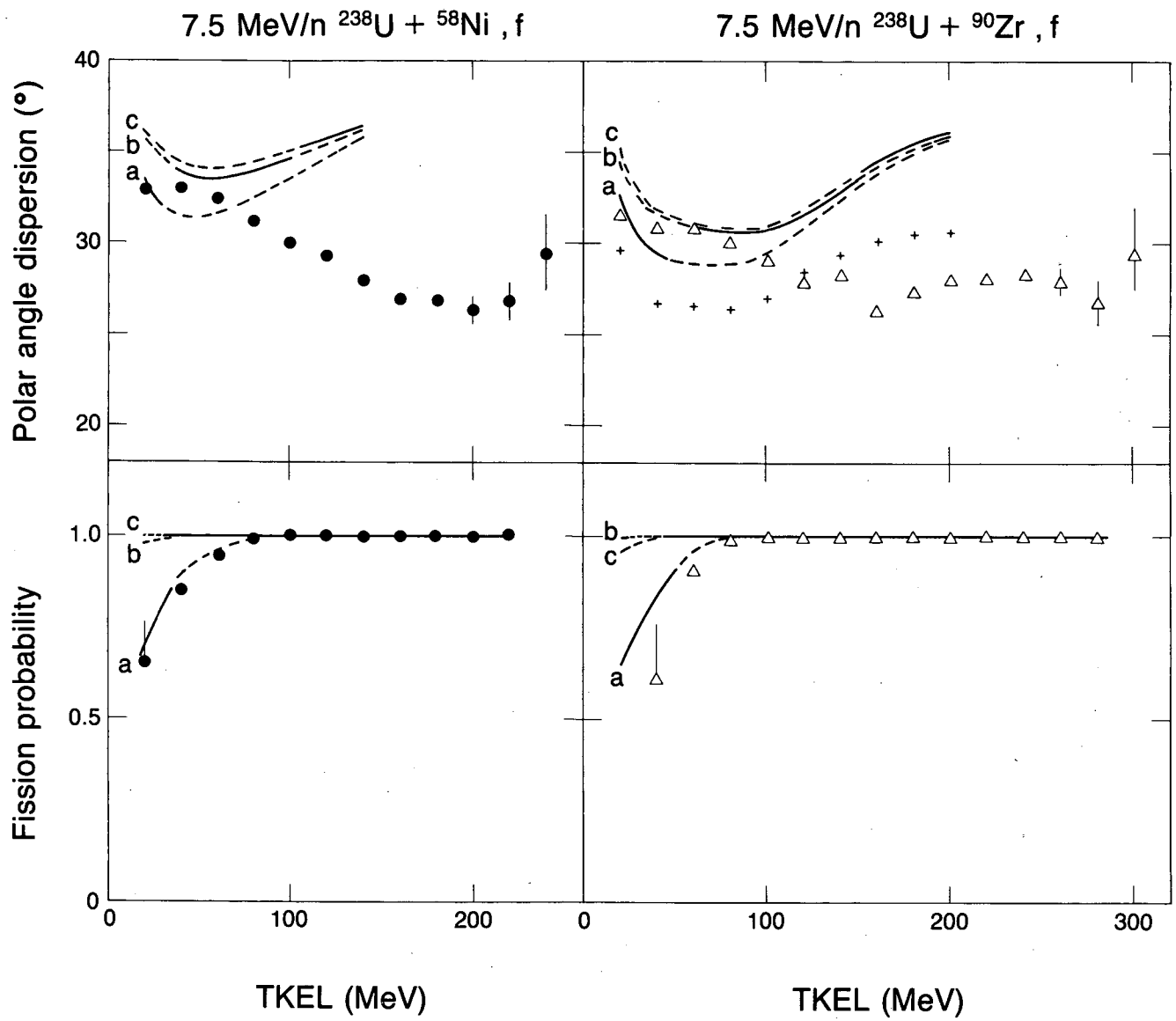
7.5 MeV/n ^{238}U + ^{58}Ni , f
7.5 MeV/n ^{238}U + ^{90}Zr , f
Polar angle dispersion (°)
Fission probability
TKEL (MeV)
TKEL (MeV)
a
b
c
40
30
20
1.0
0.5
0
0
100
200
300
XBL 8311-7315

Fig. 9

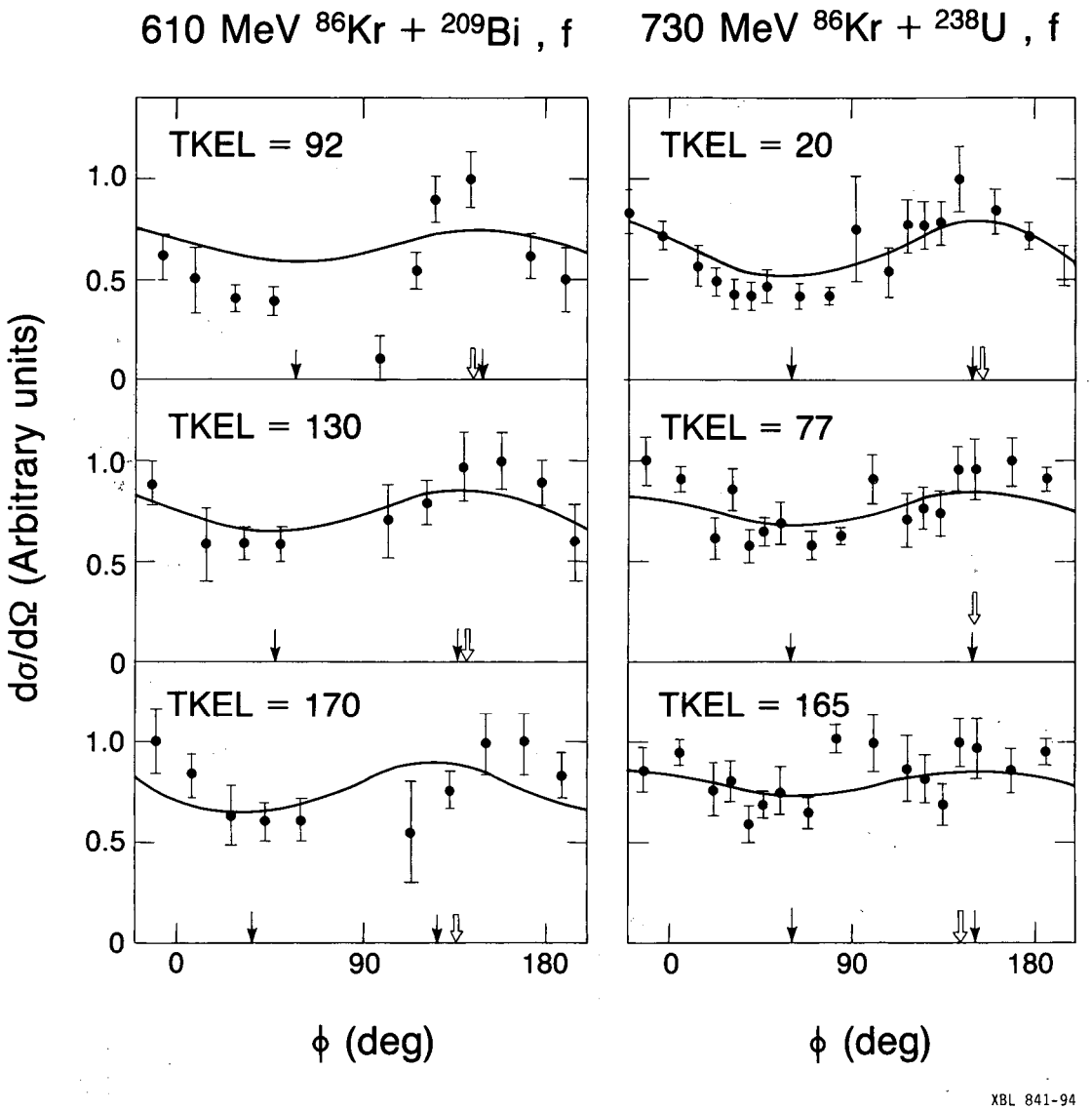
610 MeV 86Kr + 209Bi , f
730 MeV 86Kr + 238U , f
TKEL = 92
TKEL = 130
TKEL = 170
TKEL = 20
TKEL = 77
TKEL = 165
dσ/dΩ (Arbitrary units)
1.0
0.5
0
0
90
180
ϕ (deg)
XBL 841-94

Fig. 10

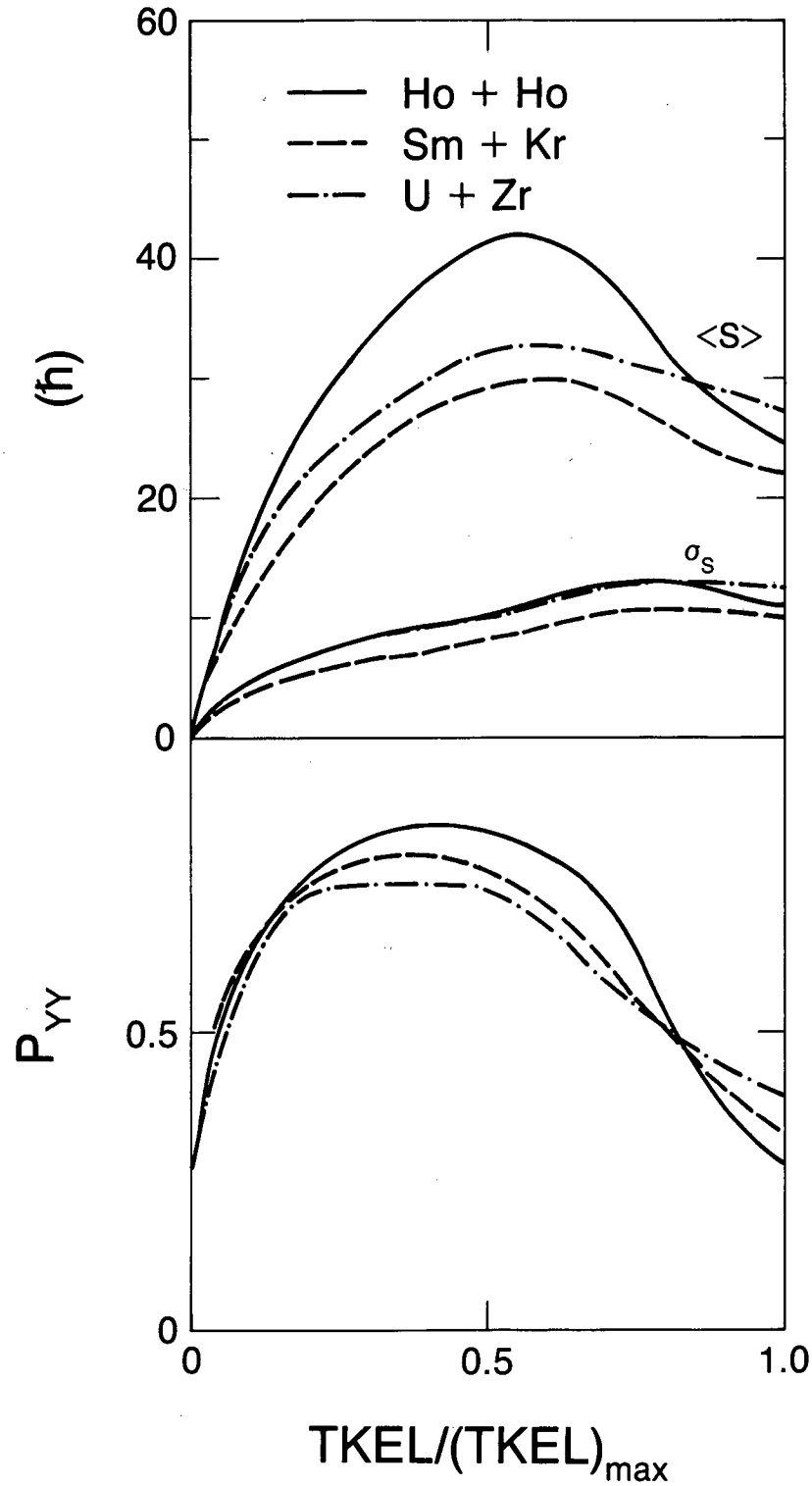

XBL 8311-7312

Fig. 11

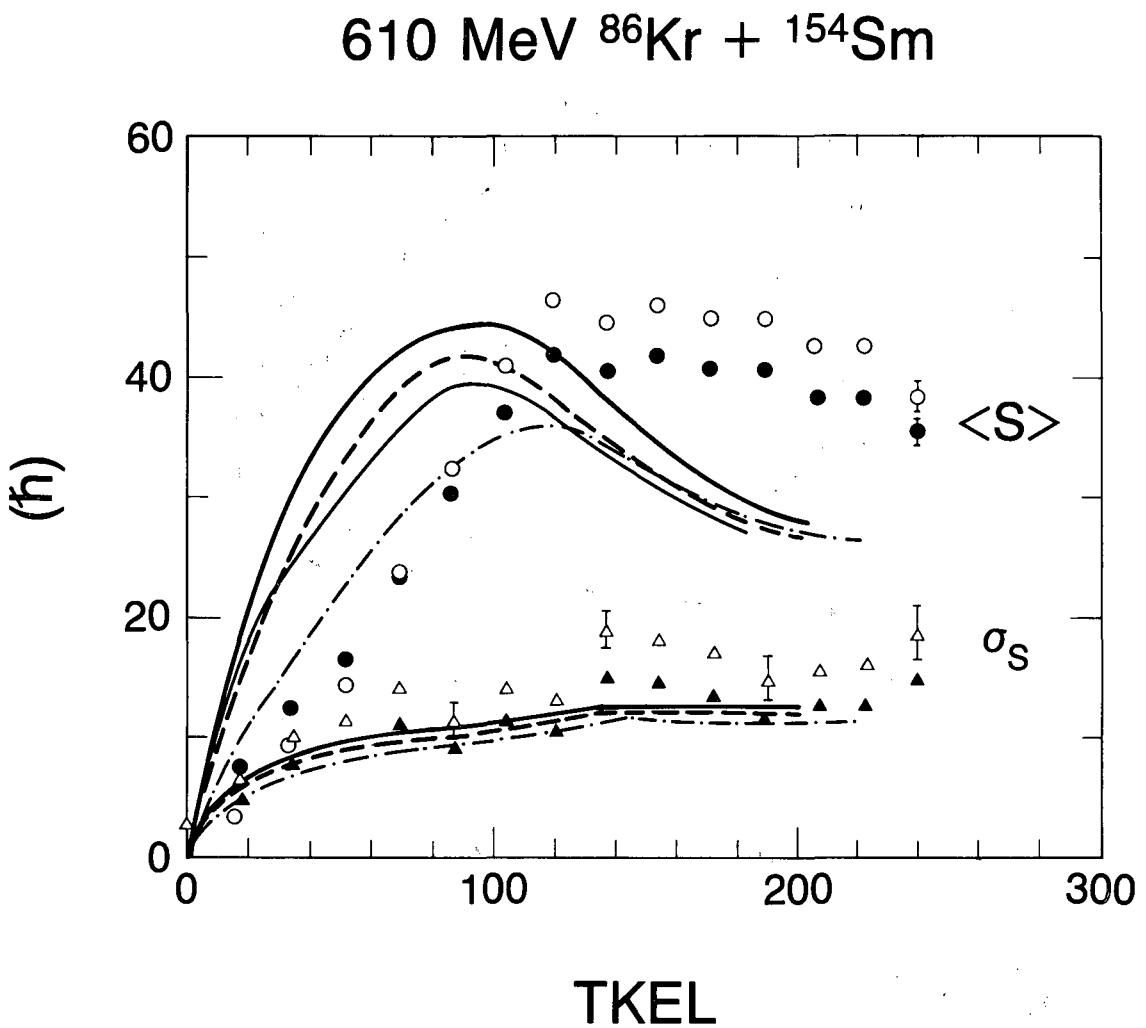

XBL 841-92

Fig. 12

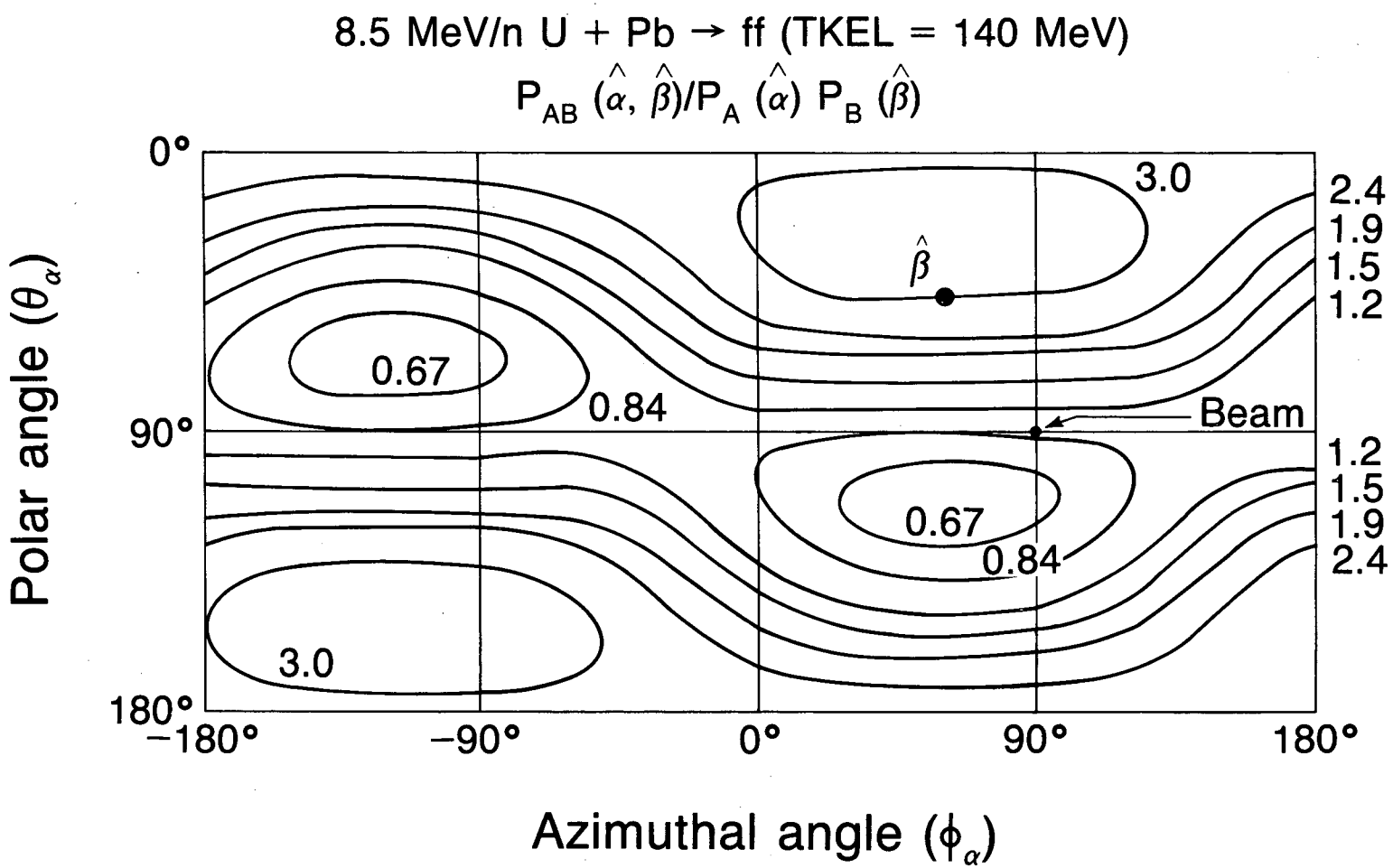

XBL 8311-7308

Fig. 13a

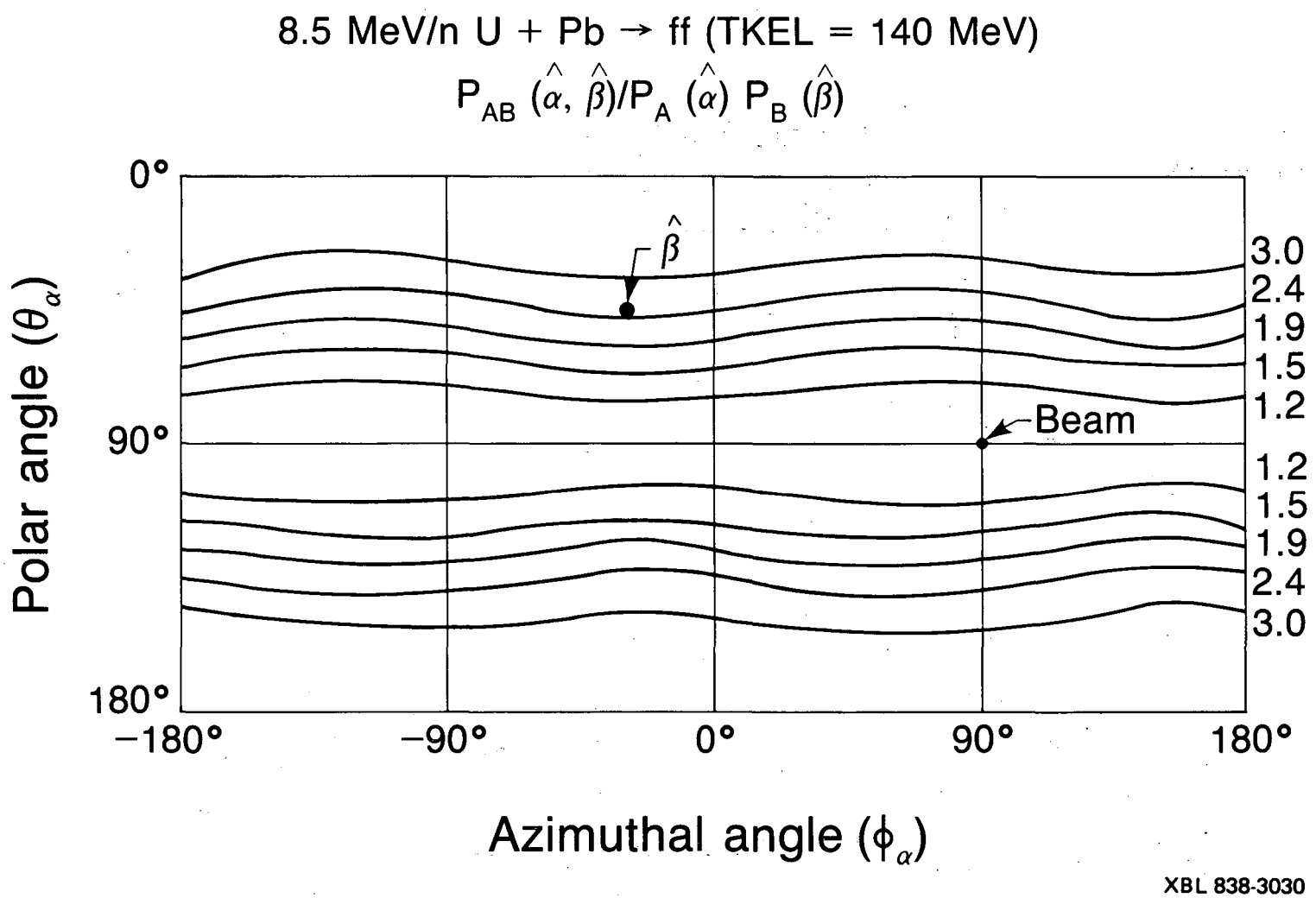
8.5 MeV/n U + Pb → ff (TKEL = 140 MeV)
$P_{AB}(\hat{\alpha}, \hat{\beta})/P_A(\hat{\alpha})\, P_B(\hat{\beta})$
0°
90°
180°
Polar angle (θ_α)
−180°
−90°
0°
90°
180°
Azimuthal angle (ϕ_α)
$\hat{\beta}$
Beam
3.0
2.4
1.9
1.5
1.2
1.2
1.5
1.9
2.4
3.0
XBL 838-3030

Fig. 13b

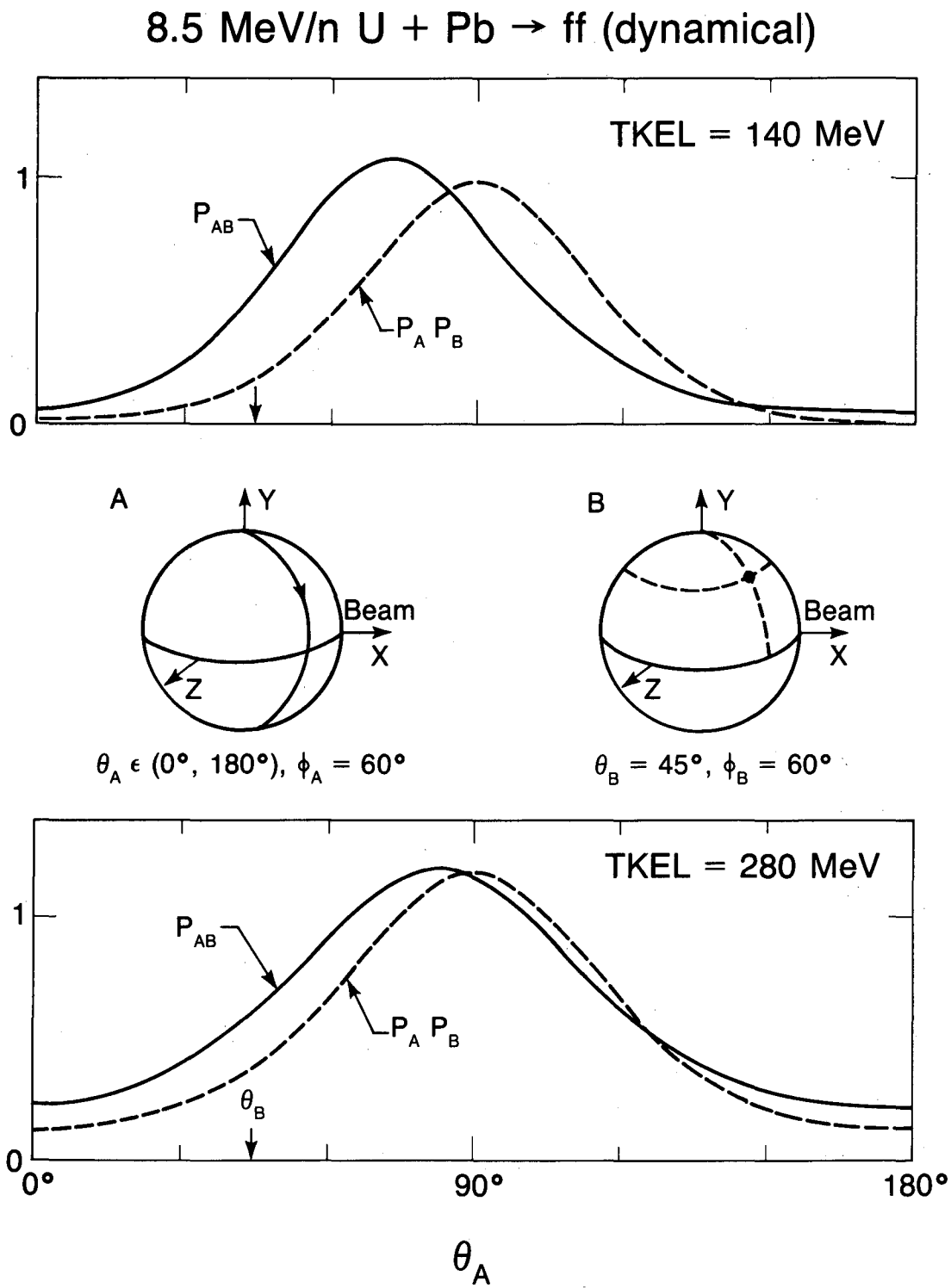

XBL 8311-7302

Fig. 14a

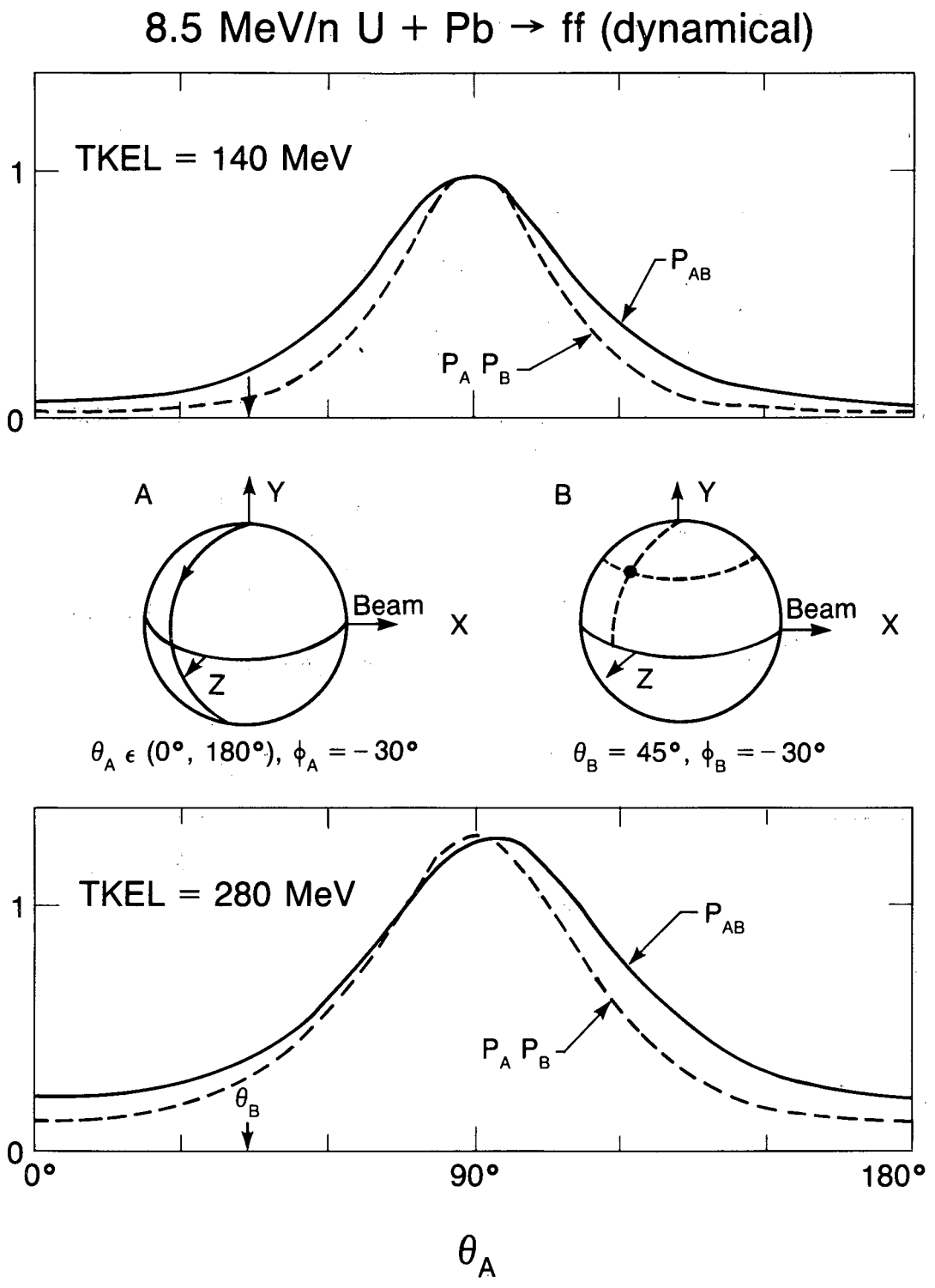

XBL 8311-7300

Fig. 14b

8.5 MeV/n U + Pb → ff (dynamical)

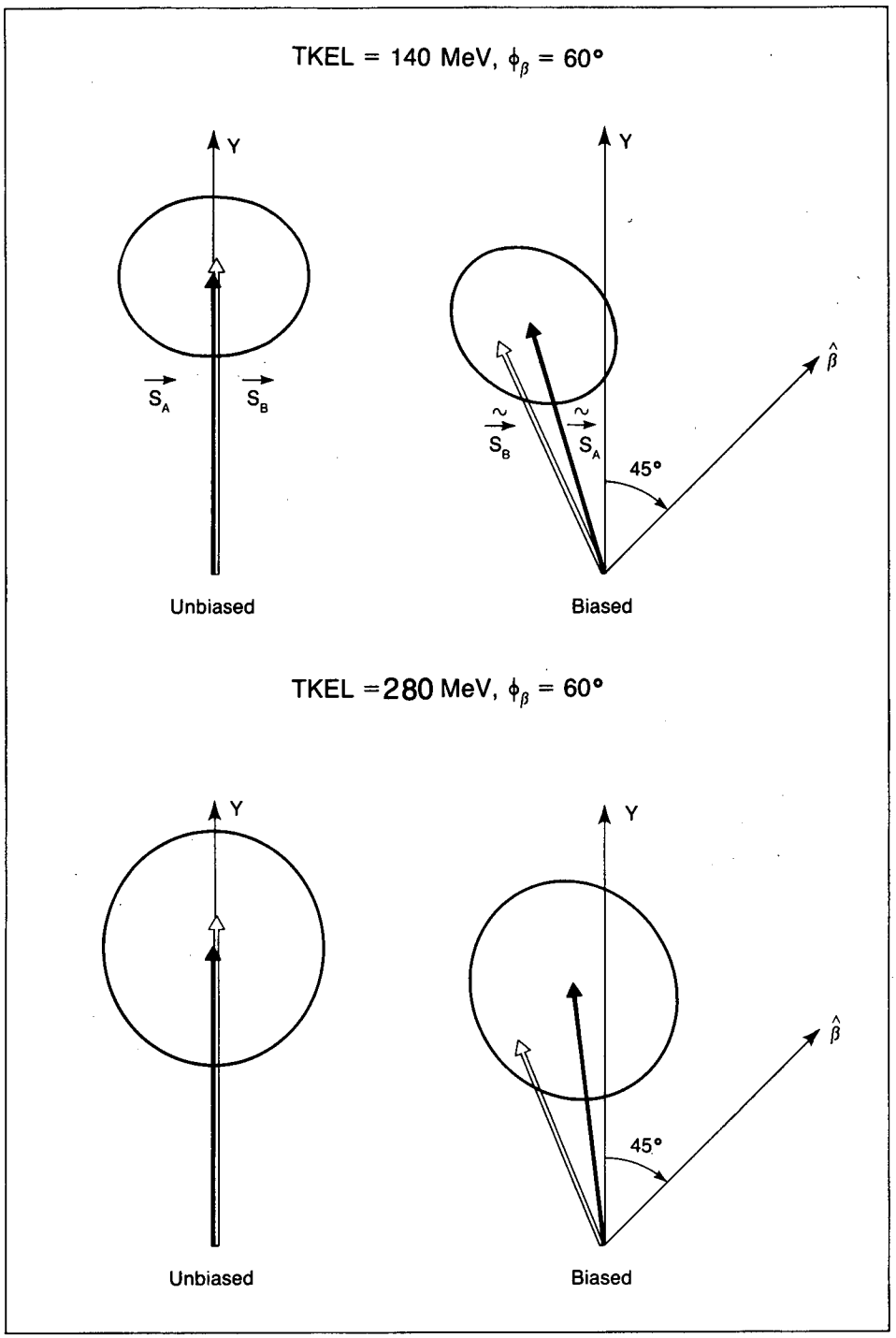

XBL 8311-7305

Fig. 15a

8.5 MeV/n U + Pb → ff (dynamical)

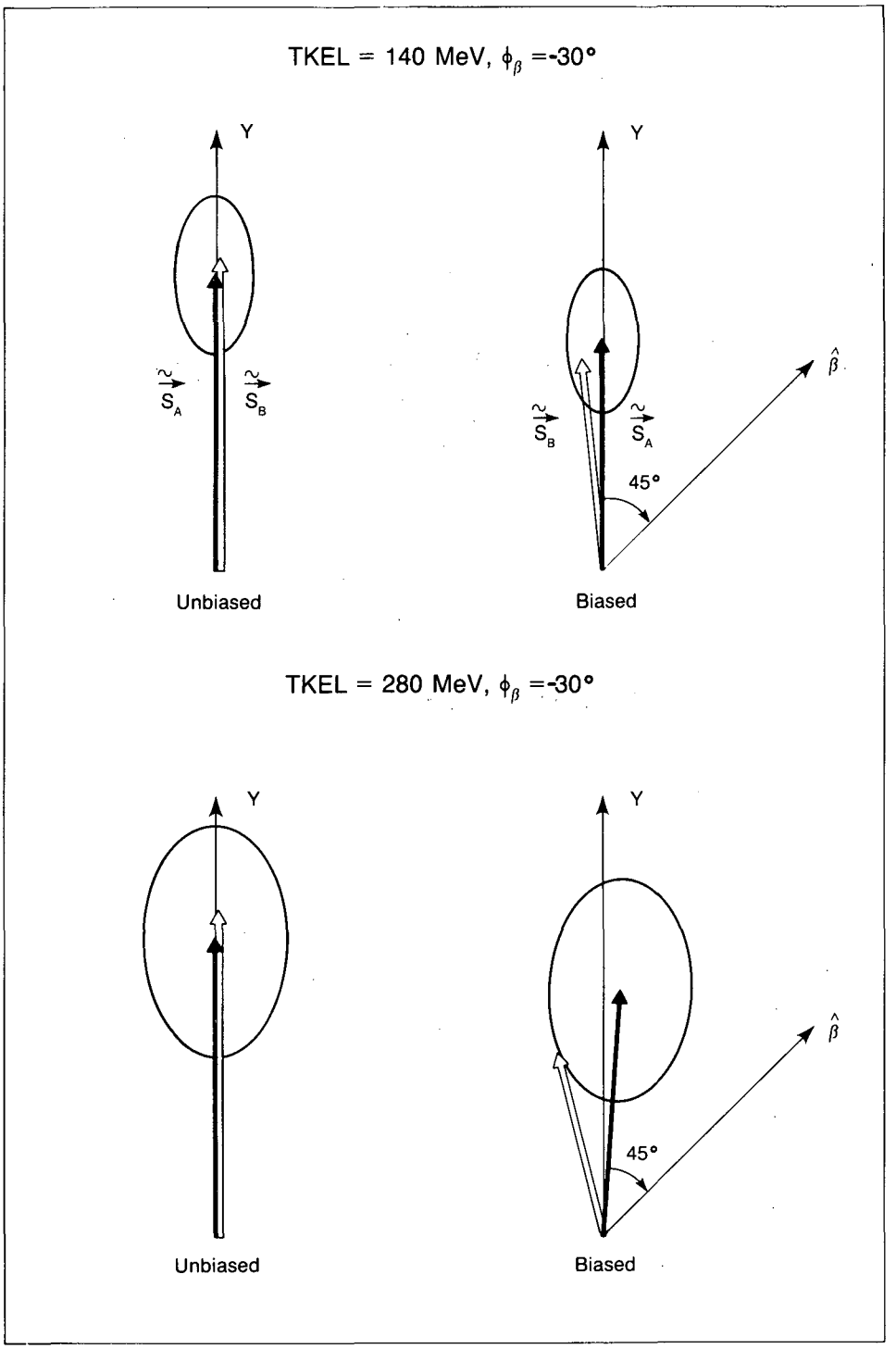

XBL 8311-7307

Fig. 15b

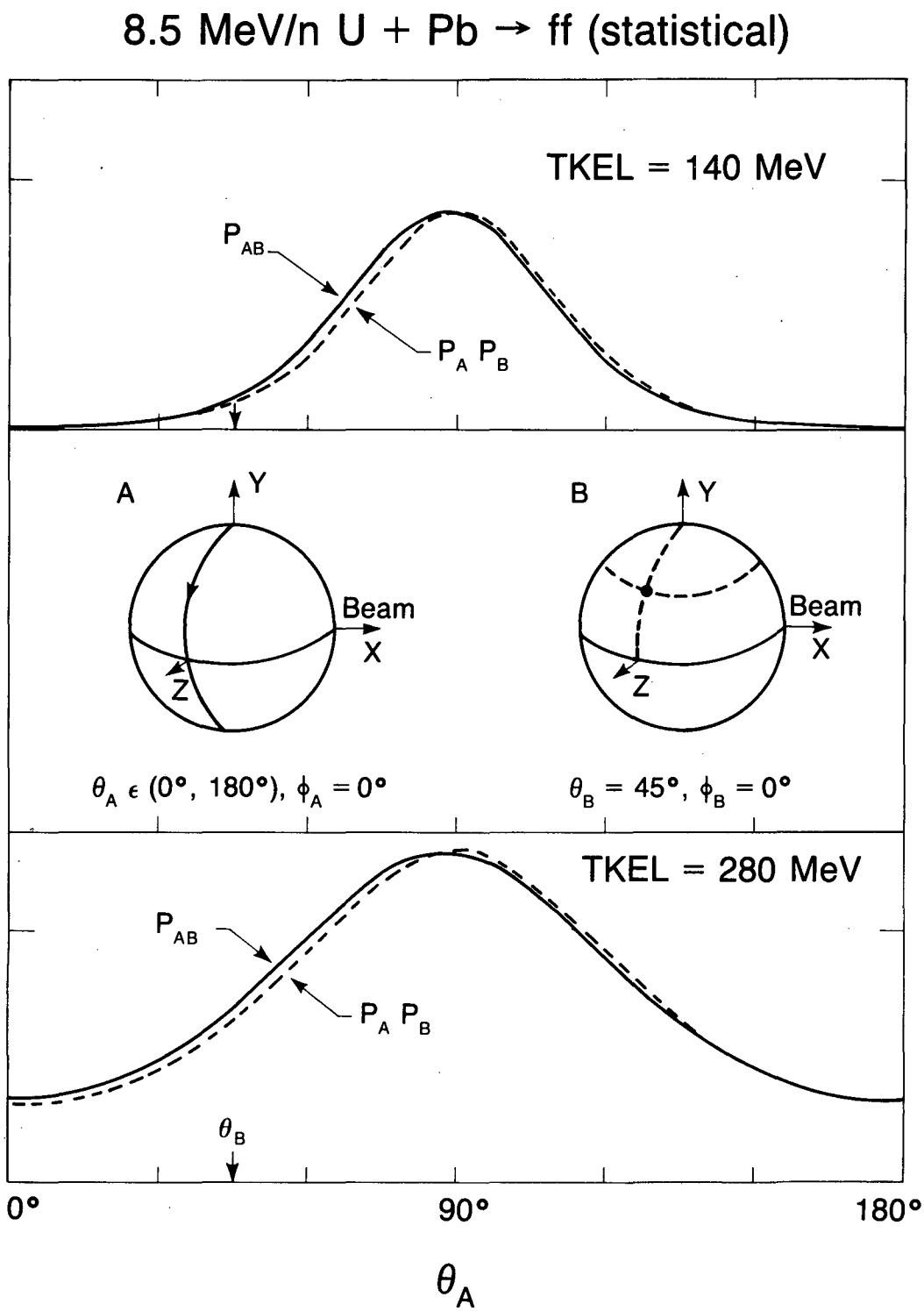

XBL 8311-7306

Fig. 16a

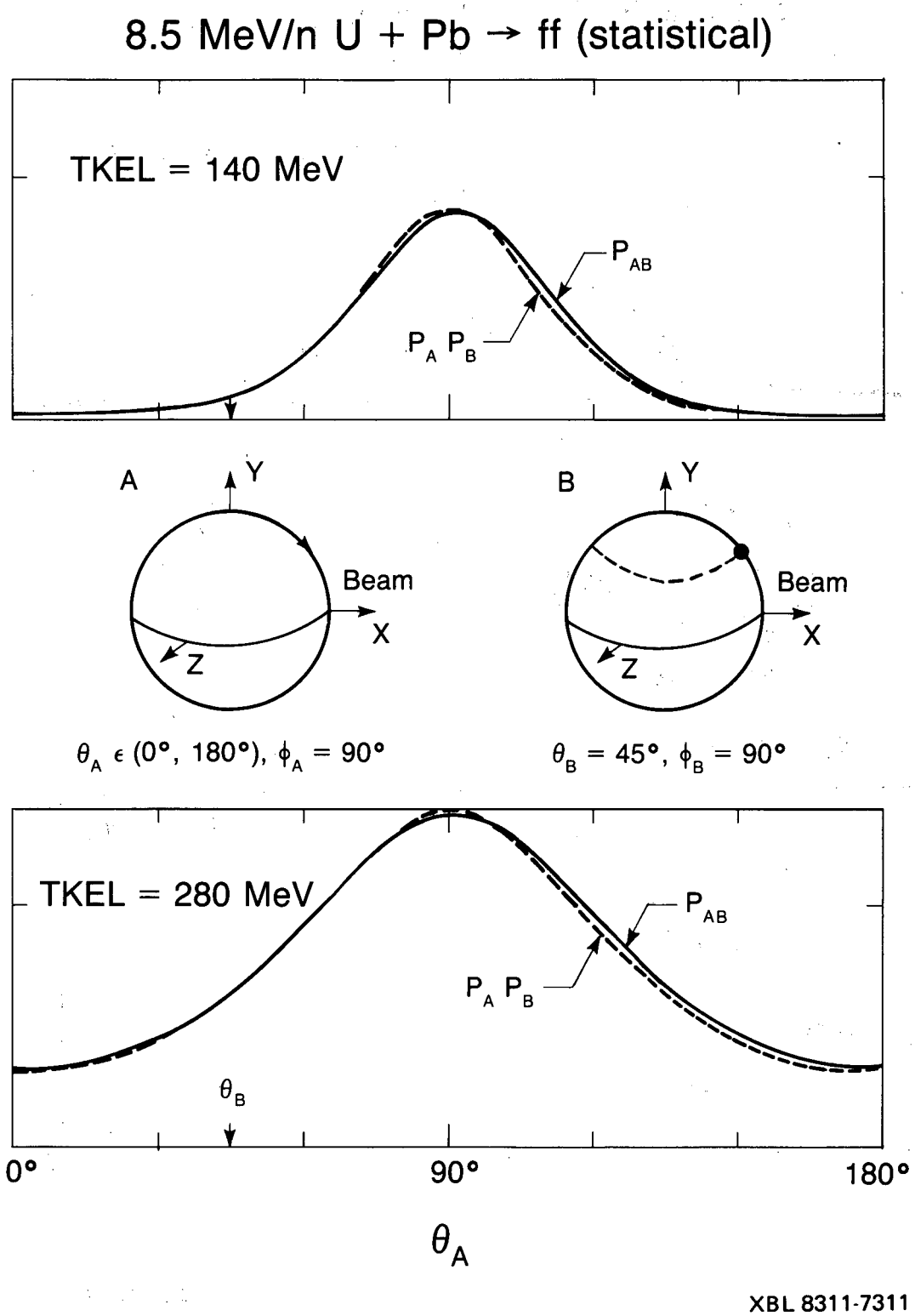
8.5 MeV/n U + Pb → ff (statistical)
TKEL = 140 MeV
P_AB
P_A P_B
A
Y
Beam
X
Z
B
Y
Beam
X
Z
θ_A ∈ (0°, 180°), φ_A = 90°
θ_B = 45°, φ_B = 90°
TKEL = 280 MeV
P_AB
P_A P_B
θ_B
0°
90°
180°
θ_A
XBL 8311-7311

Fug. 16b

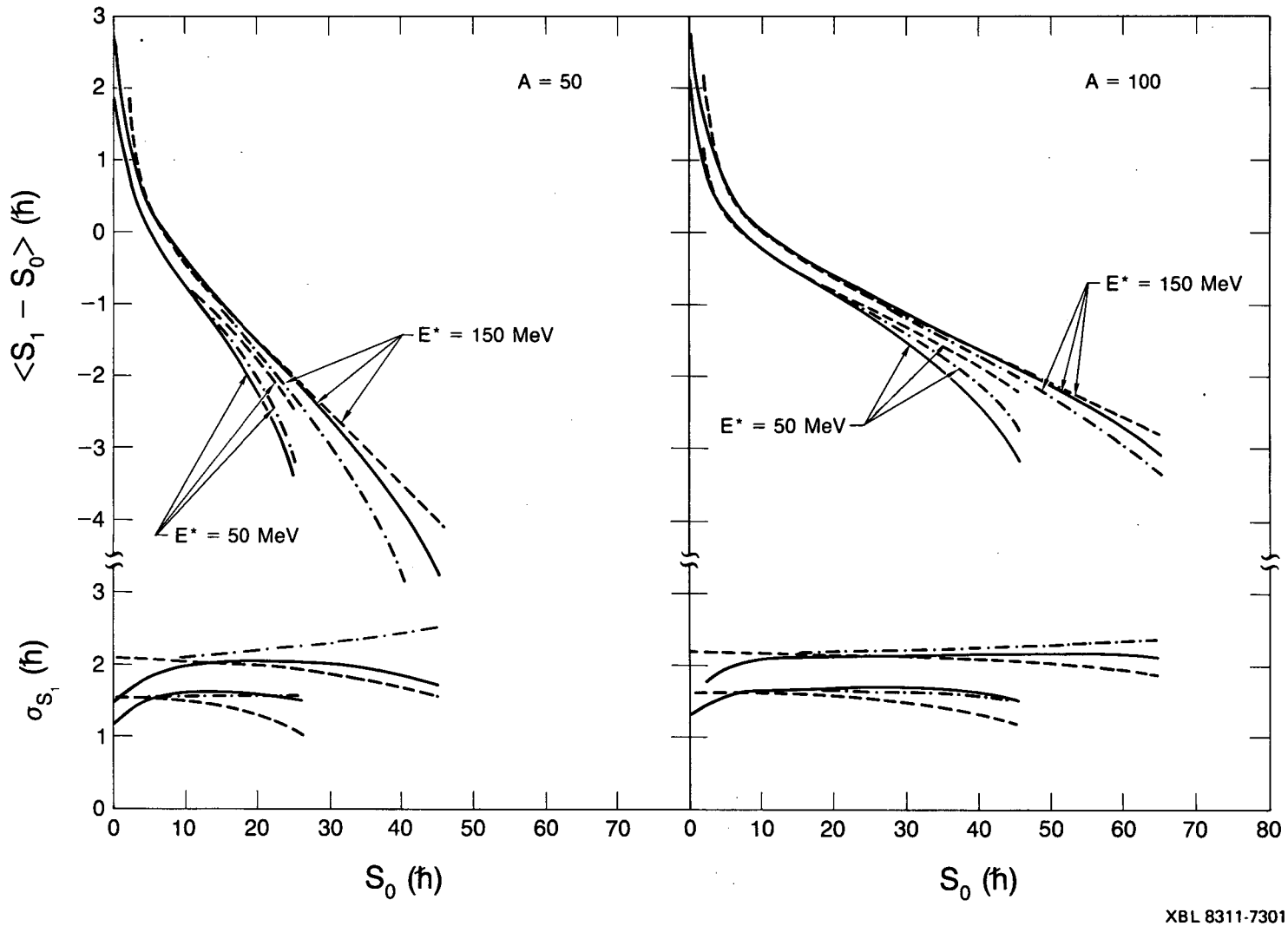
A = 50
A = 100
E* = 150 MeV
E* = 50 MeV
E* = 150 MeV
E* = 50 MeV
<S1 − S0> (ħ)
σS1 (ħ)
S0 (ħ)
S0 (ħ)
XBL 8311-7301

Fig. Ala

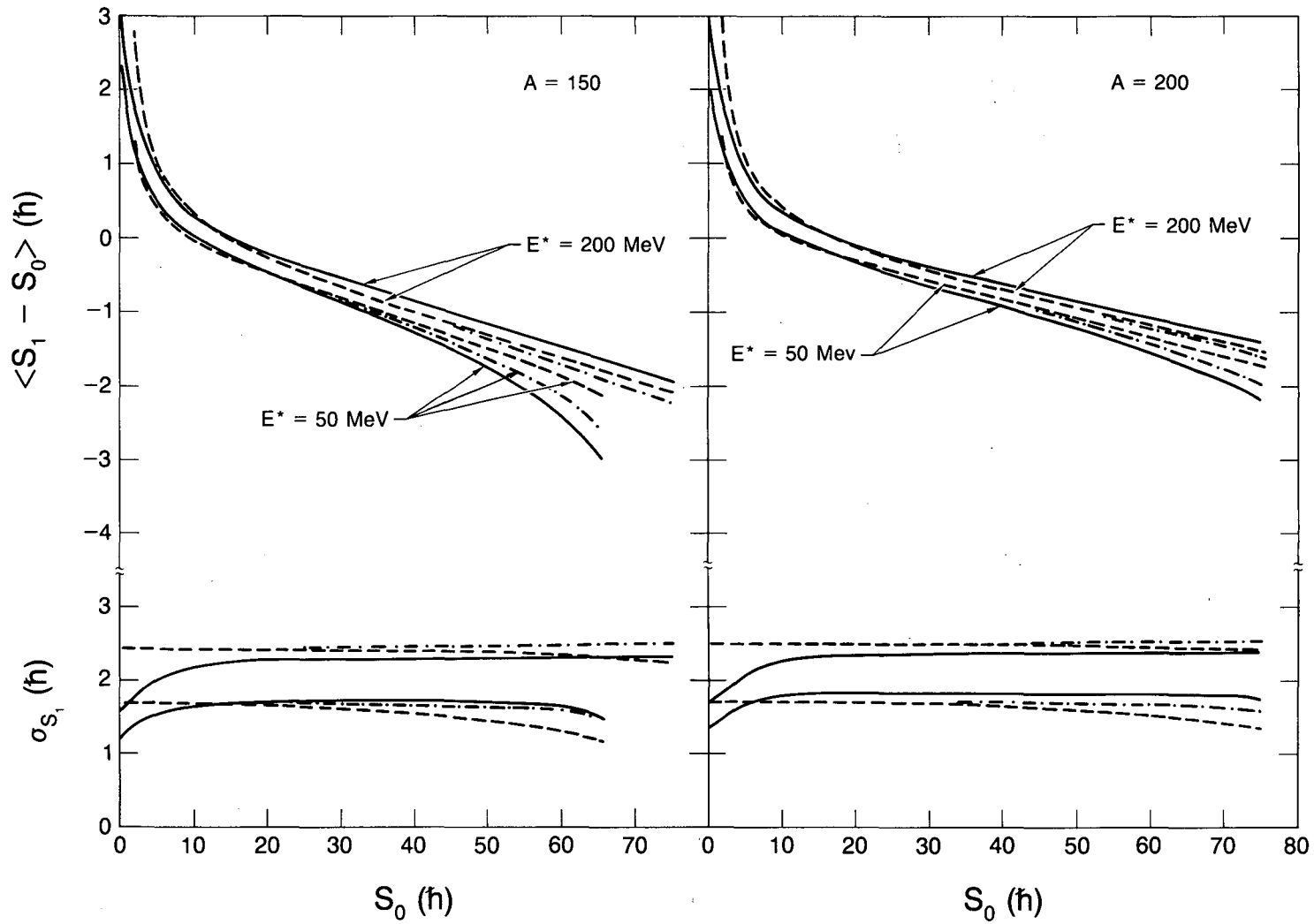
A = 150
A = 200
E* = 200 MeV
E* = 50 MeV
E* = 200 MeV
E* = 50 Mev
<S1 − S0> (ħ)
σS1 (ħ)
S0 (ħ)
S0 (ħ)
XBL 8311-7317

Fig. A1b

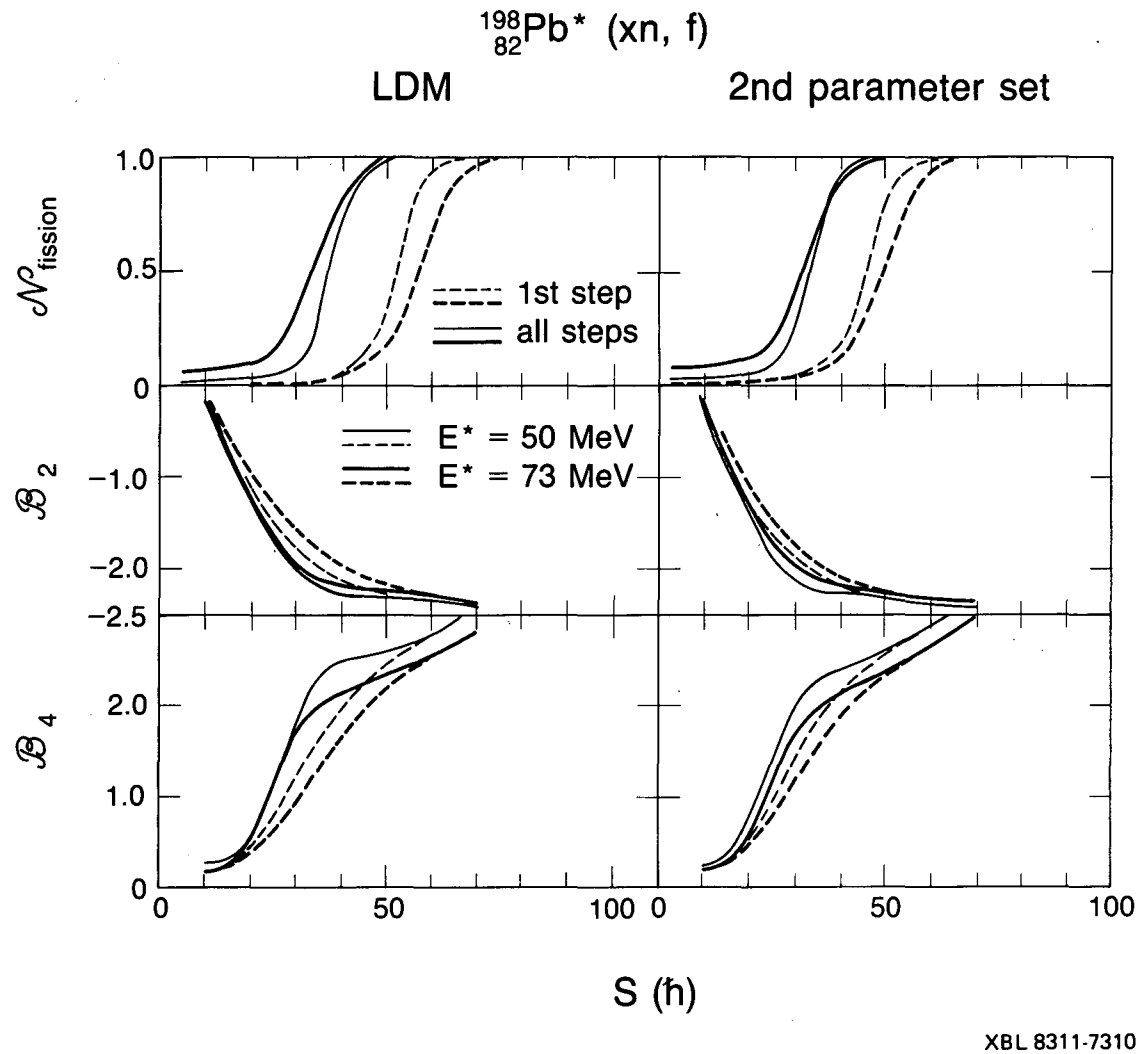
$^{198}_{82}$Pb* (xn, f)
LDM
2nd parameter set
$\mathcal{N}_{fission}$
1.0
0.5
0
1st step
all steps
E* = 50 MeV
E* = 73 MeV
$\mathcal{B}_2$
−1.0
−2.0
−2.5
$\mathcal{B}_4$
2.0
1.0
0
0
50
100
0
50
100
S (ħ)
XBL 8311-7310

Fig. B1

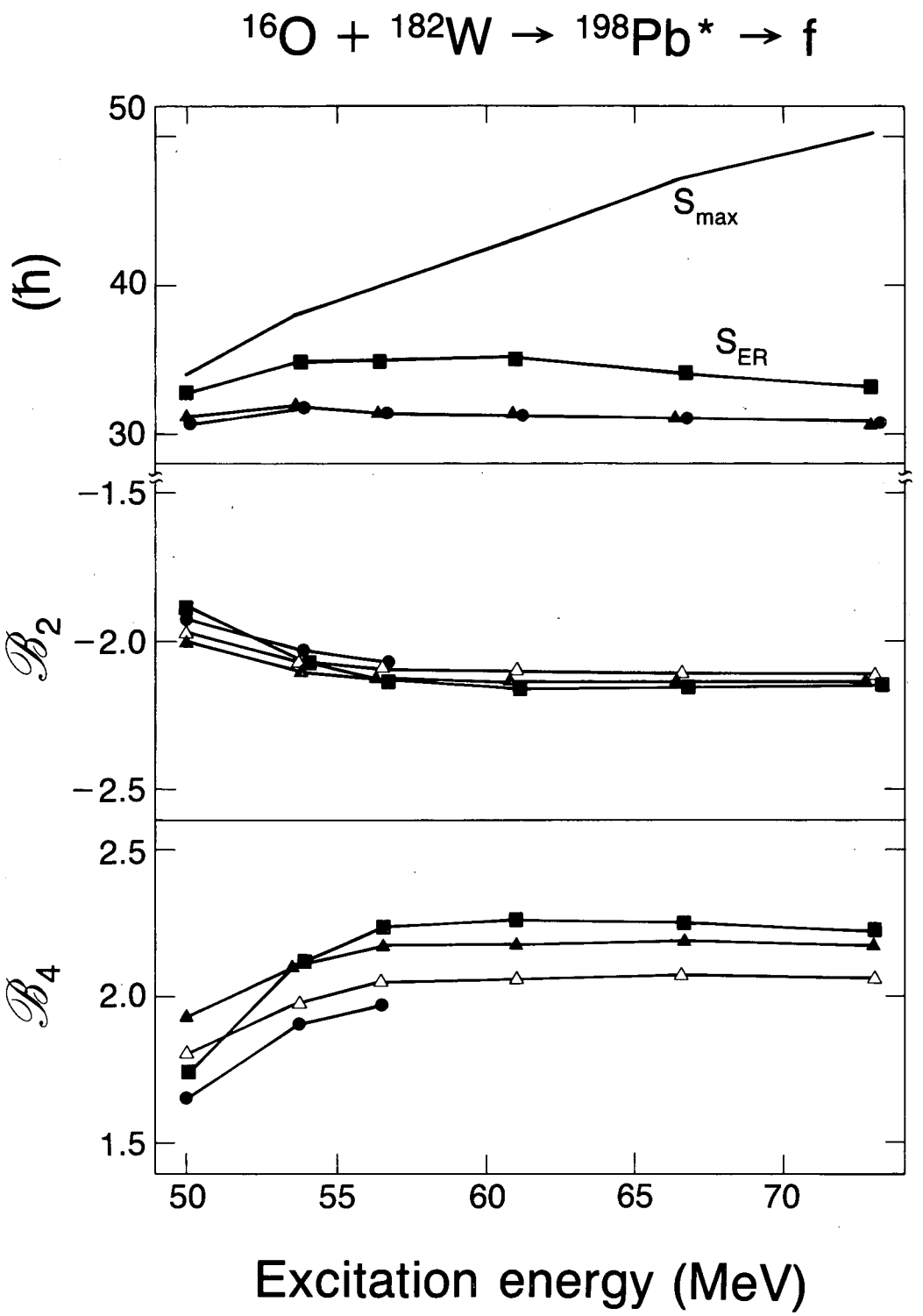

XBL 841-93

Fig. B2

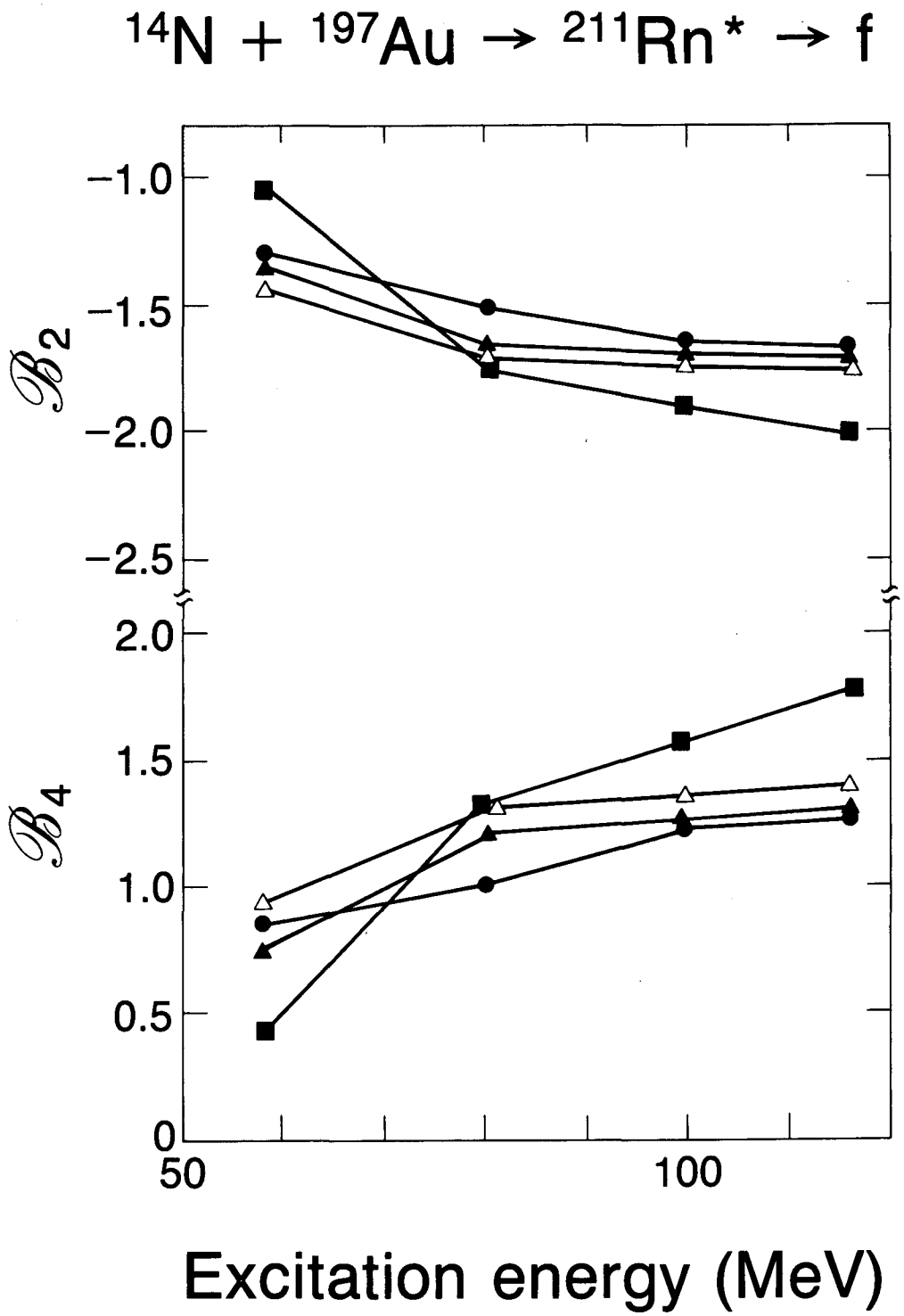

XBL 841-91

Fig. B3

This report was done with support from the Department of Energy. Any conclusions or opinions expressed in this report represent solely those of the author(s) and not necessarily those of The Regents of the University of California, the Lawrence Berkeley Laboratory or the Department of Energy.

Reference to a company or product name does not imply approval or recommendation of the product by the University of California or the U.S. Department of Energy to the exclusion of others that may be suitable.

TECHNICAL INFORMATION DEPARTMENT
LAWRENCE BERKELEY LABORATORY
UNIVERSITY OF CALIFORNIA
BERKELEY, CALIFORNIA 94720